ARCHIVES OF ACOUSTICS
10, 3, 215–228 (1985)

CHOSEN PROBLEMS OF THE AERODYNAMICS OF PLAYING THE WIND INSTRUMENTS *

ZYGMUNT PAWŁOWSKI, MAREK ŻÓŁTOWSKI

Department of Phoniatrics, Frederic Chopin Academy of Music
(00–368 Warsaw, ul. Okólnik 2)

The authors modified the aerodynamic method for the diagnostics of the function of the respiratory organ during playing the wind instruments. The essence of this method is the possibility of measuring the value of the air pressure in the respiratory tracts without puncture into the trachea and obtaining the aerodynamogram curve. This curve permits the phenomena occurring during the play to be recorded, according to the division into three periods: 1) inspiration, 2) expiration until a given sound is formed, 3) the further duration of the expiration phase until its end. In the course of the investigations, it was found that the respiratory organ of the musician compensates automatically for the sudden increase of pressure in the lungs, which is necessary for the with given pitch and intensity to form. The air pressure distribution in the respiratory organ is nonuniform — the highest value occurs in the lung vesicles, the lowest one appears in the upper parts of the respiratory tracts.

1. Introduction

It follows a review of pulmonological literature that the test spirometry and the test of intensified expiration serve to determine whether there are changes of the type of ventilatory disorders and to define their origin — obstructive, restrictive or mixed.

The obstructive ventilatory insufficiency is caused by increased resistance to air flow in the respiratory tracts.

The restrictive ventilatory insufficiency depends on a decrease in the lung area or difficulties in the respiratory movements. When both kinds of changes occur, the mixed form is identified. This occurs e.g. in advanced bronchial-derivative emphysema.

It should be recognized that the occurence of these symptoms is decidedly affected by playing a given instrument, where the age of the persons examined

* The paper was supported by the Polish Academy of Sciences, Project MR.I.24.IX.10.

is more significant then the length of their professional life. The ventilatory disorders occurring not only in musicians, but also in other professional groups i.e. nonmusicians, can suggest other reasons for these changes to occur, e.g. current chronic bronchitis, nicotinism, genetic and allergic factors. Accordingly, it should be believed that playing an instrument is not the only factor determining the formation of ventilatory disorders. This fact was confirmed by the authors' observations related to the effective efficiency of the respiratory organ of instrument-players, taking into account their age and length of playing [8].

As a result of interest in this problem, at the Department of Phoniatrics, Academy of Music in Warsaw, between 1975 and 1980, aerodynamic investigations were carried out on students and professional instrument-players, involving 82 persons, showing a repeated phenomenon of the rapid air pressure compensation in the respiratory tracts during playing instruments.

2. Review of some references

The literature devoted to the problems considered here is limited to three aspects; the aerodynamic method and phenomena occurring in playing wind instruments and the technique of hyperbaric breathing.

The aerodynamic method was elaborated and applied in clinical examinations of the vocal and respiratory organs in singing by LEDEN, YANAGIHARA, ISSHIKI and KOIKE [3–5, 14, 10]. The present authors modified this method to examine singers and musicians playing wind instruments [4]. On the basis of complex investigations, the authors have shown that phonation is an aerodynamic phenomenon, since the formation of sound consists, among other things, in the mutual interaction of two physical forces and their balance, i.e. the subglottal air pressure and the glottal resistance [14]. The characteristic of the function of the vocal and respiratory fracts was presented on the basis of physical parameters, whose values and their mutual correlation were determined by aerodynamic measurements.

Playing wind instruments should also be included among the aerodynamic phenomena, in view of the essential analogies to the formation of human voice, for there is a mutual interaction between the air pressure before the instrument inlet (foremouthpiece pressure) and the resistance of the lips and tongue of the player.

Passing to another question, the hyperbaric breathing, it should be said that a large number of papers has been published on this subject. According to VAIL [12], the pressure in the lungs in the hyperbaric conditions is increased compared with that in the normal conditions and depends on the depth of the diver's plunge in the water, the intensity of the gas flow and the kind of the respiratory mixture applied. Further, this author describes the phenomenon

of the collapse of the subsegmental bronchi at the early stage of expiration after the critical pressure has been exceeded. This closure and collapse cause a blocking of the gas exchange from the vesicles, leading to oxygen shortage in blood and the retention of carbon dioxide reflected by dyspnoea. According to SOKOŁOWSKI [11], respiratory hypertension consists in the supply of a mixture of respiratory gases to the respiratory tracts, under increased pressure, higher than the ambient one, in order to increase the oxygen partial pressure. The lungs tolerate well a 7.5 hPa value of hypertension, 15 hPa is the boundary value and the respiratory hypertension of 22.5 hPa already requires considerable muscle effort. A further increase in the pressure, e.g. 25–30 hPa, with no active tension of the respiratory muscles, causes a total expansion of the lungs, whereas 60–130 hPa causes the lung vesicles to break, pulmonary or pleural pneumatosis.

3. Assumptions and purpose of the investigations

The activity of the respiratory organ in the conditions of ordinary ventilation and physical effort has already been known and elaborated by physiologists. Essentially, breathing in singing has also been explicated by a large number of authors, although further investigations in this field are still being carried out [3–5,10]. However, communications on the role of breathing in the conditions of playing the orchestra wind instruments in the contemporary world literature are very few and they do not bring new data on the physiology and pathology of breathing. Numerous papers have only appeared on the technique, aesthetics and psychology involved in playing these instruments [1, 2, 7, 13].

The problems of breathing in the course of playing the wind instruments are much more complex than those involved in singing [8]. This results from, among other things, the specificity of particular instruments, their physical properties, different ways of blowing, duration of sounds, dynamics and the degree of difficulty in playing [1, 2, 7, 9, 13]. Therefore, it is necessary to continue the research on the function of the breathing organ in instrumentalists playing brass wind instruments (particularly those playing in the upper range of the scale and with forte intensity), also because our observations made for a large number of years have shown that the breathing organ is strained by the excessive air pressure of more than 100 hPa (100 cm H_2O). In view of this, it was decided to analyse the dependence between the excessive pressure in the respiratory tracts and the efficiency of the respiratory organ.

The purpose of these studies was to draw attention to two problems occurring when playing instruments. The first was the compensation for the high air pressure at the moment when the emitted sound formed, and the other was the air distribution in the respiratory tracts. The interest in the second

problem was caused by musicians' observations, who found that when they played, particularly brass instruments, they had to increase the air pressure in the oral cavity (irrespective of the pressure occuring at a given moment in the respiratory system) in reaching sounds in the upper range of the scale, when playing both forte and piano.

4. Selection of cases and method of the studies

Althogether 82 persons, including 24 women, underwent the examination. They were students of the Department of Wind Instruments, Chopin Academy of Music in Warsaw, and professional musicians of symphonic orchestras. The age of the persons examined varied between 22 and 45 years. Before aerodynamic investigations began, laryngological examinations were carried out, showing no significant deviations from norm. The documentation included the sex, the instrument kind, the age, the height, the weight and the number of playing years. Initially, the vital capacity of the lungs (VC) was measured by the pneumotachometer with an electronic spirometer, and then aerodynamic investigations were carried out in a plethysmographic booth. The person examined was told to play single test sounds so long as the sound could be sustained in piano and forte after a previous deep inspiration.

The aerodynamic phenomena occurring in the respiratory organ of musicians and the objective evaluation of the breathing parameters and their mutual dependence in playing were presented in two papers: partially in [9] and integrally in [6]. These parameters include: the maximum playing time (MPT), the pressure before the inlet of the instrument, i.e. before the mouthipiece (SP) the mean flow rate (MFR) through the reed or lips, the resistance of lips, tongue and reeds (GR), the expiration power (EP) and the work carried out (S).

The method used during the investigations was described in two publications [9, 10]. In order to give an idea of the problems considered, those elements which are in direct connection with the subject of this paper, will be presented.

The plethysmographic booth permits the indirect measurement of the air pressure before the inlet of the instrument — SP, before and during playing the wind instrument. Dependencies resulting from the Boyle–Mariotte law were taken as the basis of the measurement method used. It was assumed that the person examined in a hermetic plethysmographic booth after taking a maximum deep breath, contains in his respiratory system air of the volume $V = VC + RV$, where VC is the vital capacity and RV is the residual capacity. In order to sustain the instrument playing, the air contained in the respiratory system is compressed by a force caused by tension of the diaphragm and the muscles of the abdominal press. This pressure (expressed in cm H_2O) depends on the resistance of lips, tongue and the reed, on the sound intensity and pitch. The in-

dividual properties of the person examined cause a differentiation of the pressures for different persons during playing with the same sound intensity and pitch.

The illustrative flow chart in Fig. 1 explains the principle of the pressure measurement before the inlet of the instrument.

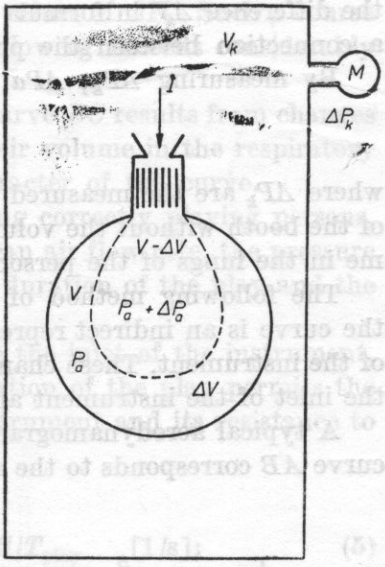

Fig. 1. A schematic diagram of the system for the measurement of the pressure before the inlet of the instrument. I – the inlet of the instrument, V – the air volume in the lungs, Pa – the air pressure in the lungs after aspiration, ΔV – the air volume difference in the lungs due to compression and, thus, the volume difference in the air contained in the plethysmographic booth, $V-\Delta V$ – the air volume in the lungs after initial compression, $Pa+\Delta Pa$ – the air pressure in the lungs after initial compression, V_k – the known booth volume, M – the difference manometer for the measurement of the pressure difference in the booth relative to the atmospheric pressure, ΔP_k – the pressure difference in the booth relative to the atmospheric pressure

Inside the plethysmographic book, there is the person examined, who contains in his respiratory system air of the volume V. When the air volume is compressed with closed lips by the pressure ΔPa, it decreases by the quantity ΔV, according to the formula resulting from the Boyle-Mariotte law saying that PV = const in isothermal conditions, $PaV = (Pa+\Delta Pa)(V-\Delta V)$; multiplication of the terms in the brackets gives $PaV = PaV+\Delta PaV-Pa\Delta V = \Delta Pa\Delta V$. The product $\Delta Pa\Delta V$ can be neglected as very small, while the equation thus simplified becomes

$$Pa\Delta V = \Delta PaV. \tag{1}$$

On the assumption that V is expressed in litres and that Pa = 1000 cm H_2O (~1 at), the quantity of the excessive pressure in the respiratory system, ΔPa (expressed in cm H_2O), of interest here, can be calculated from the formula

$$\Delta Pa = 1000\ \Delta V/V. \tag{2}$$

The air compression in the respiratory system is accompanied by a drop in the pressure inside the measurement booth. The pressure difference ΔP_k between the pressure inside the plethysmographic booth and the ambient pressure is controlled by the manometer M.

The dependence between ΔV and ΔP_k is given by the equation

$$\Delta P_k = 1000\ \Delta V / V_k, \tag{3}$$

where V_k is the air volume in the booth before the air compression in the lungs of the person examined, whereas ΔV is the volume difference before and after the compression of the air contained in the lungs. This difference is qeual to the difference ΔV in formula (2). From dependencies (2) and (3), there results a connection between the pressure changes ΔPa and the changes ΔP_k.

By measuring ΔP_k, ΔPa can thus be determined:

$$\Delta Pa = \Delta P_k V_k / V, \tag{4}$$

where ΔP_k are the measured pressure changes in the booth, V_k is the volume of the booth without the volume of the person examined and V is the air volume in the lungs of the person examined during the maximum aspiration.

The following method of the interpretation of the results was assumed: the curve is an indirect representation of the pressure changes before the inlet of the instrument. These changes can be related to the rate of air flow through the inlet of the instrument and to the resistance of the lips, tongue and reed.

A typical aerodynamogram is shown in Fig. 2. The ascending part of the curve AB corresponds to the air inspiration. The pressure in the booth changes

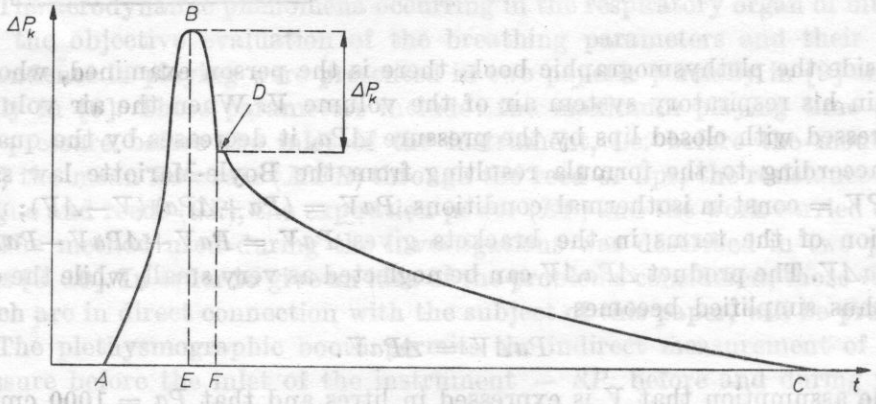

Fig. 2. A schematic representation of a typical aerodynamogram. The remaning notation is given in the text

then in the positive direction, in view of the increasing volume of the chest (the inspiration is conditioned by the formation of negative pressure in the respiratory system). The time of the preliminary compression is defined by the section EF of the foreplay. The pressure difference ΔP_k permits the pressure before the inlet of the instrument to be calculated from formula (4).

The section *DC* of the curve corresponds to the play time. The pressure changes in this part of the curve can result not only from the escape of the preliminarily compressed air from the lungs, but also from possible changes in its pressure — which should, in theory, be constant to ensure a constant sound intensity level. The duration of the play can be determined from the measurement of the section *FC*.

The section *DC* can go up, i.e. towards higher values of ΔP_k. Such a course can occur when the pressure at the moment of blowing exceeds considerably the pressure during the play.

The ascending or descending character of the curve *DC* results from changes in the fore-mouthpiece pressure and the current air volume in the respiratory system. These two quantities determine the character of the curve.

From aerodynamograms obtained by examining correctly playing persons, it is possible to determine with slight error the mean air flow rate, the pressure before the inlet of the instrument, the maximum duration of the play and the time of the foreplay.

Knowledge of the value of the pressure before the inlet of the instrument, the complete expiration volume *VC* and the duration of the play permits the mean rate of air flow through the inlet of the instrument and its resistance to be calculated.

The following dependencies are valied here:

$$\text{the mean air flow rate } MFR = VC/T_{\text{play}} \quad [1/\text{s}]; \tag{5}$$

$$\text{the resistance of lips, tongue and reeds } R = \Delta Pa/F \text{ cm } H_2O \quad [1/\text{s}]; \tag{6}$$

where *F* is the mean air flow rate [1/s]. Other quantities which can be determined on the basis of the measurement results are the work of the respiratory system and its power.

$$S = 0.01\ V\Delta Pa \quad [\text{kGm}], \tag{7}$$

where *S* is the work in kGm, *V* is the volume in litres, and ΔPa is the pressure, in cm H_2O, before the inlet of the instrument.

The work *S* can be determined as the work performed during one expiration or, alternatively, over any time.

Consideration of the quantity of work performed per unit time, e.g. in emitting sounds with given intensity and pitch, permits the expiration power necessary for the given play emission to be determined from the known dependence

$$\text{power} = \text{work/time}.$$

When considering numerical coefficients, the following dependece is valied here:

$$M = 0.098\ F\Delta Pa \quad [\text{W}], \tag{8}$$

where F is the mean air flow rate (MFR), in 1/s, and ΔPa is the pressure before the inlet of the instrument, in cm H_2O.

By using an additional measurement set-up, shown in Fig. 3, it was possible to measure and compare the results of the values of the fore-mouthpiece pressure

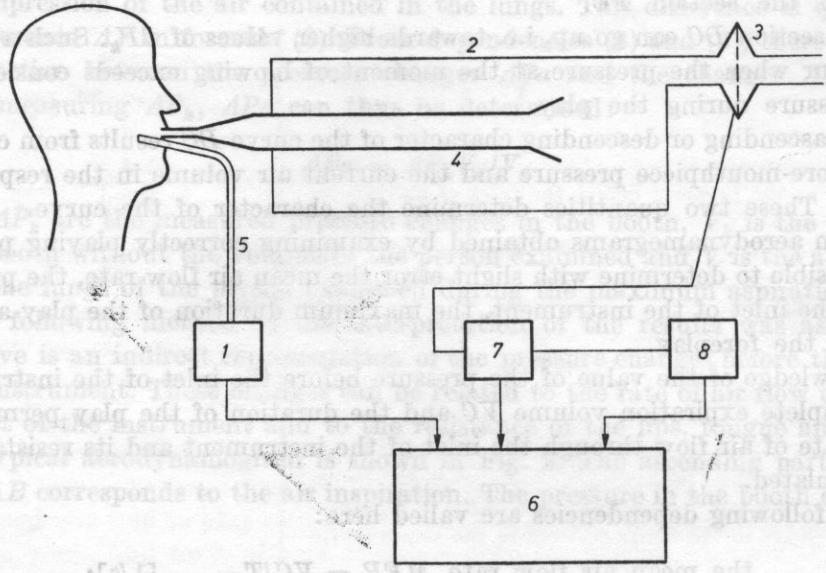

Fig. 3. A schematic diagram of the system for the simultaneous booth measurement of the air pressure both in the respiratory system and the oral cavity and the rate of air flow through the instrument. 1 — the electromanometer for the pressure measurement in the oral cavity, 2 — the instrument encasing, 3 — the pneumotachometer, 4 — the music instrument, 5 — the catheter conducting the pressure occurring in the oral cavity to the electromanometer, 6 — the multi-channel recorder, 7 — the flow signal amplifier, 8 — the electrical spirometer

and of the air flow through the instrument, obtained from direct measurements in the oral cavity (i.e. the air pressure distribution) and from indirect ones in the respiratory system, according to the measurement in the plethysmographic booth. The quantities measured in the course of the investigations were recorded according to the scheme shown in Fig. 4.

5. Results and discussion

Figs. 5 and 6 show randomly chosen aerodynamograms of two persons playing on the trumpet the sound with the pitch c^3 in piano and forte, with different conditions of calibration of recording for these persons.

It follows from the aerodynamograms shown in Fig. 5 that with different sound intensities there is a lower (in piano) or higher (in forte) degree of preli-

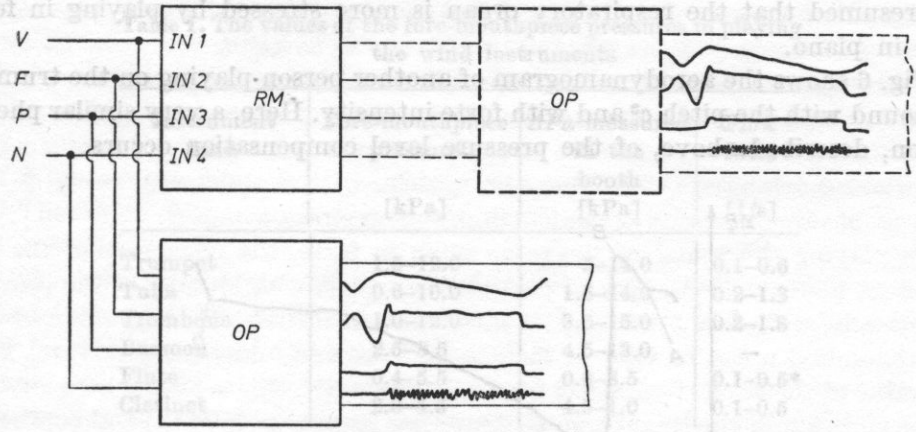

Fig. 4. A schematic diagram of the system for the recording of the measured quantities from the examinations. V – the volume, F – the flow, P – the pressure in the oral cavity, N – the sound intensity level, RM – the magnetic recorder, OP – the loop oscillograph, —— variant I, – – – – variant II

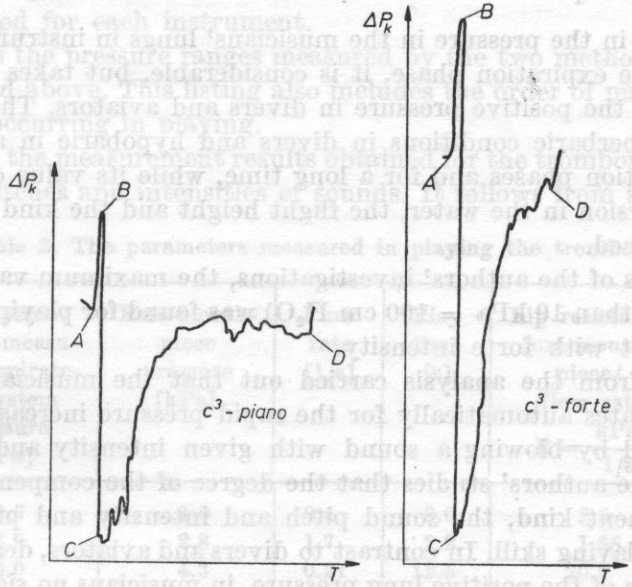

Fig. 5. Aerodynamograms of sounds played in piano and forte on the trumpet by the same person. The other notation is given in the text

minary air compression before the mouthipiece, repressented by the varying length of the section BC (with a rapid drop in the excessive pressure ΔP_k in the plethysmographic booth). Furthermore, in forte, the attainable duration of the sound (the projection of the curve CD onto the time axis) decreases. It should

be presumed that the respiratory organ is more stressed by playing in forte than in piano.

Fig. 6 shows the aerodynamogram of another person playing on the trumpet the sound with the pitch c^3 and with forte intensity. Here, a very similar phenomenon, described above, of the pressure level compensation occurs.

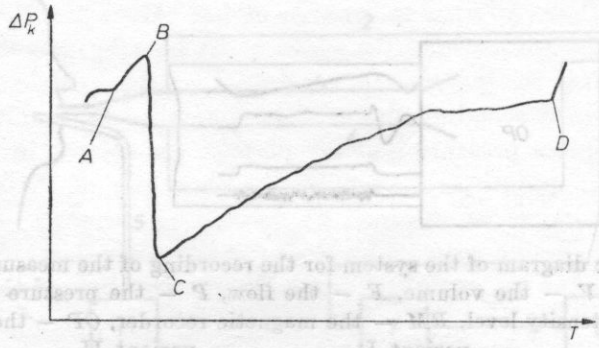

Fig. 6. The aerodynamogram of a sound played in forte on the trumpet (acc. to A. MURAS). The other notation is in the text

An increase in the pressure in the musicians' lungs in instrumental play occurs only in the expiration phase, it is considerable, but takes a shorter time compared with the positive pressure in divers and aviators. The positive lung pressure in hyperbaric conditions in divers and hypobaric in aviators occurs in both respiration phases and for a long time, while its value depends on the depth of immersion in the water, the flight height and the kind of the respiration mixture used.

On the basis of the authors' investigations, the maximum value of the lung pressure (more than 10 kPa = 100 cm H_2O) was found for playing a high sound on the trumpet with forte intensity.

It follows from the analysis carried out that the musician's respiratory organ compensates automatically for the rapid pressure increase in the lungs, which is caused by blowing a sound with given intensity and pitch. It also follows from the authors' studies that the degree of the compensation depends on the instrument kind, the sound pitch and intensity and probably on the degree of the playing skill. In contrast to divers and aviators, despite these considerable values of the positive lung pressure, in musicians no significant damages of the respiratory organ occur.

As far as the results of the pressure distribution in the respiratory system are concerned, Tables 1 and 2 give the values of the fore-mouthpiece pressure and of the air flow for play performed on 6 kinds of wind instruments.

The measurements of the fore-mouthpiece pressures were carried out by two methods: by the classical method, i.e. the direct measurement of the pressure in the oral cavity, and by the aerodynamic method, in the plethysmo-

Table 1. The values of the fore-mouthpiece pressures in playing the wind instruments

Instrument kind	Fore-mouthpiece pressure [kPa]	ΔPa measured in the booth [kPa]	Flow rates [l/s]
Trumpet	1.5–12.0	5–14.0	0.1–0.6
Tuba	0.6–10.0	1.5–14.0	0.2–1.3
Trombone	1.0–12.0	3.5–15.0	0.2–1.8
Bassoon	2.5–8.5	4.5–13.0	—
Flute	0.4–5.5	0.8–8.5	0.1–0.5*
Clarinet	2.0–4.5	4.5–1.0	0.1–0.5

* through the instrument

graphic booth. These measurements were carried out for the following instruments: trumpet, trombone, tuba, bassoon, flute and clarinet. For each instrument, the quantities of interest here were measured for low-and high-frequency sounds played in piano and in forte. Thus, 4 records of the parameters measured were obtained for each instrument.

Table 1 lists the pressure ranges measured by the two methods for the play kinds mentioned above. This listing also includes the order of magnitude of the air flow rates occurring in playing.

Table 2 lists the measurement results obtained for the trombone with playing at particular pitches and intensities of sounds. It follows from these data that

Table 2. The parameters measured in playing the trombone

Sound kind	Plethysmograph-measured respiratory system pressure [kPa]	Fore-mouthpiece pressure [kPa]	Flow rate [l/s]	Play time [s]	Lip resistance fore-mouthpiece/ /flow rate $R = \frac{\text{kPa}}{\text{l/s}}$	Expiration power [W]
F piano	1.7	1.0	0.4	8.0	2.5	0.5
F forte	3.9	2.8	1.7	2.2	1.65	5.2
c^2 piano	5.0	4.3	0.21	12.5	20.5	0.86
c^2 forte	15.0	11.5	0.98	3.5	11.7	13.1

the playing of the sound with the higher frequency and higher intensity requires that the fore-mouthpiece should be increased. This dependence is valid for playing all the instruments studied. Apart from the fore-mouthpiece pressures and flow rates, Table 2 gives the measured play time and the equivalent resistances of the lips, together with the instrument, and the expiration power were calculated. The latter two quantities seem to be of significance in attempts

to evaluate the degree of "difficulty" involved in playing the particular instruments and ensuring the appropriate playing dynamism.

Changes in the resistance of the lips reach the highest value in playing a high sound in piano. This is confirmed by the known fact when playing this kind of sound the musician must be able to apply the appropriate technique of working the oricular oris muscle, whereas the muscles of the abdominal press do not have to ensure large-power contraction and expiration power.

In playing the sound of the same pitch in forte, the resistance of the lips decreases because of the lack of possibility of further tightening of the oricular oris muscle, while the formation of this sound in forte is due to the muscles of the abdominal press, in view of their large mass and anatomic structure. Thus the value of the expiration power increases distinctly. There occurs here analogy to the emission of the singer's voice, found by ISSHIKI in 1974 [3] and confirmed by studies carried out at the Chopin Academy of Music in Warsaw in 1981 [10].

The present stage of the investigations involved the elaboration of a method for the measurement of the pressure before the lips and the reed in a least troublesome way. This method could be the aerodynamic method. The comparative measurements performed indicate some differences among the magnitudes of these pressures, depending on the method used. The highest values were obtained by using the aerodynamic method. This results from the occurrence of the following phenomena in playing the wind instruments:

1) the application of large forces by the abdominal press on the lung tissue leads to a "collapse" of part of the small respiratory tracts. The air contained in the lung vesicles or their part is bound and compressed to a considerably high degree than the air in those sections of the respiratory tracts which do not lose connection with the upper sections of the respiratory tracts.

2) as the basis for calculating the pressures in the respiratory system, it is assumed that persons playing wind instruments have the residual volume (RV) within the norms accepted for the Polish population. An increase of this quantity, with respect to the value taken from the tables, can cause an increase in the value of the calculated pressures in the respiratory system. This error can be eliminated by measuring the real residual volume before carrying out aerodynamic measurements and introducing a coefficient eliminating the error resulting from the "collapse" of small respiratory tracts as the air is compressed in the lungs.

6. Conclusions

1. The respiratory organ of the musician compensates automatically for the rapid pressure increase in the respiratory tracts, necessary for a sound with required pitch and intensity to be blown.

2. For the musicians examined, the fore-mouthpiece pressures vary between 0.4 and 12 kPa. The group of the brass instruments requires that the players should form pressures over 10 kPa (100 cm H_2O), whereas the other instruments need lower pressures.

3. The air flow rates for the mouthipiece instruments vary between 0.1 and 1.8 l/s and are lower for the others, i.e. between 0.1 and 0.5 l/s.

4. The brass instruments strain the respiratory system more than the wood ones do.

5. The dynamics of pressure changes for the brass instruments, in passing from piano to forte, or from a lower to a higher sound, is 1 : 3, whereas it is 1 : 1,5 for the groups of the reed instruments.

The values of the parameters which will be the object of the future stages of the studies, to be carried out in the successive years, were preliminarily estimated.

6. The air flow rates are determined by the resistance of the lips, or reeds, and the pressure. Sounds played in piano require lower rates than those performed in forte. There is a direct relationship between the playing time and the flow rate, resulting from the limited air volume at the disposal of the person playing the wind instruments.

7. The resistance of the lips and reeds increases as the pitch of sounds increases, in turn it decreases as the intensity of a sound with the same pitch increases.

8. The expiration power increases with increasing both the intensity and pitch of the sound. The expiration power increases at the expense of an increase in the fore-mouthpiece pressure.

References

[1] J. Banaszek, *Fundamental breathing problems in playing the oboe* (in Polish), Special Reports, PWSM, Gdańsk, 22, 169–170, 1980.

[2] A. Bourek, *Breathing in playing the wind instrument* (in Polish), Special Reports, PWSM, Gdańsk, 22, 151, 1980.

[3] N. Isshiki, *Regulatory mechanismus of voice intensity variation*, J. Speech Res., 7, 17–29 (1964).

[4] H. von Leden, *Objective measures of laryngeal function and phonation*, Annals of the New York Academy of Sciences, **155**, 56–67 (1968).

[5] H. von Leden, *Objective methods of vocal analysis in singers and actors*, Reprinted from Excerpta Medica International Congress Series, 206, 1969.

[6] A. Muras, *Analysis of breathing in musicians playing the wind instruments — by the aerodynamic method* (in Polish), Ph. D. Thesis, Academy of Medicine, Warsaw, 1981.

[7] W. Orawiec, *Essence of correct breathing in playing the bassoon* (in Polish), Special Reports, PWSM, Gdańsk, 22, 173, 1980.

[8] Z. Pawłowski, K. Orłowska, *Emission of the respiratory system in artists playing the wind instruments* (in Polish), Otolaryngologia Polska, XXIV, 4, 434, 1970.

[9] Z. PAWŁOWSKI, *Breathing in singing and playing the wind instruments* (in Polish), Special Reports, PWSM, Gdańsk, 22, 111–148, 1980.

[10] Z. PAWŁOWSKI, M. ŻOŁTOWSKI, *Fundamental aspects of aeroacoustics in singing*, Archives of Acoustics 7, 3–4 (1982).

[11] E. SOKOŁOWSKI, *Biochemical and respiratory-circulatory response of the human organism to the respiratory hyperpressure in application of oxygen: nitrogen-oxygen and helium-oxygen mixtures* (in Polish), Ass. Prof. Thesis (unpubl.), WIML, Warsaw, 1980.

[12] E. G. VAIL, *Hyperbaric respiratory mechanics*, Aerospace Medicine, **42**, 5, 536–558 (1976).

[13] A. WIERZBIŃSKI, *Role of correct breathing in forming the sound in playing the flute* (in Polish), Special Reports, PWSM, Gdańsk, 22, 161, 1980.

[14] N. YANAGIHARA, Y. KOIKE, *The regulation of sustaining phonation*, Folia Phoniatr., **19**, 1–18, 1967.

ARCHIVES OF ACOUSTICS
10, 3, 229–240 (1985)

THE CHARACTERISTICS OF THE PHENOMENON OF INITIATION (SOUND INTONATION) IN PLAYING THE WIND INSTRUMENTS *

ZYGMUNT PAWŁOWSKI, MAREK ŻÓŁTOWSKI

Department of Phoniatrics, Frederic Chopin Academy of Music
(00–368, Warsaw, ul. Okólnik 2)

It was found that the phenomenon of initiation in playing the wind instruments was characterized in particular by the value of the rise time of a sound (*RT*) and the value of the air flow during its duration. The values of the air volume (air output) and prephonation time (*TPP*) do not characterize significantly the phenomenon described.

Analysis was carried out on the physical properties related to initiation in playing the wind instruments. The instantaneous values of the air volume and flow rate were measured for the particular phases of playing.

30 musicians playing 7 groups of wind instruments were examined. The results of the investigations indicate the usefulness of the method applied in medical and didactic evaluation.

1. Introduction

The sound intonation is an essential phase of phonation. It follows from the authors' own observations and the literature communiques that the corrrect emission of the singers' voice depends on the correct phonation. In the case of instrumentalists, initiation is a counterpart of the sound intonation. There is no doubt that the quality of playing depends on the correct sound initiation.

The phenomenon is complex and affects in the further course of the play the value of the aerodynamic parameters, including the maximum play duration (*MPT*), the pressure before the instrument inlet (*SP*), the mean rate of flow through the lips and mouthpieces (*MFR*), the resistance of the lips and mouthpieces (*GR*), the expiration power (*EP*) and the work executed by the respiratory organ during the play (*S*). The problems have partly been investigated [6, 7] and are a further stage of studies in this field.

2. Intonation in singing

Both the world and Polish literature on the problem in question is scarce. The correct intonation determines the correct emission. On the other hand, it is known that hoarseness is the most important and sometimes the only symptom

* The paper was supported by the Polish Academy of Sciences, Project MR.I. 24. IX. 10.

of the inefficiency of the larynx, in the form of functional perturbations or anatomical changes [1, 2, 4]. Because of this, it is justified to continue the clinical investigations of voice and music sound formation.

According to KOIKE, HIRANO, LEDEN [3], the intonation of human voice is characterized by 4 parameters: 1. the transient rise time (*RT*), 2. the air flow rate before the transient emerges (*RF*), 3. the air volume (air output) used up in the initial 200 ms of phonation (volume), 4. the time delay from the beginning of the expiration to the transient time (the prephonation time (*TPP*)).

On the basis of the parameter values obtained, the abovementioned authors distinguished 3 characteristic kinds of voice intonation.

The soft vocal attack (soft intonation) is characterized by a gradual increase in the transient amplitude, a smooth increase in the air flow rate (*FR*) and a low air volume (Volume).

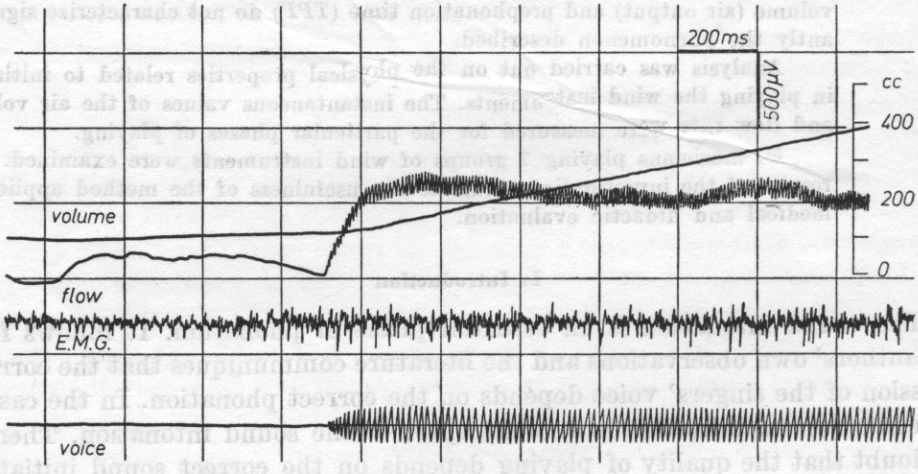

Fig. 1. Curves of changes in the volume (air output), air flow rate and sound level, according to KOIKE, HIRANO and LEDEN

Contrary to the soft intonation, the hard vocal attack (hard intonation used e.g. in staccato), is characterized by a rapid increase in the transient amplitude, a sharp increase in the air flow rate (*FR*) and a large increase in the air (Volume). A common feature of those two kinds of intonation is the fact that there is no air flow before the transient emerges.

The puffing vocal attack (the puffing intonation occuring most frequently in the pathologies of the larynx), shows a large value of the air flow rate (*FR*) before the transient begins, a distinct time delay from the beginning of the expiration to the time that the transient emerges (the prephonation time — *TPP*) and a very large volume of air. Changes in the transient amplitude envelope did not differ significantly from the soft and hard intonations.

It follows from these measurements that the values of the air volume and the prephonation time (*TPP*) are insignificant in evaluating the traditional voice intonation. In turn the values of the transient rise time (*RT*) and the air flow rate (*FR*) characterize significantly the phenomenon of voice intonation.

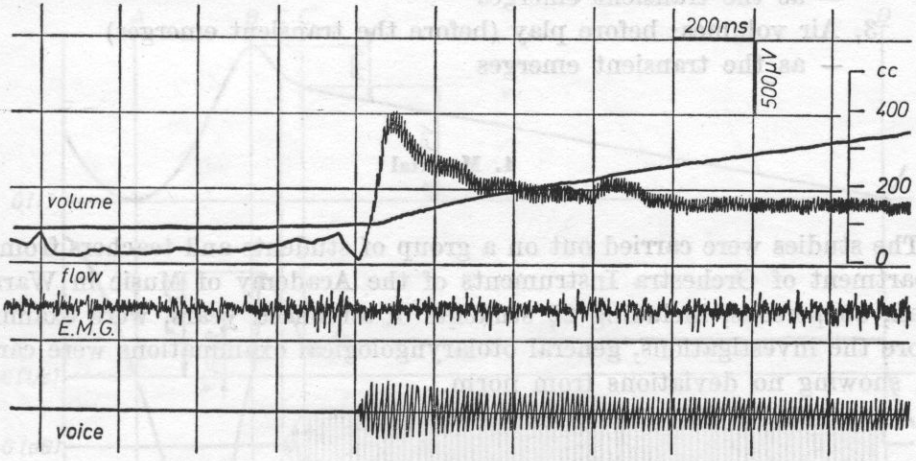

Fig. 2. Curves of changes in the volume, air flow rate and sound level, according to KOIKE, HIRANO and LEDEN

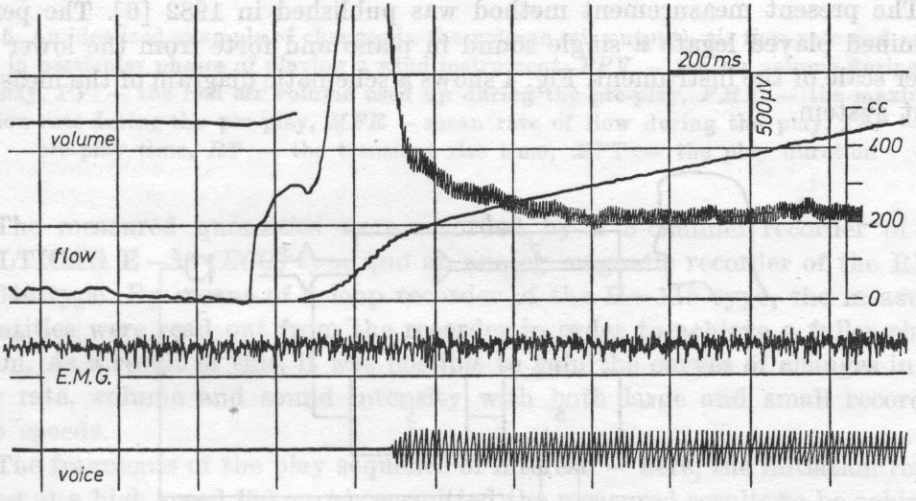

Fig. 3. Curves of changes in the volume, air flow rate and sound level, according to KOIKE, HIRANO and LEDEN

3. Assumptions and purpose of the investigations

In view of the limited literature on the physiological problems of playing the wind instruments [5–7], there is the need for these states to be complemented for the purposes of didactic certification and practice.

The aim of the investigations was to carry out an analysis of 3 parameters.

1. Pre-play time
   the transient duration
2. Flow: the maximum one before the transient emerges
   — as the transient emerges
3. Air volumes: before play (before the transient emerges)
   — as the transient emerges

4. Material

The studies were carried out on a group of students and teachers from the Department of Orchestra Instruments of the Academy of Music in Warsaw. In all, 30 persons, including 22 students of advanced years, were examined. Before the investigations, general otolaryngological examinations were carried out, showing no deviations from norm.

5. Method

The present measurement method was published in 1982 [6]. The person examined played legato a single sound in piano and forte from the lower and upper scale of the instrument. Fig. 4 shows a schematic diagram of the measurement system.

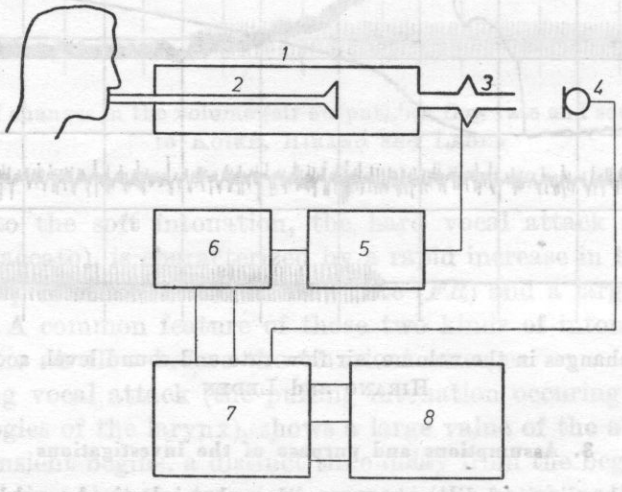

Fig. 4. A schematic diagram of the measurement system: 1. instrument encasing, 2. instrument, 3. pneumotachometer, 4. microphone, 5. flow signal amplifier, 6. electronic spirometer, 7. magnetic recorder, 8. multi-channel recorder

A full analysis of the phenomena occuring in particular phases of play requires a graphic representation of changes in the volume, flow rate and sound level as a function of time (Fig. 5).

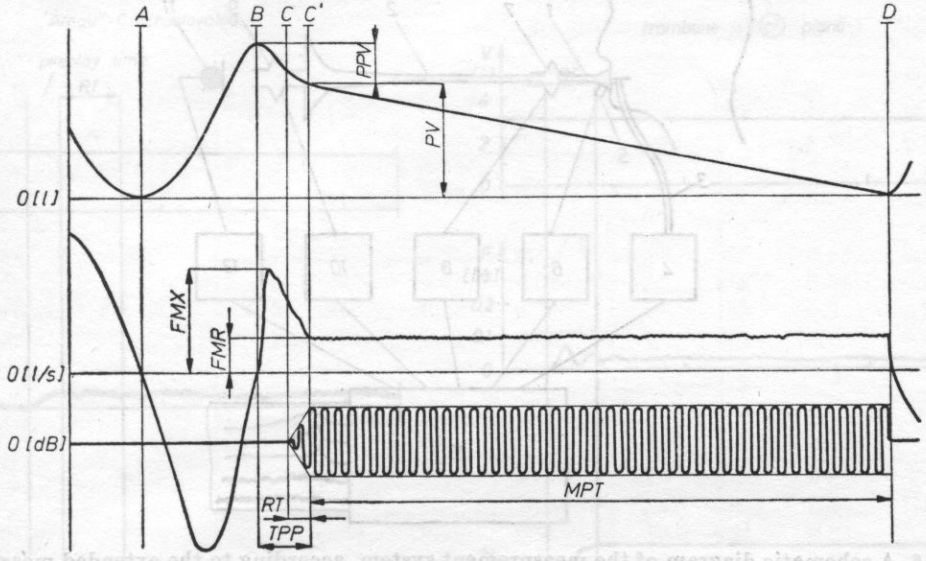

Fig. 5. An idealized example of changes in the volume (air output), air flow rate and sound level in particular phases of playing a wind instrument: *PPV* – the air volume during the pre-play, *PV* – the real air volume used up during the pre-play, *FMX* – the maximum air flow rate during the pre-play, *MFR* – mean rate of flow during the play, *TPP* – the pre-play time, *RT* – the transient rise time, *MPT* – the play duration

The measured quantities were recorded by a 3-channel recorder of the MULTICAR E–30 (*ECG*) type and an analog magnetic recorder of the RM––1040 type. By means of a loop recorder of the H–115 type, the measured quantities were read out from the recorder in order to achieve a fuller elaboration. As a result of this, it was possible to gain the curves of changes in the flow rate, volume and sound intensity with both large and small recording tape speeds.

The fragments of the play sequence of interest – here, the initiation reproduced at a high speed (50 cm/s), permitted the measured results to be achieved in a convenient form for further elaboration and interpretation. In considering the phenomena occuring in time intervals below 0.1 s (*TPP* and *RT*), some mutual displacements were found among the quantities recorded in time, depending on the situation of the microphone with respect to the instrument. In order to explain these displacements, extended measurements were carried out. They consisted in the recording of the flow rate at the inlet and outlet of an instrument and of the vibration of the mouthpiece part of the instrument

and the sound level close to inlet of the instrument. The pressure inside the oral cavity was also recorded by the direct measurement method (Fig. 6).

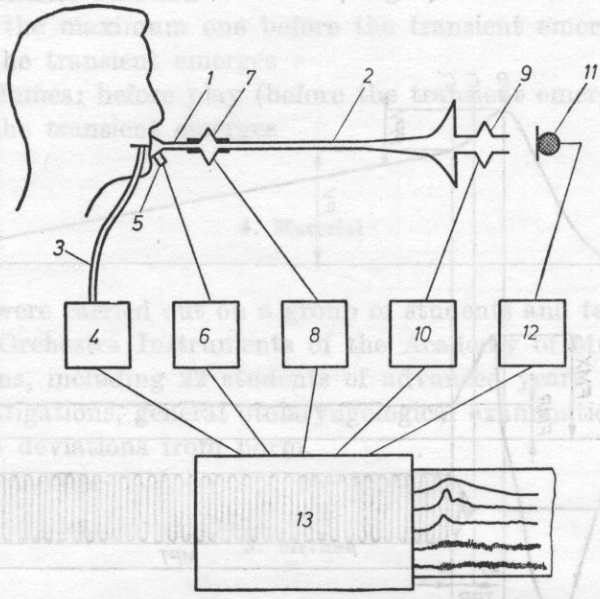

Fig. 6. A schematic diagram of the measurement system, according to the extended measurement method: 1. instrument mouthpiece, 2. instrument, 3. pressure gauge pipe, 4. pressure gauge, 5. vibration sensor, 6. vibration sensor amplifier, 7 and 9. pneumotachometers, 8 and 10. flow signal amplifiers, 11. microphone, 12. microphone amplifier, 13. multi-channel recorder

6. Results

The results were obtained from playing 7 wind instruments: trumpet, tuba, trombone, French horn, flute, clarinet and oboe. Fig. 7 shows the record of one the sounds played on the clarinet. Fig. 8. shows the corresponding record for the trombone. The successive curves represent changes in the following quantities: the volume V, the flow rate F and the sound level N in the initial stage of its formation.

In view of the large speed of the recording tape, the initiation phase is absent from the curves. The beginning of the changes in the particular quantities visualizes the first stage of the air flow and the accompanying sound formation. The diagram section shown represents about 0.5 s play. Over this interval, the air volume changes only slightly, about 0.025 l — the diagram of changes in the volume V shows no noticeable differences. The flow beginning is distinctly indicated by the course of changes in curve F and the accompanying sound effect N. The changes from the beginning of these curves to the moment when

the curves become fixed at a given mean level are transient transitional states. The duration of these states contains in itself the pro-play time and the duration of the sound transient.

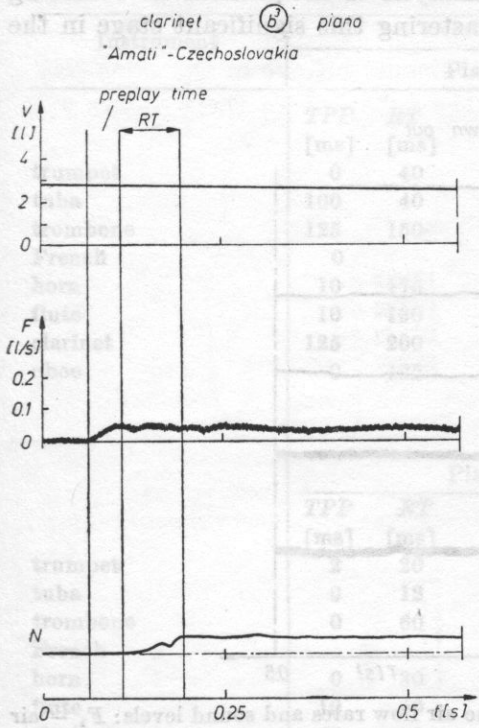

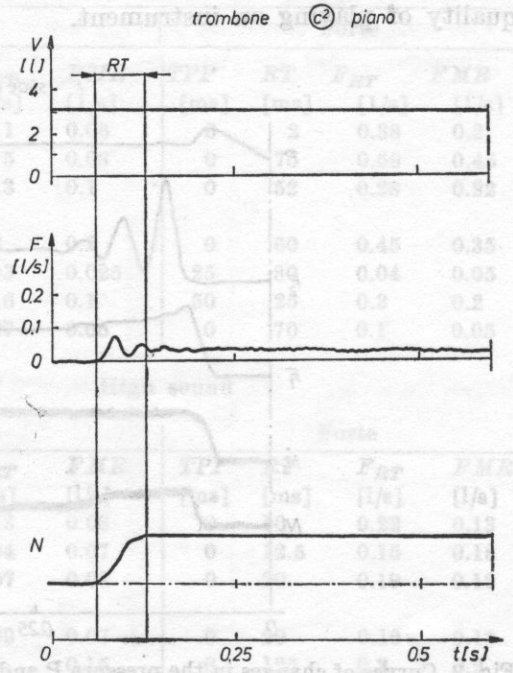

Fig. 7. Curves of changes in the volume, air flow rate and sound level during the initial stage of playing the clarinet

Fig. 8. Curves of changes in the volume, air flow rate and sound level during the initial stage of playing the trombone

Fig. 7 shows records obtained in playing the clarinet. Here, there is the distinct pre-play time (from when the flow occurs to when the sound begins to rise). Fig. 8 shows an analogous record for playing the trombone. In order to explain the doubts as to minimum time displacements in the curves of the the flow (F) and the sound level (N), additional studies were carried out following the extended methodology according to Fig. 6.

Fig. 9 shows records taking into account the flows and sound levels at the inlet and outlet of the instrument. Fig. 10 illustrates a distinctly bad sound initiation.

7. Discussion of results

The investigations and measurements carried out permit the characteristic quantities preceding the achievement of a sound at a given pitch and level to be determined for particular instruments.

The pre-play time and the transient duration, the flow occuring over these intervals, and the volume (air output) used up in these intervals, achieved by persons with sufficient music training, they can all provide the basis for characterizing the notion of initiation (Table 1). Analysis of the phenomena occurring in the initiation time can be helpful in mastering this significant stage in the quality of playing an instrument.

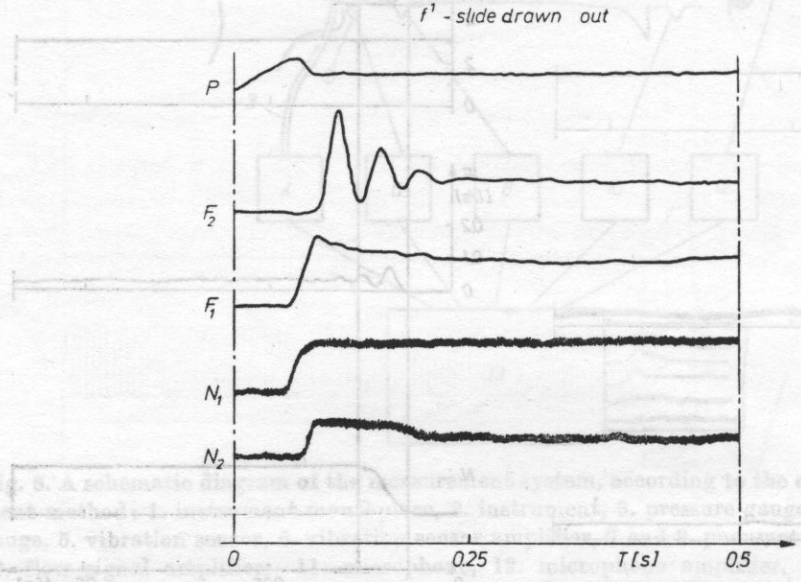

Fig. 9. Curves of changes in the pressure P and the air flow rates and sound levels: F_1 — air flow rate at the inlet to the instrument, F_2 — at the outlet, N_1 — the mouthpiece vibration amplitude, N_2 — sound amplitude at the outlet from the instrument

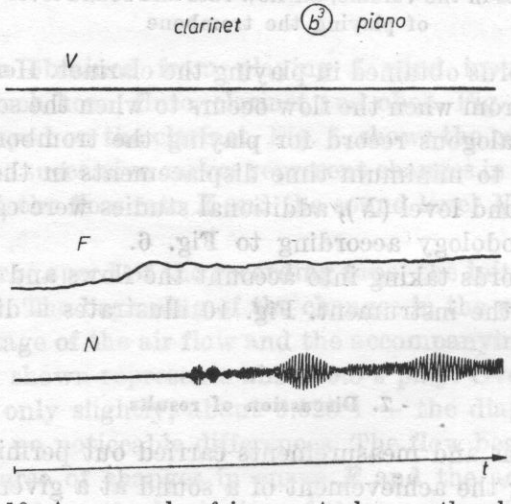

Fig. 10. An example of incorrect play on the clarinet

General observations on the pre-play times permit the following criteria of evaluation to be established.

Table 1

Instrument	Low sound							
	Piano				Forte			
	TPP [ms]	*RT* [ms]	F_{RT} [1/s]	*FMR* [1/s]	*TPP* [ms]	*RT* [ms]	F_{RT} [1/s]	*FMR* [1/s]
trumpet	0	40	0.11	0.06	0	2	0.38	0.2
tuba	100	40	0.15	0.08	0	75	0.68	0.45
trombone	125	150	0.13	0.1	0	52	0.28	0.22
French horn	0	175	0.3	0.2	0	60	0.45	0.35
flute	10	130	0.03	0.025	25	80	0.04	0.05
clarinet	125	200	0.16	0.1	50	25	0.3	0.2
oboe	0	125	0.07	0.05	0	70	0.1	0.05

	High sound							
	Piano				Forte			
	TPP [ms]	*RT* [ms]	F_{RT} [1/s]	*FMR* [1/s]	*TPP* [ms]	*RT* [ms]	F_{RT} [1/s]	*FMR* [1/s]
trumpet	2	20	0.13	0.08	0	10	0.22	0.13
tuba	0	12	0.04	0.07	0	12.5	0.15	0.18
trombone	0	60	0.07	0.03	0	20	0.19	0.12
French horn	0	30	0.09	0.07	0	20	0.16	0.13
flute	10	40	0.3	0.15	0	125	0.3	0.2
clarinet	45	85	0.05	0.04	100	75	0.12	0.08
oboe	15	60	0.08	0.04	0	60	0.05	0.03

The correctly executed initiations determine a short pre-play time, as a rule below 2 ms. The differences in the pre-play time occuring for the instruments investigated at low and high frequencies, both in piano and forte, are insignificant. The volume used up in the pre-play time is very small, as it does not exceed 20 ml. The flow accompanying these slight changes in volume and its character (with the instantaneous values exceeding largely the mean flow rate during the play) indicates a lack of coordination between the muscles of the respiratory organ and those of the articulatory one (the muscles of the lips and tongue).

In considering the subsequent stage of the play and the phenomena occurring in it, one can find that:

— The rise time *RT*, conceived as a time interval between a moment when a sound emerges and a time when it acquires given intensity, depends on afew factors.

The value of the *RT* for wood instruments when playing piano is greater than that for playing forte. Irrespective of this, the value of the *RT* changes

depending on the pitch of sounds played. However, it is the sound intensity that determines the rise time *RT*. This time is between 50 and 500 ms. Changes in the sound dynamics correspond to those in the time *RT* at a ratio of 1 : 10, whereas during the play the pitch of the sounds played changes the *RT* over the limits of 1: 2.5.

The values of the time *RT* for brass instruments behave in the same way as those for wood instruments, except for the tuba, where these values are

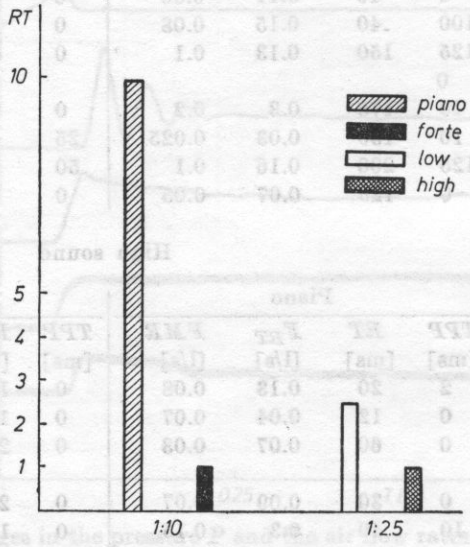

Fig. 11. An example of changes in the value ratios of the rise time (*RT*) depending on the sound intensity and pitch for wood and brass instruments

lower for playing in piano and greater in forte, both at low and high frequencies.

The volume air output used up over the rise time *RT* is small and insignificant for evaluating the inspiration, irrespective of the sound pitch and intensity for the instruments considered.

The air flows over the sound rise time are significant and concerned with:

1. brass (mouthpiece) instruments — in reference to the sound intensity and pitch. The value of the air flow rate is lower for playing in piano and greater in forte, occurring in the whole group of the instruments studied. However, the general values of the air flow rate is greater over the low sound range and lower over the high sound range.

2. in the case of wood (reed) instruments the air flow rate behaves in a way different from that in brass instruments — i.e. depending on intensity, the value of the flow increases slightly in forte, whereas, depending on the sound pitch, this value can even decrease, except for playing the flute, where the air flow rate increases.

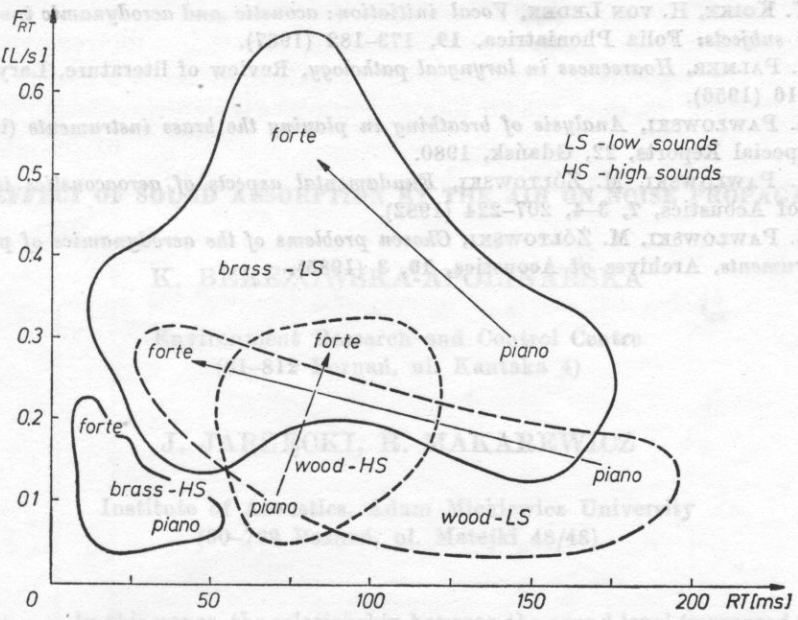

Fig. 12. Variability ranges of the air flow rates and rise times for the two groups of instruments

8. Conclusions

1. A significant feature is the value of the air flow rate, particularly over the sound rise time *RT*. Sounds played in forte are characterized by greater flow rate than that of sounds played in piano.

2. The air volume (air output) used up in the pre-play time and the rise time is small and does not characterize significantly the phenomenon of initiation.

3. The sound rise time *RT* decreases when playing in forte. As the pitch of the sounds played varies the value of the *RT* becomes slightly lower with their increasing pitch.

References

[1] R. M. Caplan, *Use of mucocutaneous sings in diagnosis of hoarseness*, Univ. Mich. Med. Bull., 26, 405–413 (1960).

[2] N. Isshiki, H. von Leden, *Hoarseness: aerodynamic studies*, Archives of Otolaryngology, **80**, 206–213 (1964).

[3] Y. KOIKE, H. VON LEDEN, *Vocal initiation: acoustic and aerodynamic investigations of normal subjects*: Folia Phoniatrica, **19**, 173–182 (1967).

[4] J. PALMER, *Hoarseness in laryngeal pathology*, Review of literature, Laryngoscope, 66, 500–516 (1956).

[5] Z. PAWŁOWSKI, *Analysis of breathing in playing the brass instruments* (in Polish). PWSM, Special Reports, 22, Gdańsk, 1980.

[6] Z. PAWŁOWSKI, M. ŻÓŁTOWSKI, *Fundamental aspects of aeroacoustics in singing*, Archives of Acoustics, 7, 3–4, 207–224 (1982).

[7] Z. PAWŁOWSKI, M. ŻÓŁTOWSKI, *Chosen problems of the aerodynamics of playing the wind instruments*, Archives of Acoustics, **10**, 3 (1985).

ARCHIVES OF ACOUSTICS
10, 3, 241–252 (1985)

THE EFFECT OF SOUND ABSORPTION BY THE AIR ON NOISE PROPAGATION

K. BEREZOWSKA-APOLINARSKA

Environment Research and Control Centre
(61–812 Poznań, ul. Kantaka 4)

J. JARZĘCKI, R. MAKAREWICZ

Institute of Acoustics, Adam Mickiewicz University
(60–769 Poznań, ul. Matejki 48/48)

In this paper, the relationship between the sound level (measured in dB(*A*)) and the distance was derived on the assumption that air absorption is the only essential factor affecting noise propagation. It was shown that at a great distance from the source "rapid sound level drop", exceeding 6 dB(*A*), occurs when the distance is doubled.

1. Introduction

In the environment of man noise is in most cases generated by the sources which can be treated as directional point sources (e.g. single means of transportation, transformer stations, construction machinery [8]). From the acoustic point of view, it is possible to shape the environment only when the explicit relations among the quantities describing the effect of noise on man are known, i.e. those among the indices of noise evaluation and quantities related to the process of noise generation and propagation, including the length of the propagation path.

In general, the annoyance of noise with time invariable spectrum is evaluated by means of sound level expressed in dB(*A*). The continuons weight function $W(f)$ corresponding to the correction curve *A* is given in the Appendix.

When the source is directionless, full information on the noise generation process is contained in the power spectral density. In Section 2.1, the function $P(f)$ that can be applied to a broad class of real sources is proposed. Table 2 gives the parameters of this function for different car types.

The sound propagation in the air is the effect of superposition of a few elementary phenomena: (classical and molecular) absorption, refraction and

interaction of waves with the ground surface. When the source is close to the ground surface and the observation point is at least a few metres over the surface, which corresponds e.g. to the case "vehicle-apartment a few storeys over the ground" (Fig. 1), only the air absorption plays a significant role. Under this assumption, the noise propagation process can be described by only two quantities: a parameter related to the absorption (Section 2.2) and the distance bet-

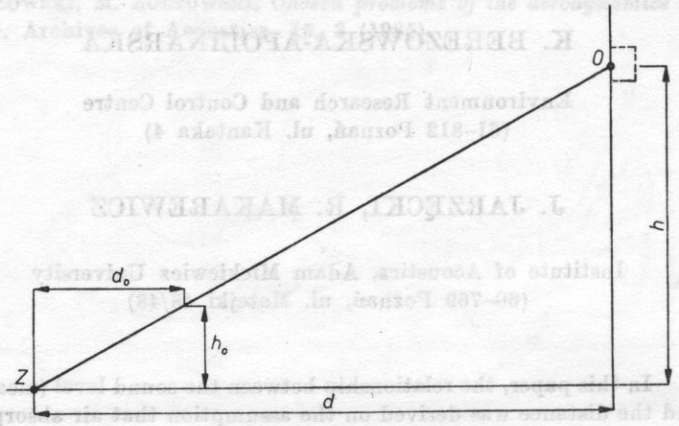

Fig. 1. Mutual position of source (Z) and the observation point (0) high over the ground surface

ween the observation point and the source. The latter quantity is of particular significance, e.g. because increasing the distance between a transportation route and buildings is one of the most effective methods of protecting the acoustic climate in the environment of man.

In Section 3, an explicit relationship between the sound level [$dB(A)$] and the distance is derived. Analysis of this dependence (Section 4) shows the usefulness of introducing the "critical distance" R which when exceeded leads to a rapid level drop (Fig. 2). Table 4 gives the values of R for a chosen car type, with varying atmospheric conditions (temperature, humidity).

2. Sound propagation in the air

When the sound source (Z) is much closer to the ground surface than the observation point (0) (Fig. 1), the effects of interaction between the acoustic wave and the ground surface — the "ground effects" [4] — can be neglected. ATTENBOROUGH showed [2] that when the height (h) of the observation point is a few meters over the ground surface, the failure to consider these effects leads to error of about 1 $dB(A)$. When the above assumption is satisfied, only the direct wave reaches the observation point.

This wave undergoes refraction. It is assumed that the atmospheric conditions, i.e. the wind speed and temperature changes with height, permit this phenomenon to be neglected. PIERCY and EMBLETON [7] emphasized that refraction plays a significant role only when the source and the observation point are at the ground surface.

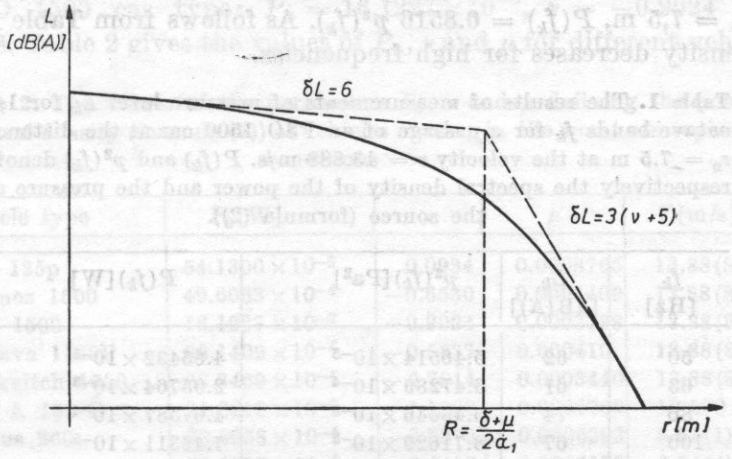

Fig. 2. Sound level drop δL for a double distance for $r \ll R$ and $r \gg R$, where R is the "critical distance" (formula (12))

It will be assumed further on that absorption by the air is the main factor affecting the sound propagation. When $p^2(f)$ is the spectral density of the acoustic pressure, then, for a source at the ground surface,

$$p^2(f) = \frac{P(f)\exp\{-2\alpha(f)\}\varrho c}{2\pi r}, \tag{1}$$

where $r = \sqrt{h^2+d^2}$ is the distance from the observation point (Fig. 1), $\varrho_0 c = 415$ [Pas/m] is the acoustic resistance of the air, $\alpha(f)$ is the absorption coefficient and $P(f)$ is the power spectral density of the source.

2.1. Power spectral density of the source

Let's assume that at the distance $r = \sqrt{h_0^2+d_0^2}$ (Fig. 1), the level of the acoustic pressure was measured in the successive frequency bands, $L_1, \ldots, L_k, \ldots, L_n$, with the centre frequencies $f_1, \ldots, f_k, \ldots, f_n$. From the definition of the pressure level, $L_k = 10 \log p_k^2/p_0^2$, $p_0 = 2 \times 10^{-5}$ Pa, it is possible to determine the values of $p_1^2, \ldots, p_k^2, \ldots, p_n^2$. When Δf_k is the width of the kth frequency band, then $p_k^2 = p^2(f_k)\,\Delta f_k$, where $p^2(f_k)$ is the pressure spectral density for the centre frequency of the band, f_k. According to formula (1), this quantity

can be related to the power spectral density of the source in the following way

$$P(f_k) = \frac{2\pi r_0^2 p^2(f_k)}{\varrho_0 c}. \tag{2}$$

(This formula has been derived under the assumption that $2\alpha(f)r_0 \ll 1$, i.e. the absorption at the distance r_0 does not play a significant role). E.g. for the distance $r_0 = 7{,}5$ m, $P(f_k) = 0.8516\ p^2(f_k)$. As follows from Table 1 the power spectral density decreases for high frequencies.

Table 1. The results of measurements of pressure level L_k for 1/3 octave bands f_k for a passage of an FSO 1500 car at the distance $r_0 = 7.5$ m at the velocity $v = 13.888$ m/s. $P(f_k)$ and $p^2(f_k)$ denote respectively the spectral density of the power and the pressure of the source (formula (2))

f_k [Hz]	L_k [dB(A)]	$p^2(f_k)$ [Pa^2]	$P(f_k)$ [W]
50	62	5.46514×10^{-5}	4.65432×10^{-5}
63	61	3.47289×10^{-4}	2.95764×10^{-3}
80	74	5.49046×10^{-5}	4.67587×10^{-4}
100	67	8.71629×10^{-5}	7.42311×10^{-5}
125	90	1.37931×10^{-2}	1.17467×10^{-2}
160	88	6.82116×10^{-3}	5.80914×10^{-3}
200	69	1.90720×10^{-5}	5.88242×10^{-5}
250	72	1.09302×10^{-4}	9.30864×10^{-5}
315	73	1.09329×10^{-4}	9.31089×10^{-5}
400	75	1.37490×10^{-4}	1.17091×10^{-4}
500	71	4.34112×10^{-5}	3.69705×10^{-5}
630	74	6.92934×10^{-5}	5.90128×10^{-5}
800	71	2.75174×10^{-5}	2.34349×10^{-5}
1000	70	1.73913×10^{-5}	1.48110×10^{-5}
1250	70	1.37931×10^{-5}	1.17467×10^{-5}
1600	68	6.82116×10^{-6}	5.80914×10^{-6}
2000	68	5.48658×10^{-6}	4.67257×10^{-6}
2500	68	4.35142×10^{-6}	3.70583×10^{-6}
3150	68	3.45730×10^{-6}	2.94436×10^{-6}
4000	67	2.17907×10^{-6}	1.85557×10^{-6}
5000	68	2.17571×10^{-6}	1.85299×10^{-6}
6300	66	1.09822×10^{-6}	9.35290×10^{-7}
8000	65	6.91208×10^{-7}	5.88658×10^{-7}
10000	60	1.73913×10^{-7}	1.48110×10^{-7}

Let us assume that

$$P(f) = P_0 f^r \exp(-\mu f). \tag{3}$$

The values of P_0, r and ν can be determined by regression analysis. Having found the logarithm of expression (3), we obtain

$$\ln P = \ln P_0 + \nu \ln f - \mu f,$$

which in the notation $y = \ln P$, $a = \ln P_0$ and $\ln f = x_1$, gives the linear dependence

$$y = a + \nu x_1 - \mu x_2. \tag{4}$$

From the measured and calculated set of values $\{x_1(k) = \ln f_k, x_2(k) = f_k, y(k) = \ln P(f_k)\}$ (see Table 1), the following coefficients were obtained for an FSO 1500 car type: $P_0 = 16.1227 \times 10^{-3}$, $\nu = -0.9024$ and $\mu = 0.0003188$. Table 2 gives the values of P_0, ν and μ for different vehicle types.

Table 2. The values of the parameters P_0, ν and μ defining the power spectral density (formula (3)) of vehicles moving in the worst atmospheric conditions

Vehicle type	P_0 [W]	ν	μ	V [m/s]
Fiat 125p	54.1300×10^{-6}	0.0934	0.0008765	13.88 (8)
Polonez 1500	49.6063×10^{-4}	−0.6530	0.0004409	13.88 (8)
FSO 1500	16.1227×10^{-3}	−0.9024	0.0003188	13.88 (8)
Zastava 1100P	38.1409×10^{-4}	−0.5677	0.000410	13.88 (8)
Moskvitch 1500	28.3469×10^{-4}	−0.7014	0.0003440	13.88 (8)
Żuk A 151 C	91.2619×10^{-3}	−1.1700	0.0002789	12.500
Ikarus 260	63.6958×10^{-4}	−0.5072	0.0006393	8.61 (1)
Jelcz 080	77.1012×10^{-4}	−0.6407	0.0006170	6.94 (4)
Star 38	43.1774×10^{-4}	−0.6199	0.0005105	10.55 (5)
Star 244 RS	27.0045×10^{-5}	−0.0381	0.0008744	10.27 (7)
Star 244	23.1085×10^{-5}	−0.0649	0.0007720	9.72 (2)
Star C 200	68.6694×10^{-5}	−0.0807	0.0008275	9.72 (2)
Tarpan F 237 R	32.8785×10^{-4}	−0.4994	0.0007091	9.72 (2)
Fiat 126p	37.2276×10^{-2}	−1.5213	−0.0002175	10.27 (7)

Expression (1), defining the pressure spectral density, includes besides the power spectral density of the source, $P(f)$, also the absorption coefficient $\alpha(f)$, which will now be considered.

2.2. Absorption coefficient

The energy of sound propagating in the air is absorbed due to heat conduction, viscosity and molecular relaxation in the medium where the acoustic wave propagates. This absorption is described by exponential function $\exp\{-2\alpha(f)r\}$ (formula (1)), where r is the length of the propagation path and α is the absorption coefficient. This coefficient is quite a complex function of frequency f, because each of the relaxation processes is described by a dependence of the form $Af^2/(B+f^2)$, where the parameters A and B depend on the temperature T and the humidity H of the medium.

In paper [1], numerical values of the absorption coefficient were given for the different frequencies, humidities and air temperatures. It was shown that

over the frequency range 100–1000 Hz the coefficient a can be apparoximated by the formula [3]

$$a = a_1 f. \tag{5}$$

Table 3 gives the values of the parameter a and of the correlation coefficient K for the temperatures $T = 0, 5, 10, 15$ and 20°C and the humidities $H = 20, 40, 60$ and 80%. In all cases $K > 0.930$ which proves a good agreement between formula (5) and the real values of a.

Standard [11], recommended by the US Federal Aviation Administration, also gives the linear dependence (5) but the values of the parameter a_1 are slightly different.

These results were to some extent confirmed by SUTHERLAND and BASS [10]. They showed that for limited frequency bands the absorption coefficient may be assumed to be $a \sim f^k$, where the exponent falls within the interval (0, 2). In the present case it was assumed that $k = 1$.

The approximation expressed by formula (5) is surprising because each of the relaxation processes and the phenomena of energy transport, responsible for classical absorption, are described by nonlinear functions of frequency. Good approximation of the real values of the coefficient $a(f)$ by the linear dependence (5) is explained by the fact that over the frequency range 10–1000 Hz the energy absorption is caused above all by the relaxation of oxygen molecules. A significant fact is that the above range is small when compared with the whole range where this relaxation occurs (we may follow the principle that each nonlinear function, in an appropriately narrow range of variability of its argument, can be replaced by a linear function).

Considering formulae (1), (3) and (5), the pressure spectral density $p^2(f)$, at the distance r from the source, can thus be expressed in the following way:

$$p^2(f) \frac{P_0 \varrho_0 c}{2\pi r^2} f^\nu \exp\{-[\mu + 2a_1 r]f\}, \tag{6}$$

where $\varrho_0 c = 415$ [Pas/m], while P_0, ν and μ are the parameters descibing power spectral density (formula (3), Table 2).

3. Sound level

The principal aim of this investigation is to determine the dependence between the sound level L and the distance r, on the assumption that the conditions specified at the beginning of Section 2 are satisfied. As follows from the definition of the sound level (formula (A2)) at first it is necessary to determine the

dependence of the (frequencyweighted) pressure on the distance. This dependence is defined by formulae (6) and (A5):

$$p_A^2 = \frac{P_0 \varrho_0 c}{2\pi r^2} \int_0^\infty W(f) f^\nu \exp\{-[\mu 2a_1 r] f\} df.$$

Substitution of the explicit weight function $W(f)$ (formula (A4)) gives

$$p_A^2 = \frac{P_0 W_0 \varrho_0 c}{2\pi r^2} \int_0^\infty f^{\nu+2} \exp\{-[\mu + \delta + 2a_1 r]\} df,$$

where $W_0 = 1.467 \times 10^{-6}$ and $\delta = 6.141 \times 10^{-4}$ (see the Appendix). Integration [5] gives

$$p_A^2 = \frac{P_0 W_0 \varrho_0 c}{2\pi r^2} \frac{\Gamma(\nu+3)}{[\mu + \delta + 2a_1 r]^{\nu+3}}, \tag{7}$$

where $\Gamma(\nu+3)$ is EULER's gamma function. From the definition of the sound level expressed in $dB(A)$ (formula (A2)), it follows thus that

$$L(r) = L_0 - 20 \log r - \Delta L(r), \quad [\mathrm{dB}(A)], \tag{8}$$

where

$$L_0 = 10 \log \left\{ \frac{P_0 W_0 \varrho_0 c \Gamma(\nu+3)}{2\pi p_0^2 [\mu + \delta]^{\nu+3}} \right\}$$

and

$$\Delta L(r) = 10(\nu+3) \log \left\{ 1 + \frac{2a_1 r}{\delta + \mu} \right\} \tag{9}$$

is a sound level drop caused by absorption. (It can readily be noticed that for $a_1 = 0$ also $\Delta L = 0$).

4. Discussion of the results

Formula (9) implies that when observation point is close to the source, so that the inequality $r \ll (\delta+\mu)(2a_1)$ is satified, then ΔL is a negligibly small quantity ($\Delta L \ll 1$ dB(A)). In this case formula (8) becomes

$$L(r) = L_0 - 20 \log r, \tag{10}$$

which means the drop $\delta L = 6$ dB(A) when the distance is doubled.

When the distance between the observation point and the source is great, $r \gg (\delta+\mu)/(2a_1)$, then the level drop δL for a double distance is much greater, for (formula (9))

$$\Delta L(r) \approx 10(\nu+3) \log \left(\frac{2a_1 r}{\delta + \mu} \right)$$

and (formula (8))

$$L(r) = L_0 + 10(\nu+3)\log\left(\frac{2\alpha_1}{\delta+\mu}\right) - 10(\nu+5)\log r. \tag{11}$$

As follows from this dependence for a double distance $\delta L = 3(\nu+5)$, which for $\nu - 1.5$ (Table 2) gives the drop $\delta L > 10\,\mathrm{dB}(A)$.

This result is a little surpising. However, it should be borne in mind that formula (11) is valid for the distances r exceeding greatly the "critical distance" R, where

$$R = \frac{\delta+\mu}{2\alpha_1}. \tag{12}$$

Substitution of $\delta = 6.141 \times 10^{-4}$ (see the Appendix), the parameter μ characterizing the power of the source (Table 2) and the quantities α_1 (Table 3) into this eguation gives the "critical distances" R for the sources of different type.

Table 3. The parameter α_1 (formula (4)) and the correlation coefficient K for the different temperatures T and humidities H

H [%] \ T[°C]		0	5	10	15	20
20	α_1	1.182×10^{-6}	1.769×10^{-6}	2.373×10^{-6}	2.744×10^{-6}	2.727×10^{-6}
	K	0.9308	0.9753	0.0012	0.9836	0.9687
40	α_1	1.960×10^{-6}	2.280×10^{-6}	2.373×10^{-6}	1.936×10^{-6}	2.727×10^{-6}
	K	0.9913	0.9753	0.9912	0.9531	0.9507
60	α_1	2.056×10^{-6}	1.956×10^{-6}	2.229×10^{-6}	1.358×10^{-6}	1.129×10^{-6}
	K	0.9792	0.9611	0.9645	0.9501	0.9571
80	α_1	1.848×10^{-6}	1.584×10^{-6}	1.289×10^{-6}	1.060×10^{-6}	9.106×10^{-7}
	K	0.9639	0.9513	0.9488	0.9547	0.9670

Table 4 gives as an example the values of R for an 1500 type car. By carying out similar calculations for the vehicles mentioned in Table 2, it can be found that for a Fiat 126p, at a temperature of 15°C and 20% humidity $R = 108$ m, while for an Ikarus $R = 228$ m. In the atmospheric conditions characterized by a tem-

Table 4. The "critical distances" R[m] (formula (12)) for an FSO 1500 car type for different atmospheric conditions

H[%] \ T[°C]	0	5	10	15	20
20	395	264	197	170	171
40	238	205	209	241	291
60	227	238	201	343	413
80	252	295	362	440	512

perature of 30°C and humidity of 80%, for a Fiat 126 p $R = 358$ m, for an Ikarus $R = 757$ m. The latter case proves that noise propagates very far. Large "critical distances" also occur for Star lorries and for Fiats 125p.

It can be discerned that for most vehicles the "critical distance" increases with increasing air humidity and temperature. However, for particular vehicle types, the temperature $T = 15$°C and the humidity $H = 20\%$ are the most favourable atmospheric parameters, since the "critical distances" are then the shortest. Noise is most effectively damped by the air in such atmospheric conditions.

Table 5. Values of the sound level drop at the "critical distance" R

Vehicle type	$\Delta L(R)$ [dB(A)]
Fiat 125 p	9.3
Polonez 1500	7.1
FSO 1500	6.3
Zastava 1100 P	7.3
Moskvitch 1500	6.9
Żuk A 151 C	5.5
Ikarus 260	7.5
Jelcz 080	7.1
Star 38	7.2
Star 244 RS	8.9
Star 244	8.8
Star C 200	8.8
Tarpan F 237 R	7.5
Fiat 126p	4.5

The "critical distance" R depends on μ (formula (12)), one of the parameters defining the spectral density of the source (formula (3)). Another parameter, ν, affects the magnitude of the sound level drop. Substitution of the definition of R (formula (12)) into (9) gives

$$\Delta L(r) = 10(\nu+3)\log\left\{1+\frac{r}{R}\right\}.$$

This is a level drop caused only by the air absorption. For $r = R$

$$\Delta L(r) = 10(\nu+3)\log 2 = 3(\nu+3). \tag{13}$$

Putting the values of ν from Table 2 into this formula we get the values of $\Delta L(r)$ for the particular vehicle type (Table 5). A comparison between them and the values of the "critical distance" calculated for these vehicles shows that the highest noise level drop caused by the absorption by the air can be observed for the noisiest wehicles (Ikarus, Star, Fiat 125, with the highest R). Despite this, e.g. at a distance of 300 m, the noisiest vehicles are still Ikaruses and Stars, which is confirmed by everyday experiences.

5. Conclusions

Many measurements of noise propagating in open areas indicate the phenomenon of a "rapid sound level drop with increasing distance". EMBLETON, PIERCY and OLSON [4] showed that close to the source the phenomenon is related to interaction between the accoustic wave and the ground surface.

In the present paper, it has been shown that a rapid sound level drop at longer distances from the source (of the order a few hundred metres) can be caused by the air absorption.

This effect follows from formula (8), which relates the sound level, the distance r, the parameters describing the source (P_0, ν, μ — formula (3)) and the damping by the air (α_1 — formula (5), Table 3). The quantities $W_0 = 1.467 \times 10^{-6}$ and $\delta = 6.141 \times 10^{-4}$, occurring there, describe the frequency correction (Appendix). As follows from this formula the sound level drop for a double distance is much higher than 6 dB(A) when $r \gg R$, where R (formula (12)) is the "critical distance" (Fig. 2). In the case of an Ikarus for which $R \cong 700$ m, the phenomenon of a rapid level drop can be observed a few hund red metres from the road, on the condition that the observation point (O) is located in the way shown in Fig. 1.

Acknowledgment. The authors wish to thank Dr Jerzy MIAZGA and Mrs. Krystyna JANICKA, M. Eng., from the Institute of Road Transportion in Warsaw, for carrying out measurements of the spectra of external vehicle noise.

References

[1] *American National Standard*, ANSI SI. 26, 1978.

[2] K. ATTENBOROUHG, *Predicted ground effect for highway noise*, Journal of Sound and Vibration, **81**, 413–424 (1982).

[3] J. BARTKOWIAK, *Sound absorption coefficient in the air* (in Polish), M. Sc. Thesis, Institute of Acoustics, Adam Mickiewicz University, Poznań, 1985.

[4] T. F. EMBLETON, J. E. PIERCY ,N. OLSON, *Outdoor sound propagation over ground of finite impedance*, J. Acoust. Soc., Am., **59**, 276–277 (1976).

[5] Y. S. GRADSTEJN, Y. M. RYZHIK, *Tablitsy integralov, summ, ryadov i proyzvedenii*, G.Y.F. — M. L. Moscow, 1963, integral 3.381.4.

[6] C. M. HARRIS, *Handbook of noise control*, McGraw-Hill, New York, 1979, pp. 2–9.

[7] J. E. PIERCY, T. F. W. EMBLETON, *Sound propagation in the open air, Handbook of noise control*, McGraw-Hill, New York, 1979.

[8] J. E. PIERCY, T. F. W. EMLBETON, G. A. DAIHLE, *Atmospheric propagation of sound*, 11th International Congress on Acoustics, Paris, 1983, **8**.

[9] J. SADOWSKI, *Architectural acoustics* (in Polish), PWN, Warsaw, 1976, p. 29.

[10] L. C. SNTHERLAND, H. E. BASS, *Infuence of atmospheric absorption on the propagation of bands of noise*, J. Acoust. Soc. Am., **66**, 886–894 (1979).

[11] *U. S. Federal Aviation Adminisration, Code of Federal Regulations*, 14, Section A 36.5, 1976.

Appendix

Despite the increasingly serious objections, the sound level expressed in dB(*A*) is generally used as the measure of the annoyance of time invariable noise. It is defined as

$$L = 10\log\left\{\sum 10^{0.1(L_k+\Delta L_k)}\right\}, \tag{A1}$$

where L_k is the pressure level in the kth 1/3 octave band, characterized by the centre frequency f_k, whereas the quantity ΔL_k corresponds to the correction curve *A*. For the centre frequencies $f_1 = 50$ Hz, $f_2 = 63, \ldots, f_{24} = 10\,000$ Hz, respectively, $\Delta L_1 = -30.2$, $\Delta L_2 = -26.2$, ..., $\Delta L_{24} = -2.5$ dB. By using futher the definition of the sound level, $L_k = 10 \log (p_k^2/p_0^2)$, formula (*A* 1) can be rewritten in the form

$$L = 10 \log\{P_A^2/p_0^2\}, \tag{A2}$$

where

$$p_A^2 = \sum 10^{0.1\,\Delta L_k} p_k^2 \tag{A3}$$

is the squared frequency – weighted pressure, according to the correction curve *A*. It can be seen that the weight function

$$W(f_k) = 10^{0.1\,\Delta L_k}, \quad k = 1, 2, \ldots,$$

takes values

$$W(f_1) = 10^{-3.02},\ W(f_2) = 10^{-2.62}, \ldots, W(f_{24}) = 10^{-0.25}.$$

It can be discerned that the set $\{f_k, W(f_k)\}$ can be approximated by the continuous function

$$W(f) = W_0 f^2 \exp\{-\delta f\}. \tag{A4}$$

The application of regression analysis to the set of points $(31, 10^{-3.02})$, $(50, 10^{-2.62})$, ..., $(10\,000, 10^{-0.25})$ gives the following values: $W_0 = 1.467 \times 10^{-6}$, $\delta = 6.141 \times \times 10^{-4}$. Hence, formula (*A*3) can be rewritten in the form

$$P_A^2 = \int_0^\infty W(f) p^2(f)\, df, \tag{A5}$$

where $p^2(f)$ is the pressure spectral density.

ARCHIVES OF ACOUSTICS
10, 3, 253–260 (1985)

A CONTRIBUTION TO THE DETERMINATION OF THE FREQUENCY DISCRIMINATION ABILITY

J. KALUŽNÝ

Strojársko technologická fakulta SVŠT, 917 24 Trnava, Czechoslovakia

V. MAJERNÍK

Katedra fyziky Pedagogickej fakulty, 949 74 Nitra, Czechoslovakia

M. KALUŽNÁ

Katedra fyziky Strojnickej fakulty SVŠT, Gottwaldovo nám. 17.801 00 Bratislava, Czechoslovakia

The *DL*'s for frequency as a function of the interstimulus intervals are experimentally determined. It is shown that the difference limens for frequency for both non-stationary and stationary signals clearly depend on the duration of the interstimulus interval up to the value ~ 256 ms. Moreover, it is shown that the recently published values of difference limen for frequency can be analytically expressed as the product of an exponential function and a resonance one where frequency and signal duration are parameters.

1. Introduction

In spite of intensive investigations the functional dependence of the difference limen for frequency (*DLf*) on various physical parameters (intensity, duration, frequency, etc.) of accoustical signals are determined unsatisfactorily. This regards mainly the influence of the interstimulus interval on the *DLf*. It is well-known that the interstimulus interval (*ISI*) between the constant and comparative acoustical signals is one of the physical parameters which affects the pitch perception and the discrimination ability of the auditory

system. The values of the ISI are (published in works dealing with the determination of the auditory discrimination ability) different and their choice has an intuitive character. However, there are some experiments performed, aimed at finding the influence of *ISI* on the perception of stationary acoustical signals. KRÚTEL' [1] investigated the dependence of the difference limen for intensity *DLI* on *ISI* and showed its influence on the values of *DLI*. HARRIS [2] and KÖNING [3] found the influence of *ISI* on *DLf* as well. HARRIS did not find any expressive changes in *DLf* on *ISI* from the interval 0.3–3.5 s. KÖNING determined the influence of *ISI* on the frequency discrimination ability of stationary signals by means of five psychometric methods. The frequency of signals he used was 1000 Hz and the loudness level was 40 dB. He changed *ISI* in the range 0.31–5 s. Five subjects participated in these experiments. KÖNING found out that the frequency discrimination ability falls only weakly with increasing *ISI*, irrespective of the psychometric method.

As we note, *ISI* had relatively large values in the experiments of HARRIS and KÖNING. It seems to us, it would be convenient to investigate the influence of *ISI* on *DLf* for the smaller values and for non-stationary signals too. In what follows we present the results of such experiments.

Several papers (see for example [4]–[8]) have dealt with the determination of difference limens for frequency where the found values of *DLf* are fitted with some functions. Unfortunately, these functions express the dependence of *DLf* on one physical parameter only. Usually, this parameter is duration or frequency. In the present paper, a function of two parameters is shown, with which one can describe the dependence of *DLf* on duration and frequency as well. This function was found for the values of *DLf* published in [4, 5].

2. Experiments

We measured the dependence of *DLf* on *ISI* for acoustical signals, with the following values of *ISI*: 0, 16, 32, 64, 128, 256 and 1024 ms. The signal duration T was 32, 64, 128, 256 ms and the frequency $f = 1000$ Hz. The experiments were performed with stimuli whose loudness level for stationary signals was 60 dB. The envelope of the signals was a rectangular one and the initial phase was zero.

The method of constant stimuli was used. The value of *DLf*, assuming Gaussian distribution of subjects' answers was determined as a 50 percent level of the required sort of answers. The experiments were carried out monaurally and individually with four subjects. Two of them had no experience in psychoacoustical experiments. The subjects were situated in anechoic chamber. The subject's answer, (whether the presented stimuli were perceived as equal or non-equal) followed the presented stimuli and only then the next pair of stimuli was presented. Each subject gave 120 answers on the presented stimuli in one

experiment. The frequency of the comparative stimulus was higher or at least equal to the frequency of the constant stimulus in the whole experiment.

A schematic diagram of the apparatus used is shown in Fig. 1. The standard stimulus and the comparative one came from generators of the sinusoidal

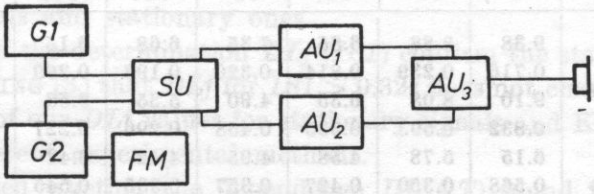

Fig. 1. A schematic diagram of the apparatus used. $G1$ and $G2$ are generators of sinusoidal signals, FM is the frequency meter, SU is the switching unit, P is the phone and AU_1, AU_2, AU_3 are the attenuation units, respectively

signals $G1$ (Brüel and Kjaer 1020) and $G2$ (Tesla BM 524), respectively. The frequency meter FM (Tesla BM 455 E) was permanently connected with $G2$ for control reasons. Signals from $G1$ and $G2$ were conducted to the switching unit SU (the laboratory product of the Institute of Physics SASc). It was possible to start the pairs of signals manully or automatically with a repeating period from the range 1–10 s. The signal duration T and interstimulus interval ISI were chosen in the SU from the range 0–1000 ms and 0–1500 ms, respectively. Then the signals from the SU were conducted through the attenuation units AU_1, AU_2, AU_3 (RFT Xa 716) which served for adjusting the required loudness level in the phone P (Melodium, Audio 15). The apparatus without the phone was located outside the anechoic chamber.

3. Results and discussion

The experimentally determined values of DLf (ISI) defined as an arithmetic mean of the frequency difference limens of the individual subjects, together with their standard deviations, are shown in Table and Figs. 2, 3. The significance of the deviation of the DLf values for the individual subjects from the arithmetic means was examined by a statistical t-test. The deviations were not significant at the 0.05 significance level and so we can consider them as random ones. By means of the t-test we also tested whether the change of the DLf value caused by the change of the interstimulus interval ISI is random or significant. It was shown for all signal durations T that the differences between DLf (ISI = = 0 ms) and DLf (ISI = 16 ms) are nonsignificant at the 0.05 significance level. Thus, it can be stated that not the presence of ISI, but its magnitude is decisive for the determination of DLf.

Table. *DLf* (*ISI*) as a function of the signal duration *T* for accoustical signals with a frequency of 1000 Hz. The upper values are *DLf*, the lower ones are the corresponding standard deviations (both are given in Hz)

T [ms]	*ISI* [ms]						
	0	16	32	64	128	256	1024
32	9.38	8.88	6.85	7.35	6.68	6.15	6.05
	0.716	0.239	0.814	0.320	0.193	0.269	0.265
64	9.10	8.08	6.35	4.90	5.35	3.58	3.48
	0.832	0.593	0.335	0.458	0.296	0.227	0.177
128	6.15	5.78	4.58	4.95	4.42	3.42	3.52
	0.568	0.350	0.427	0.357	0.335	0.545	0.150
256	5.92	5.52	4.45	4.42	3.42	2.98	3.12
	0.243	0.335	0.269	0.042	0.180	0.357	0.286

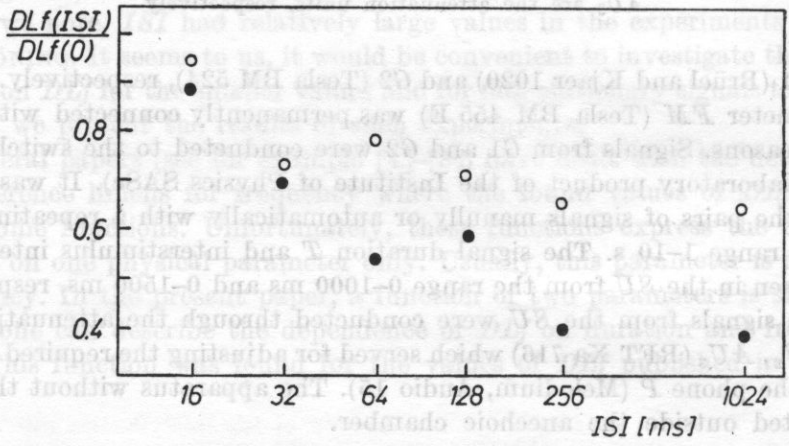

Fig. 2. The ratio *DLf* (*ISI*)/*DLf*(0) as a function of the interstimulus interval *ISI*. ○ and ● are for the signal durations $T = 32$ ms and $T = 64$ ms, respectively

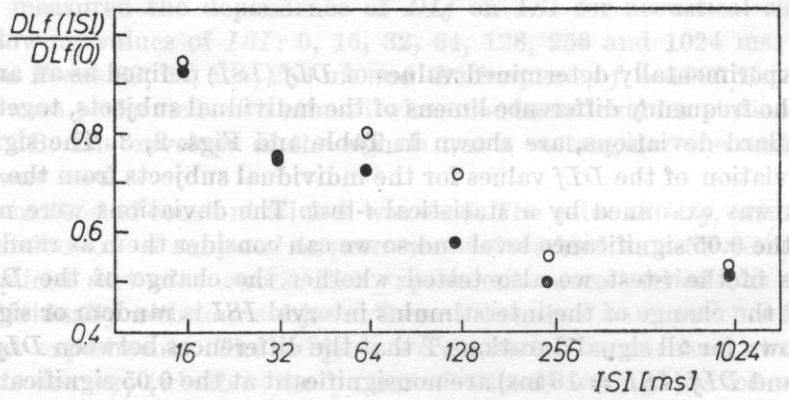

Fig. 3. The ratio *DLf* (*ISI*)/*DLf*(0) as a function of the interstimulus interval *ISI*. ○ and. ● are for the signal durations $T = 128$ ms and $T = 256$ ms, respectively

The values of *DLf* clearly decrease if *ISI* increases within the interval 16–32 ms. This kind of the dependence is broken off for non-stationary signals of durations, approximately, $T = 32$, 64 ms when $ISI \approx T$ and then continues up to the value $ISI \approx 256$ ms. *DLf* decreases if *ISI* increases for the stationary signal durations $T = 128$, 256 ms. The frequency discrimination ability does not change if *ISI* is approximately equal or more than 256 ms for both non-stationary signals and stationary ones.

Our results of the determination *DLf* (*ISI*) confirm the statements of HARRIS [2] and KÖNING [3] that *DLf* for $ISI > 0.32$s does not change significantly. The differences of our *DLf* values for stationary signals and KÖNING's ones are due to the different experimental methods.

We also tested whether the dependence *DL* $f(T)$ found for $ISI = \text{const.}$ agrees with the quantitative relationship

$$DLf = A + B/n + (B/n)^C, \tag{1}$$

determined in papers [4, 5] where n is the number of periods of the signal and A, B, C are constants. We showed that our results fulfil this equation but the constants A, B, C are other than in papers [4, 5] for a signal frequency of 1000 Hz. The agreement in the qualitative relationship may be considered as a certain criterium of the confidence of the results achieved. The differences in A, B, C are probably caused by the differences in the performance of the experiments.

In order to explain the dependences plotted in Figs. 2, 3 we assume that the values of *DLf* for short *ISI* are affected by the perstimulating and the poststimulating fatigue. When $ISI \to 0$ the masking phenomenon must be considered between standard stimulus and the comparative one. The poststimulating fatigue is manifested by an increase in the perception threshold during the short time till the full stimulation sensibility of the auditory system is restored. The interval of less sensibility depends on the intensity of the presented signals and differs for individual subjects. Adaptation phenomena can be explained by means of actions which are running in the peripheral auditory organ when the weak stimuli are presented. In the case of strong stimuli the adaptation phenomena in the brain might also cause the decrease of the sensibility of the competent analyzing elements.

4. The analytical expression of *DL* $f(f, T)$

Many authors interested in the investigation of the dependence of the frequency discrimination ability on the auditory system attempted to express analytically the empirical results. OETINGER [6] succeded in the determination of *DLf* as an analytical function of duration T of the signal in a short inter-

val of duration. The results of LIANG CHIAN and ČISTOVIČ [7] can be also expressed through an analytical function of the form

$$\Delta z = \frac{\Delta z_0}{1-\exp(-T/T_0)},$$

where Δz_0 and T_0 are constants [8], if the frequency is recalculated in pitch (mels). Δz is the differences limen for pitch.

The analytical form of the curve of $DLf(T)$ for the most important range of frequency (from the point of view of the transfer information ability) of non-stationary signals was obtained by means of numerical calculations in papers [4, 5]. In these papers it has been shown that if the signal duration is expressed as a number of periods n, the function which fits best the empirical dependence DLf on n has the form of (1). The constants A, B, C are dependent on the signal frequency f. Equation (1) expresses one form of the auditory uncertainty relation [5].

It was shown that the experimental data of DLf from papers [4, 5] can be also expressed by the exponential function

$$DLf(f) = a\exp(bf), \tag{2}$$

where a, b are constants for a given frequency. The calculations showed that the values of b were constant ($b = 4\times10^{-4}\mathrm{Hz}^{-1}$) and a was a function of the signal duration T. The function $a(T)$ is a decreasing one. The most suitable form of $a(T)$ from all types of functions which were investigated is

$$a(T) = K_1 + \frac{K_2}{(K_3+T)^2}, \tag{3}$$

where K_1, K_2, K_3 are constants. The most suitable values of K_1, K_2, K_3 and thereby the dependence $a(T)$ were found by means of the iteration procedure. By putting (3) into (2) one can obtain the following determination of $DLf(T,f)$:

$$DLf(T,f) = \left\{K_1 + \frac{K_2}{(K_3+T)^2}\right\}\exp(bf), \tag{4}$$

where $K_1 = 1.85$ Hz, $K_2 = 625.5$ s, $K_3 = 1.42$ s, $b = 4\times10^{-1}\mathrm{Hz}^{-1}$.

The analytical expression (4) of the frequency discrimination ability describes empirical dependence sufficiently precisely mainly for signals of frequencies up to 4 kHz. The new analytical expression (4) of the function $DLf(T,f)$ is suitable mainly for the calculation of some information-theoretical parameters of the auditory system e.g. information content of acoustical signals as a function of duration and frequency [9].

5. Conclusion

From what has been said so far, it follows that:

1) *DLf* for signals of 1000 Hz frequency and durations from 32 ms up to 256 ms represents a function of the interstimulus interval *ISI*.

2) *DLf* reaches its maximum value if *ISI* is equal to zero. If *ISI* increases up to ~256 ms the *DLf* decreases. For $ISI > 256$ ms *DLf* is practically constant.

3) *DLf* can be expressed in a wide range of signal durations as a product of an exponential function and a resonance one.

Acknowledgement. The authors wish to express their thanks to the workers of the Department of Acoustics of the Institute of Physics of the Slovak Academy of Sciences for the technical assistance during the experimental work.

References

[1] J. KRUTEL, *Thesis*, Bratislava, 1970.

[2] D. J. HARRIS. *Discrimination of pitch: suggestions toward method and procedure*, J. Exper. Psych. 43, 96 (1952).

[3] E. KÖNING, *Effect of time on pitch discrimination thresholds under several psychophysical procedures: comparison with intensity discrimination thresholds*, J. Accoust. Soc. Amer., 29 606 (1957).

[4] J. KALUŽNÝ, *Quantitative expression of the frequency discrimination ability of the auditory system*, Studia Psychologica, 20, 243 (1978).

[5] V. MAJERNIK, J. KALUŽNÝ, *On the uncertainty relations*, Acustica, 43, 132 (1979).

[6] R. OETINGER, *Die Grenze der Hörbarkeit von Frequenz und Tonzahländerungen bei Tonimpulsen*, Acustica 9, 430 (1959).

[7] LIANG CHIAN, L. ČISTOVIČ, *Dependence of the frequency differential thresholds on the duration of the tone signals*, Akust. Zhur., 6, 81 (1960).

[8] V. MAJERNÍK, *Some information theoretical characteristics of human ears for nonstationary accoustical stimuli*, Proc. of 4th Intern. Congr. of Cybernetics., Namur, 1964.

[9] V. MAJERNÍK, J. KALUŽNÝ, *Intensity of the acoustical signals as an information carrier in auditory transfer channel*, Acoustica, 32, 74 (1975).

ARCHIVES OF ACOUSTICS
10, 3, 261–272 (1985)

CALCULATION OF THE SOUND-ABSORBING PANELS BASED ON THE PRINCIPLE OF ELECTROACOUSTIC ANALOGIES AND CONSIDERING THE RAYLEIGH IMPEDANCE

M. LEŚNIAK, A. DRZYMAŁA, S. KLIMCZYK

Physics Department, I. Łukaszewicz
Technical University
(35–959 Rzeszów, ul. W. Pola 2)

R. WYRZYKOWSKI

Acoustics Department, Pedagogical College
(35–310 Rzeszów, ul. Rejtana)

This paper reports on calculations of the parameters of a bothsided perforated sound-absorbing system, based on the "electric model" and considering the Rayleigh impedance. Both the absorption coefficient for perpendicular incidence and the reverberation coefficient over a broad frequency range were calculated.

1. Introduction

This paper reports on calculations of bothsided perforated sound-absorbing panels, based on the electroacoustic analogies applied in acoustics [1, 3–5, 7]. The calculations were based on a new "electric model", taking into account the Rayleigh impedance both at the input and the output of the perforated system. The results obtained in the form of a curve of the absorption coefficient versus frequency are comparable to the characteristic of series-made sound-absorbing panels. Analysis of this is given in the Conclusions.

2. Theoretical basis of the calculations

A bothsided perforated sound — absorbing panel filled with some sound--absorbing material can be represented in the form of an equivalent electric system, whose schematic diagram is shown in Fig. 1. It was considered in the

calculations that this sound-absorbing system has n holes per 1 m² of the plate, therefore, the quantities m, r and L define, respectively, the equivalent impedance for n holes connected in parallel. According to the system of electroacoustic

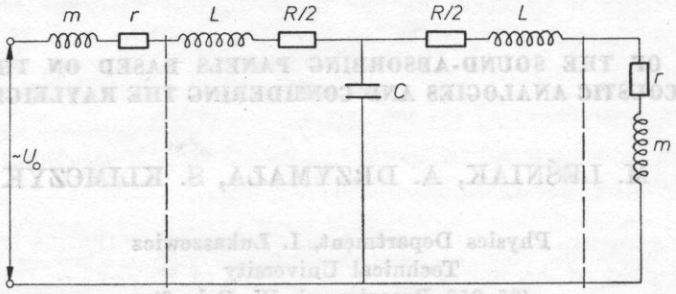

Fig. 1. An equivalent electric system of the two-sided perforated sound-absorbing panel

analogies accepted in acoustics, L corresponds to the acoustic mass of the air in the holes, R — to the resistance of the ports and C — to the acoustic compliance of a chamber of the system. The calculations were carried out by taking the quantities characterizing the plates as concentrated constants, which, for sizes occurring in practice, is valid up to about 8 kHz, with further increase of the frequency the approximation becomes increasingly "gross". By referring all the quantities to unit area and considering the existence of n holes connected in parallel, the following substitutions can be applied [1, 3–5, 7]:

$$R = R_{ac}d, \quad C = \frac{D}{\varrho c^2}, \quad L = \frac{\varrho l}{p}, \tag{1}$$

where d is the thickness of the layer of sound-absorbing material, R_{ac} is the flow resistance of the sound-absorbing material, l is the thickness of the perforated plate, D is the distance between the perforated plates and p is the perforation coefficient of the plates, defined as the ratio of the surface area of the holes in unit surface of the plate to this unit surface:

$$p = \frac{nS}{1\text{m}^2}, \tag{2}$$

where n is the number of ports per 1 m², S is the surface area of a port, ϱc is the acoustic resistance of the air, ϱ is the density of the air and c is the sound speed.

This system also considers the Rayleigh impedances r and m resulting from the diffraction effects at the holes. Practically over the whole working frequency range of soundabsorbing panels, and quite certainly for the approximations applied here, it can be assumed that the air vibrates in a port as a

rigid piston. The Rayleigh impedance for a single port [4] is given by the formula

$$Z' = \frac{\varrho c}{S}\left[1 - \frac{J_1(2ka)}{ka} + i\frac{S(2ka)}{ka}\right], \tag{3}$$

where J_1 is a Bessel function of the first order, S is a Struwe function of the first order, k is a wave number and a is the radius of the port.

For $ka \ll 1$, in the series expansion of both Bessel and Struwe functions, the terms of higher orders can be neglected. On this assumption, from [2], the Bessel and Struwe functions can be given in the following way:

$$J_1(2ka) = ka - \tfrac{1}{2}k^3a^3, \qquad S(2ka) = \frac{8k^2a^2}{3\pi}. \tag{4}$$

Substitution of $J_1(2\ ka)$ and $S(2\ ka)$ in (3) and consideration that $Z' = r_1 + i\omega m_1$ give

$$r_1 = \frac{\varrho\omega^2a^2}{2cS}, \qquad m_1 = \frac{8a\varrho}{3\pi p}. \tag{5}$$

Since the sound-absorbing system considered contains n holes connected in parallel, the resultant Rayleigh impedance, referred to unit area, will be

$$r = \frac{\varrho\omega^2a^2}{2cp}, \qquad m = \frac{8a\varrho}{3\pi p}. \tag{6}$$

The aim of the calculations is to find the parameters of the system on the assumption that the absorption coefficient reaches a maximum for a predetermined resonance frequency. This coefficient is defined as the ratio between the energy absorbed by the system and the energy incident on the system. The energy incident on the system (P_1) is partly absorbed (P_2), partly reflected (P_3), and part of the energy is transmitted through the system (P_4) — according to the diagram shown in Fig. 2.

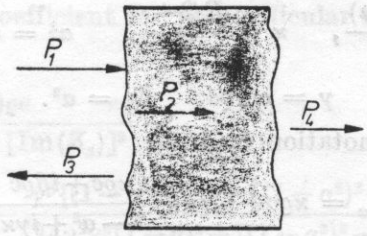

Fig. 2. A schematic representation of the distribution of energy incided on the absorbing material

By taking into account this notation, the absorption coefficient is defined in the following way:

$$\eta = \frac{P_2}{P_1}. \tag{7}$$

Applying the notation in Fig. 2, it can be written that

$$P_2 = P_1 - P_3 - P_4. \tag{8}$$

From that point of view,

$$\eta = \frac{P_1 - P_3 - P_4}{P_1} = 1 - \frac{P_3}{P_1} - \frac{P_4}{P_1}. \tag{9}$$

We begin with a plane wave for perpendicular incidence on the boundary between two media, and then the second term of expression (9) becomes [6, 7]

$$\frac{P_3}{P_1} = \left| \frac{\varrho c - Z_a}{\varrho c + Z_a} \right|^2, \tag{10}$$

where Z_a is the acoustic impedance of the sound-absorbing system, whose equivalent diagram is shown in Fig. 1.

Expression (10) is the definition of the reflection coefficient. After separating the real and imaginary parts of Z_a, the reflection coefficient becomes [6]

$$\frac{P_3}{P_1} = \frac{[\varrho c - \mathrm{Re}(Z_a)]^2 + [\mathrm{Im}(Z_a)]^2}{[\varrho c + \mathrm{Re}(Z_a)]^2 + [\mathrm{Im}(Z_a)]^2}; \tag{11}$$

or, by combining the first two terms of expression (9), there is

$$1 - \frac{P_3}{P_1} = \frac{4\ \mathrm{Re}(Z_a)\varrho c}{[\varrho c + \mathrm{Re}(Z_a)]^2 + [\mathrm{Im}(Z_a)]^2}. \tag{12}$$

The acoustic impedance for a given sound-absorbing system was calculated by means of an equivalent electric system:

$$Z_a = r + R/2 + i\omega(L+m) + \frac{r + R/2 + i\omega(L+m)}{1 - \omega^2 C(L+m) + i\omega C(R/2+r)}. \tag{13}$$

For simplification, the following notation will be introduced:

$$\beta = \frac{\omega(L+m)}{\varrho c}, \quad \varkappa = \frac{R/2+r}{\varrho c}, \quad \alpha^2 = \omega^2(L+m)C,$$

$$\gamma = \omega C \varrho c, \quad \beta\gamma = \alpha^2. \tag{14}$$

Introduction of this notation leads to

$$Z_a = \varkappa\varrho c + i\beta\varrho c + \frac{\varkappa\varrho c + i\beta\varrho c}{1 - \alpha^2 + i\gamma\varkappa}. \tag{15}$$

Some simple transformations lead, respectively, to

$$\mathrm{Re}(Z_a) = \varkappa\varrho c + \frac{\varkappa\varrho c(1-\alpha^2) + \beta\gamma\varkappa\varrho c}{(1-\alpha^2)^2 + \gamma^2\varkappa^2}, \tag{16a}$$

$$\mathrm{Im}(Z_a) = \beta\varrho c + \frac{\beta\varrho c(1-\alpha^2) - \gamma\varkappa^2\varrho c}{(1-\alpha^2)^2 + \gamma^2\varkappa^2}. \tag{16b}$$

The third term of expression (9) $-P_4/P_1$ — can also be calculated by applying an equivalent electric system. The power of the incident wave is calculated as the power of the plane wave, and, in order to retain the logical continuity of reasoning, in keeping with the principle of electroacoustic analogies, the amplitude of the accoustic pressure p_0 can be replaced by U_0. Thus, this expression can be given in the form

$$\frac{P_4}{P_1} = \frac{|I_3|^2 r}{U_0^2/\varrho c} = \frac{|I_3|^2 r \varrho c}{U_0^2}, \tag{17}$$

where I_3 is the intensity of the current flowing through the elements r and m (Fig. 1) and U_0 is the *rms* value of the tension.

I_3 now remains to be calculated. This can be done by taking advantage of the Kirchhoff laws in reference to the circuit shown in Fig. 1.

$$I_3 = \frac{U_0 \dfrac{1}{i\omega C}}{\left[\dfrac{R}{2} + r + i\omega(L+m) + \dfrac{1}{i\omega C}\right]^2 - \left[\dfrac{1}{i\omega C}\right]^2}. \tag{18}$$

By using the notation in (14), expression (18) becomes

$$I_3 = \frac{i\gamma U_0 \dfrac{1}{\varrho c}}{[i\gamma\varkappa + (1-a^2)]^2 - 1}. \tag{19}$$

Substitution of (19) in (17) and transformations give

$$\frac{P_4}{P_1} = \frac{\gamma^2\{(1-a^2)^2\varkappa^2\gamma^2 - [(1-a^2)^2 - (1+\gamma^2\varkappa^2)]^2}{\{4\gamma^2\varkappa^2(1-a^2)^2 + [(1-a^2)^2 - 1 + \gamma^2\varkappa^2)]^2\}^2} \frac{r}{\varrho c}. \tag{20}$$

Finally, the absorption coefficient for perpendicular incidence is given by the relationship

$$\eta_\perp = \frac{4\,\mathrm{Re}(Z_a)\varrho c}{[\varrho c + \mathrm{Re}(Z_a)]^2 + [\mathrm{Im}(Z_a)]^2} - \frac{\gamma^2\{(1-a^2)^2\gamma^2\varkappa^2 - [(1-a^2)^2 - (1+\gamma^2\varkappa^2)]^2\}}{\{4\gamma^2\varkappa^2(1-a)^2 + [(1-a^2)^2 - (1+\gamma^2\varkappa^2)]^2\}^2} \frac{r}{\varrho c}. \tag{21}$$

The above formula permits the absorption coefficient for perpendicular incidence to be calculated as a function of frequency with predetermined parameters of the sound-absorbing system. The absorption coefficient depends on the angle of the wave incidence on the surface of the sound-absorbing material. Because of this, the sound absorption coefficient for a plane wave incident at an angle φ on the surface of the material was called the directional absorp-

tion coefficient. The dependence of the absorption coefficient on the wave incidence angle can be given in the following way [6]:

$$\frac{P_3}{P_1} = \frac{[\varrho c - \mathrm{Re}(Z_a)\cos\varphi]^2 + [\mathrm{Im}(Z_a)]^2\cos^2\varphi}{[\varrho c + \mathrm{Re}(Z_a)\cos\varphi]^2 + [\mathrm{Im}(Z_a)]^2\cos^2\varphi} \tag{22}$$

or by calculating

$$1 - \frac{P_3}{P_1} = \frac{4\,\mathrm{Re}(Z_a)\varrho c\cos\varphi}{[\varrho c + \mathrm{Re}(Z_a)\cos\varphi]^2 + [\mathrm{Im}(Z_a)]^2\cos^2\varphi}. \tag{23}$$

The expression of the directional coefficient becomes then

$$\eta_\varphi = \frac{4\,\mathrm{Re}(Z_a)\varrho c\cos\varphi}{[\varrho c + \mathrm{Re}(Z_a)\cos\varphi]^2 + [\mathrm{Im}(Z_a)]^2\cos^2\varphi} - \frac{\gamma^2\{(1-\alpha^2)^2\varkappa^2\gamma^2 - [(1-\alpha^2)^2 - (1+\gamma^2\varkappa^2)]^2}{\{4\gamma^2\varkappa^2(1-\alpha^2)^2 + [(1-\alpha^2)^2 - (1+\gamma^2\varkappa^2)]^2\}^2} \frac{r}{\varrho c}. \tag{24}$$

When scattered sound, i.e. sound composed of waves travelling in all directions, is incident on the material, the absorption coefficient has some mean value and is called the reverberation coefficient of sound absorption. This coefficient can be given, depending on the directional absorption coefficient η_φ for any incidence angle φ, in the following way [7]:

$$\bar{\eta} = \int_0^{\pi/2} \eta_\varphi \sin 2\varphi d\varphi. \tag{25}$$

Substitution of (24) in (25) gives the following expression of the reverberation absorption coefficient:

$$\bar{\eta} = \int_0^{\pi/2} \left\{ \frac{4\,\mathrm{Re}(Z_a)\varrho c\cos\varphi}{[\varrho c + \mathrm{Re}(Z_a)\cos\varphi]^2 + [\mathrm{Im}(Z_a)]^2\cos^2\varphi} - \frac{\gamma^2\{(1-\alpha^2)^2\gamma^2\varkappa^2 - [(1-\alpha^2)^2 - (1+\gamma^2\varkappa^2)]^2\}}{\{4\gamma^2\varkappa^2(1-\alpha^2)^2 + [(1-\alpha^2)^2 - (1+\gamma^2\varkappa^2)]^2\}^2} \frac{r}{\varrho c} \right\} \sin 2\varphi d\varphi \tag{26}$$

or

$$\bar{\eta} = \int_0^{\pi/2} \frac{4\,\mathrm{Re}(Z_a)\varrho c\cos\varphi}{[\varrho c + \mathrm{Re}(Z_a)\cos\varphi]^2 + [\mathrm{Im}(Z_a)]^2\cos^2\varphi} \sin 2\varphi d\varphi - \frac{\gamma^2\{(1-\alpha^2)^2\gamma^2\varkappa^2 - [(1-\alpha^2)^2 - [1+\gamma^2\varkappa^2)]^2\}}{\{4\gamma^2\varkappa^2(1-\alpha^2)^2 + [(1-\alpha^2)^2 - (1+\gamma^2\varkappa^2)]^2\}^2} \frac{r}{\varrho c}. \tag{27}$$

Finally, after calculating the integral, the reverberation coefficient is given

by the formula

$$\eta = \frac{8\varrho c \operatorname{Re}(Z_a)}{|\operatorname{Re}(Z_a)|^2 + |\operatorname{Im}(Z_a)|^2}\left\{1 - \frac{\varrho c \operatorname{Re}(Z_a)}{[\operatorname{Re}(Z_a)]^2 + [\operatorname{Im}(Z_a)]^2} \times \right.$$

$$\times \left[\ln\left([\varrho c + \operatorname{Re}(Z_a)]^2 + [\operatorname{Im}(Z_a)]\right)^2 - \ln(\varrho c)^2\right] + \frac{\varrho c}{\operatorname{Im}(Z_a)} \times$$

$$\times \left(\frac{2[\operatorname{Re}(Z_a)]^2}{[\operatorname{Re}(Z_a)]^2 + [\operatorname{Im}(Z_a)]^2} - 1\right)\left(\operatorname{arctg}\frac{[\operatorname{Re}(Z_a)]^2 + [\operatorname{Im}(Z_a)]^2 + \varrho c \operatorname{Re}(Z_a)}{\varrho c \operatorname{Im}(Z_a)} - \right.$$

$$\left.\left. - \operatorname{arctg}\frac{\operatorname{Re}(Z_a)}{\operatorname{Im}(Z_a)}\right)\right\} - \frac{\gamma^2\{(1-\alpha^2)^2\gamma^2\varkappa^2 - [(1-\alpha^2)^2 - (1+\varkappa^2\gamma^2)]^2\}}{\{4\gamma^2\varkappa^2(1-\alpha^2)^2 + [(1-\gamma^2\varkappa^2) - (1+\gamma^2\varkappa^2)]^2\}^2}\frac{r}{c}. \quad (28)$$

Just as (21), formula (28) considers only a real part of the absorption coefficient. These expressions permit the calculation of the absorption coefficient as a function of frequency. They also make it possible to calculate the parameters of the system on the assumption that the absorption coefficient reaches a maximum for a predetermined resonance frequency. The resonance frequency is matched to a frequency at which in the noise spectrum there is the maximum accoustic pressure level. Expression (21) reaches the highest value when the following conditions are satisfied:

$$\operatorname{Re}(Z_a) = \varrho c, \quad \operatorname{Im}(Z_a) = 0. \quad (29)$$

By taking into account these conditions (29), one can calculate the resonance frequency or the parameters of the soundabsorbing system, and the value of the absorption coefficient for the resonance frequency. In order to do this, from the condition $\operatorname{Im}(Z_a) = 0$, it is obtained from equation (16*b*) that

$$\beta\varrho c[(1-\alpha^2)^2 + \varkappa^2\gamma^2] + \beta\varrho c(1-\alpha^2) - \gamma^2\varkappa^2 = 0. \quad (30)$$

From condition (14), i.e., that $\beta = \alpha^2/\gamma$, equation (30) becomes

$$\alpha^6 - 3\alpha^4 + \alpha^2(2 + \varkappa^2\gamma^2) - \varkappa^2\gamma^2 = 0. \quad (31)$$

The substitution $\alpha^2 = u$ gives

$$u^3 - 2u^2 + u(2 + \varkappa^2\gamma^2) - \varkappa^2\gamma^2 = 0. \quad (32)$$

This equation is satisfied when $u = 1$, i.e. $\alpha^2 = 1$. From the condition obtained, the value of the resonance frequency can be calculated:

$$1 = \alpha^2 = \omega_{\text{res}}^2(L+m)C,$$

hence

$$\omega_{\text{res}} = \sqrt{\frac{1}{C(L+m)}}. \quad (33)$$

When expressing L, m, C by the parameters of the sound-absorbing system, it

is possible to calculate the resonance frequency. By dividing the left side of equation (32) by $(u-1)$, it is obtained that

$$u^2-2u+\varkappa^2\gamma^2=0. \tag{34}$$

Solution of equation (34) gives its roots in the form

$$u_{1,2}=1+\sqrt{1-\varkappa^2\gamma^2}. \tag{35}$$

Becouse of the physical sense of $\varkappa$ and γ, the latter condition can be given in the form

$$0<\varkappa\gamma<1. \tag{36}$$

In recapitulating, equation (32) is satisfied when $\alpha^2=1$ for any values of the product $\varkappa\gamma$ and for

$$1<\alpha^2<2 \quad \text{and} \quad 0<\alpha^2<1 \quad \text{when } 0<\varkappa\gamma<1. \tag{37}$$

In turn, from the conditions $\mathrm{Re}(Z_a)=\varrho c$ and $\alpha^2=1$,

$$\gamma^2=\frac{1}{\varkappa(1-\varkappa)}. \tag{38}$$

From (38) and in view of the physical sense, $\varkappa$ must satisfy the condition

$$0<\varkappa<1. \tag{39}$$

Since for $\alpha^2=1$ and the product $\varkappa\gamma$ no condition is imposed, γ can take any values, certainly positive ones, which can be seen from expression (38).

The conditions obtained for $\varkappa$ and γ permit the calculation of the parameters of the sound-absorbing system.

3. Numerical calculations

It follows from conditions (33) and (37) that there can be three resonance frequencies: one for any $\varkappa\gamma$ and two frequencies for the condition $0<\varkappa\gamma<1$. By carrying out calculations for typical sound-absorbing barriers it can be found that $\varkappa\gamma$ must always be larger than 1. From that point of this, condition (37) is eliminated and one resonance frequency remains, which can be calculated from condition (33). The parameters of the system for a predetermined frequency at which in the noise spectrum there is the maximum acoustic pressure level, i.e. for the resonance frequency, can be calculated from dependencies (1), (6), (14) and (38),

$$\left(\frac{c}{2\pi f}\right)^2=\left(\frac{1}{p}+\frac{8a}{3\pi p}\right)D, \tag{40a}$$

$$\varkappa = \frac{R_{ac}d + \dfrac{\varrho a^2\omega^2}{cp}}{2\varrho c}, \tag{40b}$$

$$\left(\frac{2\pi f}{c}\right)^2 = \frac{1}{D^2\varkappa(1-\varkappa)}. \tag{40c}$$

In practice, it is most convenient to assume that $D = d$. From relations (40), it is possible to calculate the parameters of the system, by assuming, e.g., a typical tin perforation and typical values of the transmission resistance.

Knowledge of the parameters of the sound-absorbing system permits the calculation of the absorption coeffient for perpendicular incidence as a function of frequency, based on expression (21), and of the reverberation coefficient, from expression (28).

Fig. 3 shows the dependence of the absorption coefficient for perpendicular incidence, $\eta_\perp$ (curve 1), and of the reverberation coefficient, $\bar{\eta}$ (curve 2), as a function of frequency. The calculations were carried out for a sound-absorbing system with the tin thickness $l = 0.4 \times 10^{-3}$m, for the typical perforation $p = 0.280$ with the port diameter $2a = 4.5 \times 10^{-3}$ m, by assuming $D = 7 \times 10^{-2}$ m and that the consition $D = d$ is satisfied. Therefore, such a sound-absorbing system was chosen for calculations, since the parameters of sound-absorbing systems of the "Deska" type, produced by the Poznań Factory of Cork Products, are the same. In order to compare the results in Fig. 3, the frequency dependence of the reverberation coefficient of sound absorption (curve 3) was marked for

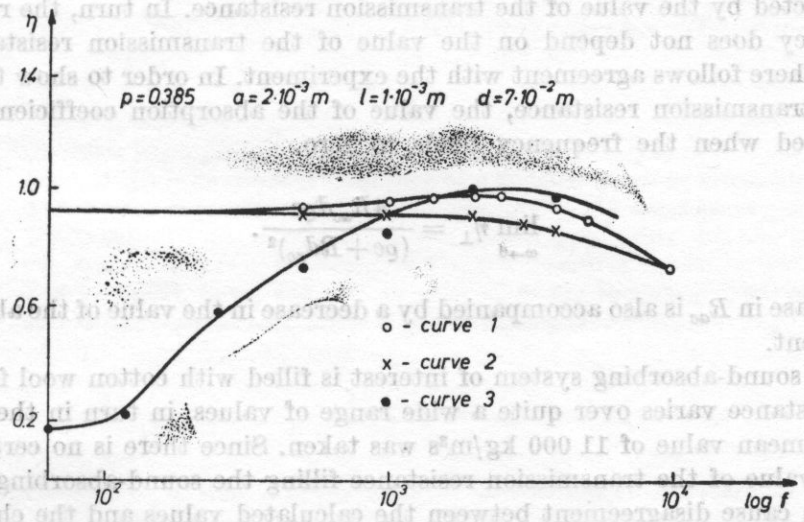

Fig. 3. Dependence of the absorption coefficient, respectively, for perpendicular incidence (curve 1), reverberation (curve 2) and the reverberation absorption coefficient for the system of the "Deska" type (curve 3) versus frequency

the above-mentioned absorbers of the "Deska" type. These results were drawn from technical data on the product and obtained at a conference with the representatives of the producer.

4. Conclusions

It follows from comparison of these curves that the measured maximum of the absorption coefficient is close to the measured frequency. The calculations indicate that the resonance frequency is equal to 2253 Hz, whereas it follows from the technical data that it is about 3000 Hz. A decidedly, however, lower value is taken by the reverberation absorption coefficient, drawn from the data of the ready panels, than that calculated on the basis of electroacoustic analogies for the part of the low frequencies. It follows from formula (21) that the value of the absorption coefficient from the part of the low frequencies is decidedly affected by the value of the transmission resistance. In turn, the resonance frequency does not depend on the value of the transmission resistance and hence, there follows agreement with the experiment. In order to show the effect of the transmission resistance, the value of the absorption coefficient can be calculated when the frequency tends to zero.

$$\lim_{\omega \to 0} \eta_{\perp} = \frac{4R_{ac}d\varrho c}{(\varrho c + Rd_{ac})^2}. \tag{41}$$

A decrease in R_{ac} is also accompanied by a decrease in the value of the absorption coefficient.

The sound-absorbing system of interest is filled with cotton wool for which the resistance varies over quite a wide range of values, in turn in the calculations a mean value of 11 000 kg/m³s was taken. Since there is no certainty as to the value of the transmission resistance filling the sound-absorbing system, this can cause disagreement between the calculated values and the characteristics of the panels produced.

The research was carried art at the Rzeszów Technical University within the contract U-946.

References

[1] A. DRZYMAŁA, M. LEŚNIAK, S. KLIMCZYK, R. WYRZYKOWSKI, *Parameters of sound-absorbing systems for predetermined frequencies* (in Polish), Proceedings of the XXXth OSA, Committee on Acoustics of the Polish Academy of Sciences, Gdańsk.

[2] E. JANKE, F. EMDE, F. LOSCH, *Spetstyalnye funktsi*, Izd. Nauka, Moscow, 1968.

[3] I. MALECKI, *Theory of acoustics waves and systems* (in Polish), PWN, Warsaw, 1964.

[4] E. SKUDRZYK, *The foundations of acoustics*, Wien-New York, 1971.

[5] R. WYRZYKOWSKI, A. PUCH, J. SNAKOWSKI, *Acoustic filters* (in Polish), Pedagogical College Press, Rzeszów, 1977.

[6] R. WYRZYKOWSKI, *Linear theory of the acoustic field of gaseous media* (in Polish), Pedagogical College Press, Rzeszów, 1972.

[7] Z. ŻYSZKOWSKI, *The fundamentals of electroacoustics* (in Polish), WNT, Warsaw, 1966.

ARCHIVES OF ACOUSTICS
10, 3, 273–280 (1985)

APPLICATION OF A PHASE LOOP SYSTEM TO ANALYSIS OF A DOPPLER SIGNAL IN ULTRASONIC SYSTEMS

MACIEJ PIECHOCKI

Institute of Fundamental Technological Research, Polish Academy of Sciences
(00–049 Warsaw, ul. Świętokrzyska 21)

MICHEL XHAARD, PIERRE PERONNEAU

Instrumentation et Dynamique Cardiovasculaire INSERM U265, Hopital Broussais
(75674 Paris, 96, rue Didot)

This paper presents a way of applying a phase loop system to the measurement of the instantaneous frequency of a Doppler signal in ultrasonic systems. This system was used to verify experimentally the dependence proposed by ANGELSEN [1], connecting the instantaneous probability distribution of the signal with its power spectrum. It presents measured results for two, laminar and turbulent, flows, and also an example of the operation of the phase loop system for a signal with a low signal to noise power ratio.

1. Introduction

The tendency to extend applications of ultrasonic flowmeters in medical diagnosis has brought about developments in the methods of analyzing signals they provide. Generally, it is assumed that a good mathematical description of such a signal is the Gaussian stochastic process, which is stationary for stationary flows [1-3]. Full information on the properties of this process, i.e., also on those of the flow observed, is contained in the power spectrum or the auto-correlation function of this process. Since, however, the spectral analysis requires sophisticated equipment, it is still essential to carry on studies on the possibilities of measuring the flow properties through the analysis of zero crossings, or that of its instantaneous frequencies.

In 1976 SAINZ *et al.* published the results of their investigations on the use of the phase loop system (*PLL*) to analyze a Doppler signal [7]. In the interpretation of the results, however, no account was taken of the stochastic nature

of the signal, thus, making it hardly convincing. Because of a lack of a theoretical description of the measured phenomenon, the conclusions are intuitive in nature.

The present paper is devoted mainly to an experimental verification of a dependence connecting the properties of the instantaneous frequencies of a signal with its power spectrum. The instantaneous frequency of a signal is defined by the time derivative of the instantaneous phase of the signal [1]. This dependence was proposed by ANGELSEN in 1981; it permits the determination of the mean value and standard deviation of the signal power spectrum from the probability distribution of its instantaneous frequencies. The ratio between these quantities, i.e. the ratio between the standard deviation of the power spectrum and its mean frequency, is called the turbulence index — accepted in medical diagnosis as the index of the degree of flow turbulence [4, 5].

The dependence, proposed by ANGELSEN, between the parameters of the signal power spectrum and the probability distribution of its instantaneous frequencies is given by the formula

$$p(\omega_c) = \frac{\sigma_s^2}{2\left[(\omega_c - \overline{\omega})^2 + \sigma_s^2\right]^{3/2}}, \tag{1}$$

where $p(\omega_c)$ is the probability distribution of the instantaneous frequencies of a signal, ω_c is the instantaneous frequency of a signal and $\overline{\omega}$ is the mean frequency in the power spectrum.

It follows from formula (1) that by knowing $\overline{\omega}$ — the mean frequency in the power spectrum, and σ_s^2 — the variance in the signal power spectrum, it is possible to calculate $p(\omega_c)$, the probability distribution of the instantaneous frequencies of this signal. Conversely, by knowing the distribution $p(\omega_c)$, the values of $\overline{\omega}$ and σ_s^2 can be found. The dependencies permitting the determination of these two parameters of the power spectrum have the following form:

$$\overline{\omega} = \overline{\omega}_c; \quad \sigma_s = 0.654 \Delta_{1/2\omega_c}, \tag{2}$$

where $\overline{\omega}_c$ is the mean value of the instantaneous frequencies and $\Delta_{1/2\omega_c}$ is the distribution width of $p(\omega_c)$ at half its height.

From dependencies (1) and (2) an additional conclusion follows, that, if they are valid, knowing the whole distribution $p(\omega_c)$, the only information on the power spectrum of this signal which can be determined, from $p(\omega_c)$, are the values of $\overline{\omega}$ and σ_s, i.e. the mean value and the standard deviation of the power spectrum. In turn, the shape of the power spectrum is not directly related to that of the distribution $p(\omega_c)$.

Dependence (1) was given in [1] without assumptions restricting its validity range. However, a previous publication by ANGELSEN [2] contained dependencies resembling formula (1), obtained for narrow-band signals, i.e. on the assumption that the ratio $\sigma_s/\overline{\omega}$ tended to zero.

A further part of this paper gives a system permitting the measurement of the instantaneous frequency of a signal and comparison between the theoretical dependencies given above and the measured results.

2. Construction principles of the system

Fig. 1 shows a schematic diagram of an impulse flowmeter where a phase loop system (*PLL*) was used to measure the instantaneous frequency of a Doppler signal.

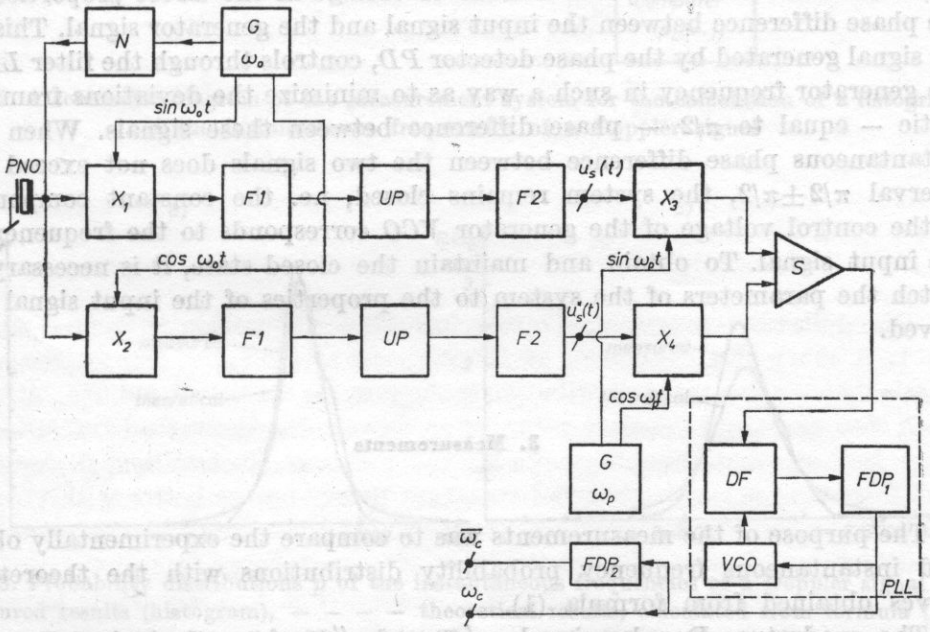

Fig. 1. A simplified schematic diagram of the impulse flowmeter with a (*PLL*) phase loop system for the measurement of the instantaneous and mean frequencies of the Doppler signal. X_1, X_2 – multiplying systems, S – summator, N – transmitter, F_1 – low-pass filter after demodulation, F_2 – low – pass filter after sampling, $G\omega_0$ – carrier frequency generator, $G\omega_p$ – generator of the centre frequency of the system *VCO*, *UP* – sampling and hold units, *PD* – phase detector, LPF_1 – low-pass filter in the *PLL* system, LPF_2 – filter averaging the instantaneous frequency, *VCO* – voltage controlled oscillator $u_s'(t)$, $u_s''(t)$ – quadrature Doppler signals, ω_c – instantaneous frequency of Doppler signal, $\overline{\omega_c}$ – mean frequency of Doppler signal

The classical pulsed Doppler flowmeter demodulates, samples and filters the high-frequency signal detected in two independent channels shifted in phase by $+90°$, or $-90°$, depending on the flow direction. The two low-frequency signals thus obtained, $u_s'(t)$ and $u_s''(t)$, called quadrature signals, are fed

to the detector of instantaneous frequencies through a single side band modulation system, consisting of the multiplying units X_3 and X_4, and the sumator S. The task of this system is to shift the spectrum of the Doppler signal described by $u_s'(t)$ and $u_s''(t)$ towards higher frequencies, while retaining information on the flow direction. The new carrier frequency ω_p corresponds to the frequency of the generator *VCO* at zero control voltage.

The phase loop system itself consists of three functional units: the phase detector *PD*, the low-pass filter LPF_1 and the voltage controled oscillator *VCO* with its frequency depending on the control voltage. The principle of the operation of the system is also such control of the frequency of the generator *VCO* so that the phase difference between the input and the generated signals would be constant. To that end, use is made of voltage in the direct proportion to the phase difference between the input signal and the generator signal. This error signal generated by the phase detector *PD*, controls through the filter LDF_1 the generator frequency in such a way as to minimize the deviations from the static — equal to $\pi/2$ — phase difference between these signals. When the instantaneous phase difference between the two signals does not exceed the interval $\pi/2 \pm \pi/2$, the system remains closed, i.e. the constant component of the control voltage of the generator *VCO* corresponds to the frequency of the input signal. To obtain and maintain the closed state, it is necessary to match the parameters of the system to the properties of the input signal observed.

3. Measurements

The purpose of the measurements was to compare the experimentally obtained instantaneous frequency probability distributions with the theoretical curves obtained from formula (1).

The quadrature Doppler signals, $u_s'(t)$ and $u_s''(t)$, from the pulsed Doppler flowmeter manufactured at the CNRS ER 248 Laboratory were recorded on magnetic tape. The measurements were carried out for two stationary flows in a rigid pipe with 16 mm internal diameter. The transducer diameter was 16 mm, the sample volume was set on the flow axis. One of the flows investigated was laminar with the Reynolds number $Re = 700$, and the other was turbulent $Re = 5000$.

Fig. 2 shows a schematic diagram of the measurement system used to determine the probability distributions of the instantaneous frequency of the signal. The quadrature Doppler signals, $u_s'(t)$ and $u_s''(t)$, were fed to the instantaneous frequency detector, based on a *PLL* system. The voltages occurring at the output ω_c (Fig. 1) of this system were sampled by the *A/D* convertor at a frequency of 50 kHz and introduced to the computer memory.

Further signal processing was carried out in a software manner. The programme elaborated by the authors analyzed successively the input data in order to produce a histogram from them. Points on the instaneous frequency axis, ω_c, correspond to the discrete voltages fed to the computer (Fig. 3). The

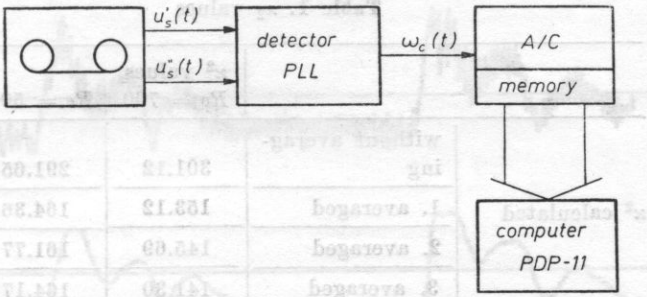

Fig. 2. A schematic diagram of the measurement system for the calculation of a listogram of the instantaneous frequencies of a Doppler signal

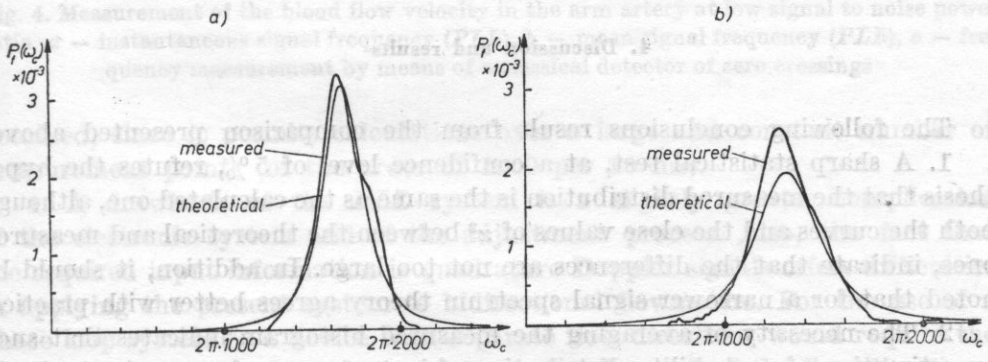

Fig. 3. Probability distributions p of the instantaneous frequencies of a Doppler signal — measured results (histogram), — — — — theoretical results, calculated from formula (1); a — laminar flow ($Re = 700$), b — turbulent flow ($Re = 5000$)

y-axis describes the number of times the given voltage, representing the respective instantaneous frequency, occurred in the signal recorded. Each of these values is divided by the total number of the samples analyzed so as to normalize the distributions obtained. The histograms thus obtained were smoothed by local averaging, i.e. each value of the original histogram was replaced by the arithmetic mean of five values — the one currently calculated and the two adjacent ones on both sides.

The measured curves shown in Fig. 3 were smoothed by using the method presented above, three times in succession. In order to compare the theoretical and measured curves, the $\varkappa^2$ statistical test was used. When the value of $\varkappa^2$, calculated as a function of the difference between the theoretical and measured

curves, is less than a specific constant value, it can be accepted that the theoretical curve represents a correct description of the phenomenon, the observation of which was the basis for determining the measurement curve.

Table 1 represents a comparison of the calculated and theoretical $\varkappa^2$ values.

Table 1. $\varkappa_2$ values

		$\varkappa^2$ values $Re = 700$	$Re = 5000$
$\varkappa^2$ calculated	without averaging	301.12	291.65
	1. averaged	153.12	164.36
	2. averaged	145.69	161.77
	3. averaged	141.30	164.17
$\varkappa^2$ theoretical	$\varkappa^2$ at 5% confidence level	101.67	101.67

4. Discussion and results

The following conclusions result from the comparison presented above:

1. A sharp statistical test, at a confidence level of 5%, refutes the hypothesis that the measured distribution is the same as the calculated one, although both the curves and the close values of $\varkappa^2$ between the theoretical and measured ones, indicate that the differences are not too large. In addition, it should be noted that for a narrower signal spectrum theory agrees better with practice.

2. The necessity of averaging the measured histogram indicates that such an estimation of probability distribution of instantaneous frequencies is slowly convergent. Each of the histograms presented (Fig. 3, Table 1), is the result of calculations for 8000 measurement points.

In practical implementation, one should count on gathering about 20×10^{-3}s 50×10^3 Hz $= 1000$ measurement points over 20 ms, at a sampling frequency of 50 kHz. A higher sampling frequency is not justified. Therefore, it should be surmised that, in order to obtain good estimation of the mean value and the instantaneous frequency probability distribution width, it would be necessary to average results over a few cardiac cycles. The $\varkappa^2$ test results shown in Table 1 show that it is very interesting to use local histogram averaging. Perhaps, this operation can to a large extent replace averaging results for successive cardiac cycles, although the lack of theoretical elaborations makes it difficult to draw motivated conclusions here.

3. By comparing the features of the phase loop system with a classical detector of zero crossings, it is indicated that it has the following advantages:

— better performance at low signal to noise ratios, as illustrated by Fig. 4;

— when applied to the analysis of the flow nature, the phase loop permits the measurement of the parameters of the signal which are related directly to its spectrum by relations (1) and (2), and ensures greater stability of the results

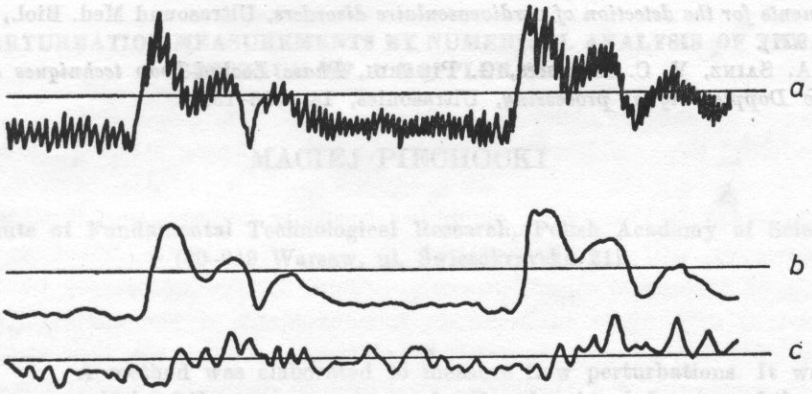

Fig. 4. Measurement of the blood flow velocity in the arm artery at low signal to noise power ratio. *a* — instantaneous signal frequency (*PLL*), *b* — mean signal frequency (*PLL*), *c* — frequency measurement by means of a classical detector of zero crossings

obtained, since it permits calculations over a large and constant number of measurement points (of the order of 1000 per 20 ms).

4. A drawback of the *PLL* system is a slightly greater complication of the electronic system and of the adjustment process. Also, the fact that the required input information is quadrature Doppler signals offers difficulties in applying the present system to bidirectional flowmeters. For the use of a phase loop system to a device with separate flow directions would require the formation of additional quadrature components for each of the flow directions.

Despite these difficulties, the phase loop system can be applied in Doppler diagnostic equipment, in particular where the measurement of flow perturbations is significant or where the signal to noise ratio is low.

Acknowledgment. The authors are grateful to Prof. L. FILIPCZYŃSKI for a discussion of the paper and a number of valuable pieces of advice.

References

[1] B. A. J. ANGELSEN, *Instantaneous frequency, mean frequency and variance of mean frequency estimators for ultrasonic blood velocity Doppler signals*, IEEE Trans. on Biomed. Enging., **28**, 11 (1981).

[2] B. A. J. ANGELSEN, *Spectral estimation of a narrow-band gaussian process from the distribution of the distances between adjacent zeros*, IEEE, Trans. Biom. Enging., **27** (1980).

[3] W. R. BRODY, I. D. MEINDEL, *Theoretical analysis of the C. W. Doppler ultrasonic flowmeter*, IEEE, Trans. Biom. Enging., **21**, 3, 183–192 (1974).

[4] P. M. BROWN, K. W. JOHNSTON, M. KOSSAM, R. S. COBBOLD, *A critical study of ultrasound Doppler spectral analysis for detecting carotid disease*, Ultrasound in Med. Biol., **8**, 5, 515–523 (1982).

[5] F. K. FORSTER, *The applications and limitations of Doppler spectral broadening measurements for the detection of cardiovasculaire disorders*, Ultrasound Med. Biol., **38**, 1223–1226 (1977).

[6] A. SAINZ, V. C. ROBERTS, G. PINARDI, *Phase Locked-Loop techniques applied to ultrasonic Doppler signal processing*, Ultrasonics, 14, 128–132.

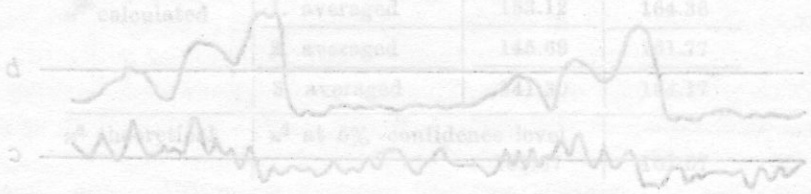

ARCHIVES OF ACOUSTICS
10, 3, 281–302 (1985)

FLOW PERTURBATION MEASUREMENTS BY NUMERICAL ANALYSIS OF THE POWER SPECTRUM OF A DOPPLER SIGNAL

MACIEJ PIECHOCKI

Institute of Fundamental Technological Research, Polish Academy of Sciences
(00–049 Warsaw, ul. Świętokrzyska 21)

A method was elaborated to measure flow perturbations. It was based on analysis of the power spectrum of a Doppler signal. In view of the simplifications assumed, it concerns pulsed flowmetres. The process of the formation of the Doppler signal is described mathematically, its power spectrum is calculated. A numerical model of the signal power spectrum is pressented. It has been constructed to calculate the effect of the gradient of the mean velocity in the sample volume, and also to determine the effect of the passage of blood particles through the sample volume on the shape of the power spectrum.

This model was verified experimentally. On the basis of it, a corrected turbulence index was proposed. This index describes with greater precision the flow perturbations.

1. Introduction

The introduction of measurements of the degree of the perturbation into diagnostic studies of the circulatory system results from a tendency to expand the application range of Doppler flowmeters, by fuller use of information on the flow contained in the signal obtained. The measurement of perturbations permits the quantization of the flow properties, which are now evaluated qualitatively from the detection of Doppler signals. The published investigations confirm the usefulness of such a measurement in studies on the stenosis of blood vessels and on the intra-operational investigations of the correctness of the vessel reconstruction [5, 8].

The commonly applied measure of the flow perturbation is the so-called turbulence index, defined as the percentage ratio between the standard deviation and the mean frequency of the power spectrum of a Doppler signal or its time interval histogram [5, 8].

In considerable approximation, it is assumed that if the velocity measurement is carried out with a sample volume that is small compared with the size of a vessel, the indices mentioned above correspond approximately to the ratio between the standard deviation of the instantaneous velocity oscillation and the mean velocity in the area studied. For laminar flow, the value of the turbulence index should, therefore, be zero [8]. Unfortunately, the interpretation given here is only too oversimplified. For, in practice, the values of the turbulence index never drop down to zero, as the width of the power spectrum also depends on factors other than flow perturbation. Because of this, the indices presented here are hardly sensitive to the real magnitude of flow perturbations.

Another essential problem, occurring for flow perturbation measurements, which, however, will be reflected here, is the difficulty in obtaining accurate estimation of a Doppler signal power spectrum for real, pulsating blood flows. This involves difficulties in accurate measurement of the turbulence index.

The aim of this paper is to analyze relations between the flow studied and the power spectrum of a Doppler signal and to develop a method permitting a more precise flow perturbation measurement than that allowed by the turbulence index. It was assumed that the shape of the sample volume and the distribution of the mean velocity inside this volume can be just any.

The process of the generation of the Doppler signal was described and its power spectrum calculated in order to determine factors defining the parameters of this spectrum. The dependencies obtained permitted the construction of an approximate, numerical method for the calculation of the power spectrum and its parameters, based on measurements of the mean flow velocity profile in a vessel and the parameters of the flowmeter. By comparing the power spectrum, measured for a given signal and a synthesized one, we can conclude on the existence of flow perturbations.

A numerical model of the power spectrum of a signal is also the basis for the introduction of an improved turbulence index, proposed in this paper. This index is defined in a way that is slightly different than that given in the literature. From the spectrum variance the effects are detracted which are related to the factors expanding the spectrum, and not connected with the flow perturbations. The detracted values can be determined numerically from measurements of the shapes of the samples volumes and the mean profiles of the flow velocity.

2. Signal generation process

The description of the signal generation process aims at obtaining a mathematical form of a Doppler signal, depending on the properties of the investigated flow and on the parameters of the equipment. This description provides the

basis for calculating the signal power. To that end, analysis was successively performed on operations implemented by a typical Doppler flowmeter (Fig. 1) and on the effect of these operations on the final form of the signal.

The following assumptions were made:

1. The signal detected by the transducer is the sum of independent dissipations from randomly placed particles.

2. The amplitudes and phases of scattered waves are random.

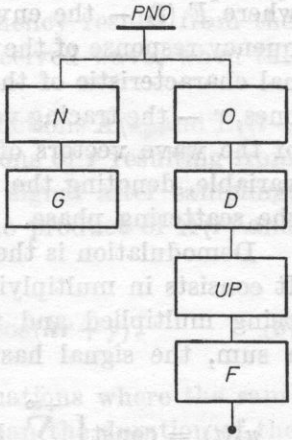

Fig. 1. A simplified schematic diagram of a flowmeter with pulsed emission. *G* — generator, *N* — transmitter, *O* — receiver, *D* — demodulator, *UP* — sampling unit, *F* — low-pass filter, *PNO* — transmit-receive transducer

3. All the scatterred waves, giving significant components of a signal with respect to the noise field, come from the nearest sample volume.

4. The sample volume is so small and far from the transducer that the scattered waves reaching the transducer can be recognized as plane.

5. The velocity of the scattering particles is constant in the course of passing through the sample volume and is parallel to the flow axis.

The first two assumptions are generally assumed in the analysis of a Doppler signal [16, 24] and lead to a random model of this signal.

A third assumption aims at avoiding the components of the signal which do not come from the sample volume and which can occur as a result of the known phenomenon of ambiguity in the measurement of distance by the impulsed apparatus [10].

The fifth assumption is satisfied for laminar flow in straight vessels. For perturbed flows, it is reduced to the requirement that the sample volume should be respectively small.

For a pulsed flowmeter, the voltage exciting the transmitter transducer to vibrate has the form:

$$x(t) = \sum_{n=-\infty}^{+\infty} E(t-n\tau_p)\cos\omega_0(t-n\tau_p), \qquad (1)$$

where $E(t)$ — the envelope of the transmitted impulse, ω_0 — the working frequency of the flowmeter, τ_p — the repetition period of the transmitted impulse. Thus, the signal $x(t)$ is an infinite sum of the identical pules.

With the given assumptions, the voltage at the receiving transducer, generated by the sum of waves scattered by a single particle, is expressed by

$$u_0(t) = \text{const}\Big[\sum_{n=-\infty}^{+\infty} E_1(t-n\tau_p-\boldsymbol{kr}/\omega_0)\Big]\, aA(\boldsymbol{r})\cos(\omega_0 t-\boldsymbol{kr}+\gamma), \tag{2}$$

where $E_1(t)$ — the envelope of the transmitted impulse, modified by the frequency response of the transducer at detection; $A(\boldsymbol{r})$ — the resultant directional characteristic of the transducer, made up of the transmitted and received ones, $\boldsymbol{r}$ — the tracing vector of the particle, describing its position, $\boldsymbol{k}$ — the sum of the wave vectors of the transmitted and scattered waves, a — a random variable, denoting the scattering amplitude, γ — a random variable denoting the scattering phase.

Demodulation is the first operation carried out on the received signal $u_0(t)$. It consists in multiplying the signal by a sinusoid at the frequency ω_0. After being multiplied and transforming the product of the cosine function into a sum, the signal has the form

$$u_d(t) = \text{const}\Big[\sum_{n=-\infty}^{+\infty} E_1(t-n\tau_p-\boldsymbol{kr}/\omega_0)\Big]\, aA(\boldsymbol{r})\times$$

$$\times 1/2\,[\cos(-\boldsymbol{kr}+\gamma)+\cos(2\omega_0 t-\boldsymbol{kr}+\gamma)]. \tag{3}$$

It is the sum of two components. The first, related to $\cos(\boldsymbol{k}, \boldsymbol{r}+\gamma)$, which changes slowly (through the dependence of $\boldsymbol{r}$ on time), is the one of interest. The other, related to the curve of a double carrier frequency $2\omega_0$, can easily be filtered off, without losing information on the particle velocity. Thus, the final result of the demodulation will have the form

$$u_d(t) = \text{const}\Big[\sum_{n=-\infty}^{+\infty} E_1(t-n\tau_p-\boldsymbol{kr}/\omega_0)\Big]\, aA(\boldsymbol{r})\cos(\boldsymbol{kr}-\gamma). \tag{4}$$

Sampling operation

Another operation which is performed on a signal in a pulsed flowmeter is signal sampling in order to define the depth at which its analysis is carried out. This sampling will be written as a multiplication of the signal $u_d(t)$ by the sampling function $f_p(t)$, which is a periodic function with the period τ_p. Let us now introduce a delay t_r of this function with respect to the transmitter, correspond-

ing to the depth analysed. The form of the signal is, after the operation of sampling, given by the following formula

$$u_p(t) = \text{const}\Big[\sum_{n=-\infty}^{+\infty} f_p(t-n\tau_p-t_r)E_1(t)-n\tau_p-\boldsymbol{kr}/\omega_0)\Big]\times$$
$$\times aA(\boldsymbol{r})\cos(\boldsymbol{kr}+\gamma). \quad (5)$$

It is usually assumed that the sampling function is a sequence of Dirac impulses $\delta(t)$. The time difference between particular samples equals the repetition period of the transmitter impulses. The filling is a sinusoidal function with a frequency coresponding to the movement of a particle. This frequency results from the Doppler effect, i.e., a change in the frequency of the received wave, when the source or observer moves.

The envelope of the signal $u(t)$ is the product of the functions $A(\boldsymbol{r})$ and $E_1(t-$ $-n\tau_p-\boldsymbol{kr}/\omega_0)$ for $t = n\tau_p+t_r$ and the successive positions of $\boldsymbol{r}$ resulting from the movements of a particle. Thus, in describing the signal after sampling, we can introduce the function $H(\boldsymbol{r}, t_r)$, representing the product of $A(\boldsymbol{r})$ and $E_1(t-n\tau_p-\boldsymbol{kr}/\omega_0)$ for $t = n\tau_p-t_r$, namely:

$$u_p(t) = \text{const}\Big[\sum_{n=-\infty}^{+\infty}\delta(t-n\tau_p-t_r)\Big]\, aH(\boldsymbol{r}, t_r)\cos(\boldsymbol{kr}+\gamma). \quad (6)$$

However, in practice, we meet quite frequently situations where the sampling duration (when $f_r(t) \neq 0$) is equal to or greater than the duration of the transmitted impulse (when $E_1(t) \neq 0$). In practical solutions, as a rule systems calculating the mean value of a sample and memorizing it until the next value comes are used. Such a solution maximizes the energy contained in the spectrum concentrated around zero with respect to the remaining replications. By introducing the averaging process into our notation, we can simplify it. Thus, again, for a constant time delay we can define the function $H(\boldsymbol{r}, t_r)$ describing the envelope of the signal $u_p(t)$ defined by a change in the position of a particle [14].

$$H(\boldsymbol{r}, t_r) = \int_{-\infty}^{+\infty} f_p(\tau)E_1(\tau+t_r-\boldsymbol{kr}/\omega_0)\,d\tau A(\boldsymbol{r}). \quad (7)$$

Again, the signal after the sampling operation can be written in the form of a sequence of impulses set for $\tau = 0$,

$$u_p(t) = \text{const}\Big[\sum_{n=-\infty}^{+\infty}\delta(t-n\tau_p-t_r)\, aH(\boldsymbol{r}, t_r)\cos(\boldsymbol{kr}-\gamma). \quad (8)$$

The final form of the Doppler signal

The function $H(\boldsymbol{r}, t_r)$ describes the effective, from the viewpoint of the spectrum of the signal received, distribution of acoustic energy in space, which is usually called the sample volume. In further considerations, the parameter

t_r will be regarded as constant, i.e., the position of the sample volume in the flow field will be considered constant.

In order to obtain the total signal form after sampling it is necessary to sum up the contributions coming from all the particles. This procedure results from the independence of particular scatterings. The summary signal at the input of the sampling system will thus have the form

$$u_s(t) = \text{const}\Big[\sum_{n=-\infty}^{+\infty} \delta(t-n\tau_p-t_r)\Big]\Big[\sum_{i=1}^{N} a_i H(\boldsymbol{r}_i)\cos(\boldsymbol{k}\boldsymbol{r}+\gamma_i)\Big], \tag{9}$$

where N is the number of particles occurring at the same time in the sample volume.

The position of the particle $\boldsymbol{r}_i$ is a function of time. We assumed that the particle velocity $\boldsymbol{v}_i$ was constant and parallel to the flow axis as the particle flowed through the sample volume. The position of the particle can be given as

$$\boldsymbol{r}_i = \boldsymbol{r}_i^0 + \boldsymbol{v}_i t, \tag{10}$$

where $\boldsymbol{r}_i^0$ is the tracing vector of the particle for the time $t = 0$. The product of the position $\boldsymbol{r}$ and the wave vector $\boldsymbol{k}$ equals that of the Doppler frequency and time.

In addition, we can introduce the notation

$$a_i = \boldsymbol{k}\boldsymbol{r}_i^0. \tag{11}$$

a_i is a random variable with a distribution related to the distribution of the initial position of the particle in the sample volume, which from the assumption is taken as uniform.

Thus, the signal takes the following form:

$$u_s(t) = \text{const}\Big[\sum_{n=-\infty}^{+\infty} \delta(t-n\tau_p-t_r)\Big]\Big[\sum_{i=1}^{N} a_i H(\boldsymbol{r}_i)\cos(\omega_i t+a_i+\gamma_i)\Big]. \tag{12}$$

In this equation, the quantities a_i, a_i, γ_i, ω_i and $\boldsymbol{r}_i$ are random variables. The signal $u_s(t)$ (formula (12)) is the sum of functions of these quantities. Since the number of the factors summed up is very large (N is of the order of 10^6), and the probability distributions for each component of it are the same, $u_s(t)$ is a random, approximately Gaussian, process. For this process to be stationary, i.e., for the probabilistic quantities related to it to be constant in time, the flow field must be stationary. In addition, we assume that this is an ergodic process — where the values averaged over the set equal respectively the corresponding values averaged in time. In these conditions, all the information available on this process is contained in its second-order characteristics, i.e., in the auto-correlation function or the power spectrum.

Thus, to obtain maximum information on this flow, we should look for it in one of these measured characteristics. Such a solution would require, however, an extremely complicated measurement equipment and a good theoretical description of the process of spectrum formation.

3. Analysis of the signal power spectrum

To define the form of the power spectrum of the signal $u_s(t)$, we assume a definition of the power spectrum which is quite often used in technology:

$$S(\omega) = \lim_{T\to\infty} \frac{1}{2T} \left| \int_{-T}^{T} u_s(t) \exp(-j\omega t)\, dt \right|^2, \tag{13}$$

where $u_s(t)$ is the time form of the signal and $S(\omega)$ is the power spectrum of the signal.

For the signal $u_s(t)$ (formula (12)) $S(\omega)$ is expressed as

$$S(\omega) = \lim_{T\to\infty} \frac{1}{2T} \left| \int_{-T}^{T} \text{const} \left[\sum_{n=-\infty}^{+\infty} \delta(t - n\tau_p - t_r) \right] \left[\sum_{i=1}^{N} a_i H(\boldsymbol{r}_i) \times \right. \right.$$

$$\left. \left. \times \cos(\omega_i t + a_i + \gamma_i) \exp(-j\omega t)\, dt \right| ^2 . \right. \tag{14}$$

The first term (under the integral) of the signal, which contains the sum of the Dirac impulses, corresponds to the signal sampling. In the spectral representation, it involves the existence of successive copies of the spectrum of the second term, which are distant by

$$\omega_p = 2\pi \frac{1}{\tau_p}. \tag{15}$$

By assuming that the spectrum of the second term describing the signal is limited and zero for $\omega > \omega_p/2$, we only consider the spectrum concentrated round the pulsation equal to zero. It corresponds to the practical signal filtration narrowing its band to the useful interval $(0; \omega_p/2)$. Thus, we obtain

$$S(\omega) = \lim_{T\to\infty} \frac{1}{2T} \left| \int_{-T}^{T} \text{const} \left[\sum_{i=1}^{N} a_i H(\boldsymbol{r}_i) \cos(\omega_i t + a_i + \gamma_i) \times \right. \right.$$

$$\left. \left. \times \exp(-j\omega t)\, dt \right| ^2 . \right. \tag{16}$$

Let us denote the terms which we achieve as the integral has been introduced under the sum sign as

$$F_i(j\omega) = \left| \int_{-T}^{T} a_i H(\boldsymbol{r}_i) \cos(\omega_i t + a_i + \gamma_i) \exp(-j\omega t)\, dt \right|^2. \tag{17}$$

By substituting this determination in formula (16) and calculating the squared modulus of the sum, we obtain

$$S(\omega) = \text{const} \lim_{T\to\infty} \frac{1}{2T}\left[\sum_{i=1}^{N} R_2^2 F_i(j\omega) + \sum_{i=1}^{N} \operatorname{Im}^2 F_i(j\omega)\right] +$$

$$+ \lim_{T\to\infty} \frac{1}{2T}\left(\sum_{k=1}^{N}\sum_{i=1}^{N} [\operatorname{Re} F_k(j\omega) \operatorname{Re} F_i(j\omega) + \operatorname{Im} F_k(j\omega) \operatorname{Im} F_i(j\omega)]\right). \quad (18)$$

The second term in formula (18) applies to the products of functions of independent scatterings and is zero.

Thus, the signal spectrum becomes

$$S(\omega) = \text{const} \lim_{T\to\infty} \frac{1}{2T} \sum_{i=1}^{N} a_i^2 \left| \int_{-T}^{T} H(\boldsymbol{r}_i) \cos(\omega_i t + a_i + \gamma_i) \exp(-j\omega t)\, dt \right|^2. \quad (19)$$

For our signal the operation of passing to the limit in time causes the fact that the number of particles giving the spectral components should tend to infinity. And the integrals in formula (19) will tend to the Fourier transforms of the subintegral functions. These transforms exist, as the subintegral functions are limited in time in view of the bounded dimensions of the sample volume. Thus, the components of the sum can be replaced by the squared moduli of the respective Fourier transforms. We denote as $\mathscr{F}$ the Fourier transformation. By calculating the squared modulus of the Fourier transform of the subintegral function, on the assumption that $\mathscr{F}[H(\boldsymbol{r}_i) = 0]$ for $|\omega| > \omega_i$ we obtain the dependence

$$|\mathscr{F}[H(\boldsymbol{r}_i)\cos(\omega_i t + a_i + \gamma_i)]|^2$$
$$= |\mathscr{F}[H(\boldsymbol{r}_i)]|^2 * \delta(\omega + \omega_i) + |\mathscr{F}[H(\boldsymbol{r}_i)]|^2 * \delta(\omega - \omega_i). \quad (20)$$

The sum from formula (18) should be extended to all particles flowing through the sample volume in the measurement time. We shall denote it as a boundary transition, by designating as M the number of particles which are summed up. We replace the normalising factor $1/T$ by $1/M$. Since the random variable a_i is, when squared, averaged, and its mean square value $\overline{(a^2)}$ can be made part of the constant term, we obtain

$$S(\omega) = \text{const} \lim_{M\to\infty} \frac{1}{M} \sum_{i=1}^{M} \left(|\mathscr{F}[H(\boldsymbol{r}_i)]|^2 * \delta(\omega + \omega_i) + |\mathscr{F}[H(\boldsymbol{r}_i)]|^2 * \delta(\omega - \omega_i)\right), \quad (21)$$

or otherwise

$$S(\omega) = \text{const}\left(\lim_{M\to\infty} \frac{1}{M} \sum_{i=1}^{M} |\mathscr{F}[H(\boldsymbol{r}_i)]|^2 * \delta(\omega + \omega_i) + \right.$$
$$\left. + \lim_{M\to\infty} \frac{1}{M} \sum_{i=1}^{M} |\mathscr{F}[H(r_i)]|^2 * \delta(\omega - \omega_i)\right). \quad (22)$$

The signal power spectrum, expressed by formula (22), consists of two identical and separate, in view of the assumption $\mathscr{F}[H(\boldsymbol{r}_i)] = 0$ for $|\omega| > \omega_i$, components situated on the pulsation axis symmetrically with respect to zero.

In the further part, considerations will be limited to one of those components only, ie., the one on the positive semi-axis of pulsation, so as to shorten the notation of the formula. In addition, we shall neglect the constant proportionality factor. Thus, we obtain the simple form of the spectrum:

$$S(\omega) = \lim_{M\to\infty} \frac{1}{M} \sum_{i=1}^{M} |\mathscr{F}[H(\boldsymbol{r}_i)]|^2 * \delta(\omega - \omega_i). \tag{23}$$

The next transformation executed here is now strictly related to the numerical nature of the description of the spectrum to be constructed. The continuous velocity axis will be replaced by a discrete one. I.e., we assume that the velocity, and, thus, the Doppler frequency, will take a finite number of values, whereas the two adjacent quantities differ by a finite quantity, called the discretization step.

This way of frequency representation permits the next spectrum transformation to be carried out. Among the components of the sum represented in formula (23), let us choose those in which the Doppler frequency ω_k is the same. They are the components of the spectrum from particles moving at the same velocity. First, the separability of the convolution operation with respect to addition permits us to sum up the contributions from these factors, and then convolute the result with the Dirac delta, corresponding to this frequency. For the velocity v_k the summation result will be:

$$\delta(\omega - \omega_k) * \left(\lim_{M_k\to\infty} \frac{1}{M_k} \sum_{i=1}^{M_k} |\mathscr{F}[H(\boldsymbol{r}_i)]|^2 \right). \tag{24}$$

To get the whole spectrum, the above contributions must be summed up for all velocities:

$$S(\omega) = \sum_{k=1}^{L} \left\{ \delta(\omega - \omega_k) * \left(\lim_{M_k\to\infty} \frac{1}{M_k} \sum_{i=1}^{M_k} |\mathscr{F}[H(\boldsymbol{r}_i)]|^2 \right) \right\}, \tag{25}$$

where L is the number of discrete values of velocity in the vessel.

In the spectral form, the internal sum according to the index i represents the effect of a passage through the sample volume of particles at velocity corresponding to the frequency ω_k. Indeed, a time change in $\boldsymbol{r}_i$ corresponds to the particle path through the sample volume, while $H(\boldsymbol{r}_i)$ describes a change in the scattered acoustic energy in passing through the sample volume. The external sum, according to the index k corresponds to the summation of the effects for all the particle motion velocities existing in the sample volume.

We can note that the existence of a large number of velocities in the sample volume can result from the presence of a specific velocity profile in the vessel.

It can also result from instantaneous velocity oscillations related to the flow perturbations. Since the estimation of the signal spectrum directly from its temporary form, as used here and applied generally in analysing equipment, requires a very long observation time, it is not possible to distinguish between the contributions from the velocity gradient and the instantaneous oscillations. In other words, having only the signal spectrum, we cannot say whether there are instantaneous velocity perturbations, since the effect of a constant velocity gradient on the spectrum can be the same. To be able to make this distinction, we must have more information on the flow. Let us assume that we know the mean velocity profile in the sample volume, for such a profile can be measured by a pulsed flowmeter in the same time in which we collect data for spectral analysis. Knowing the flow profile in the vessel the position and shape of the measurement volume, we can, e.g. by numerical calculations, try to find the spectrum $S(\omega)$ of the signal, by calculating successively the functions $H(\boldsymbol{r}_i)$ and their Fourier transforms. In practice, it is, however, very difficult, mainly because of the geometrical complexity of the function $H(\boldsymbol{r}_i)$. Let us then use approximations. First, we shall calculate the energy distribution of scattered waves as a function of velocity. In other words, for each frequency ω_k, some distribution of the power of the scattered wave $B_k(\omega)$

$$B_k(\omega) = \lim_{M_k \to \infty} \frac{1}{M_k} \sum_{i=1}^{M_k} |\mathscr{F}[H(\boldsymbol{r}_i)]|^2, \tag{26}$$

caused by the effect of particles passing through the sample volume, will be replaced by a line of the same power from the appropriate distribution.

$$P_k = \int_{-\infty}^{+\infty} B_k(\omega)\, d\omega. \tag{27}$$

Thus, the power distribution of scattered waves as a function of velocity is given by the formula

$$S_G(\omega) = \sum_{k=1}^{L} P_k \delta(\omega - \omega_k), \tag{28}$$

for each of the frequencies ω_k is, from the Doppler formula, related to the the respective velocity v_k.

Let us note that distribution (28) would correspond to the spectrum of the Doppler signal if we neglected the effect of the finite time of the particle passage through the sample volume. For if $H(\boldsymbol{r}_i)$ were functions changing very slowly in time, their spectra would be very strongly concentrated close to zero, i.e., equal practically to the constants P_k introduced here. This would require that the width of the spectrum of the function $H(\boldsymbol{r}_i)$ should be negligible with respect to the quantities ω_k.

4. Numerical model synthesis

The spectrum analysis is now at a moment where as a result of the simplifications used, it is easy to introduce numerical calculations, to calculate for known parameters the specific form of the power distribution of the received signal as a function of velocity (formula (28)).

It is easier to calculate this distribution in a way other than that resulting from the analysis carried out. Instead of following the paths of particular particles, we should calculate the sums of the powers existing at these points of the sample volume where the velocity is constant [14]. Since we cannot neglect the effect of the finite time of the particle passage through the sample volume, for it influences greatly the spectral shape, some approximation was added to the numerical calculations. To some limited extent, the flow perturbations will also be considered in the model built. Its construction will begin with representing an approximation of the particle passage effect (the transit time effect).

For each discrete value of the velocity v_k related to ω_k, we introduce an arbitrary approximation of this effect, as

$$B_k(\omega) = P_k N(0, \sigma_k), \tag{29}$$

where

$$N(0, \sigma_k) = \frac{1}{\sqrt{\sigma_k}} \exp(-\omega^2/2\sigma_k^2). \tag{30}$$

$N(0, \sigma_k)$ is thus a Gaussian function symmetrical with respect to zero, with a standard deviation σ_k.

For each velocity v_k the shape of the fuzziness of the power spectrum was approximated by a Gaussian curve. The coefficient P_k ensures equality of the total scattered power for each velocity v_k between our approximation and the exact value. We shall define intuitively the width of the Gaussian curve as an approximation of the transit time effect, expressed by σ_k, and then the value of the whole approximation will be verified experimentally.

It follows from considerations made in the conclusion of the previous section that for a given sample volume the width of fuzziness of the power spectrum is the greater the shorter the time spent by particles in the sample volume. Thus, this width should be proportional to the particle velocity and inversely proportional to the length of the particle path in the sample volume. The particle velocity is a known parameter. Unfortunately, it is difficult to determine the length of the particle path in the sample volume. However, it should be expected that the power P_k scattered by particles moving at the velocity v_k is related to the mean particle path length at this velocity in the sample volume. The deviation σ_k can thus be defined in the following way:

$$\sigma_k = \frac{v_k}{b(P_k)^{1/\beta}}, \tag{31}$$

where b and β are constant parameters determined experimentally from the dependence on the geometry of the sample volume. The above approximation resembles the one which Gabrini used successfully in [6].

For the purposes of our model of the Doppler signal spectrum, it is convenient to desscribe perturbed flow through the mean profile of this flow and instantaneous velocity fluctuations round this profile, Anyway, this description is accepted in fluid mechanics [17]. Let $\bar{v}_k$ denote the mean velocity in the elementary volume ΔV_i, resulting from the position of the sample volume with respect to the mean velocity profile in the vessel. We denote as $p_i(v)$ the probability that the instantaneous velocity $\mathrm{v} = \bar{v}_k + v$ occurs at this point. Thus, v denotes the difference between the instantaneous and mean velocities. We continue to maintain the assumption that the velocity is parallel to the axis of the vessel. For strongly perturbed flows, in stenotic vessels, and for pulsating flows, unfortunately, this assumption can deviate strongly from reality. When the measurement time is sufficiently long, the power scattered in the elementary fragment of the sample volume ΔV_i (Fig. 2), defined as $dH^2(\xi_i)$,

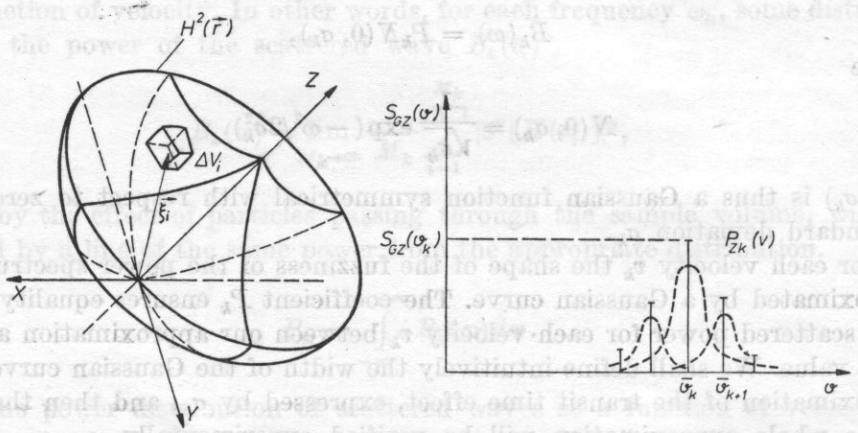

Fig. 2. The idea of the numerical calculations of the power spectrum of scattered waves as a function of velocity ΔV_i — the elementary fragment of the sample volume, $H^2(\boldsymbol{r})$ — the sample volume, $P_{zk}(v)$ — the probability distribution of the deviation of the instantaneous velocity by v from the mean velocity $\bar{v}_k$

is divided among all the velocities occurring in ΔV_i, in proportion to their occurrence frequency, defined by $p_i(v)$. The vector ξ_i denotes the position of each of the elementary fragments of the sample volume ΔV_i (Fig. 2). By summing up all the powers related to the given mean velocity $\bar{v}_k$, we obtain the magnitude of power related to this velocity:

$$P_{zk}(v) = \sum_{i=1}^{I_k} \Delta V_i dH^2(\xi_i) p_i(v). \tag{32}$$

Instead of the line of the power P_k, just as in the case of laminar flow, we obtain a certain distribution on the velocity axis. When $p_i(v)$ is constant, we obtain, in all the elementary volumes, where v_k is the same:

$$P_{zk}(v) = p_k(v) \sum_{i=1}^{I_k} \Delta V_i dH^2(\xi_i), \tag{33}$$

where $p_k(v)$ is the probability that v deviates from the mean velocity at those points where it equals $\bar{v}_k$. Thus, this probability is now related to the velocity profile and not to the space.

The latter formula can be changed to the form

$$P_{zk}(v) = p_k(v) P_k. \tag{34}$$

The values of P_k are defined by the sum in formula (33) and refer to the mean velocity profile. Thus, the power distribution of the Doppler signal as a function of velocity becomes

$$S_{Gz}(v) = \sum_{k=1}^{L} P_k p_k(v) * \delta(v - v_k). \tag{35}$$

This distribution contains two factors with a significant effect on the width and shape of the signal power spectrum. They are the flow perturbations and the existence of the mean velocity gradient in the measurement volume. It should be completed by the effect of the finite time of the particle passage. When the flow perturbations are not too large, we can approximate this effect, just as for laminar flow, from the mean velocity profile. Thus, just as we did previously, for each discrete value of the mean velocity $\bar{v}_k$ we introduce the Gaussian curve $N(0, \sigma_k)$ as its approximation. The standard deviation σ_k is defined as previously from formula (31), thus, it is based on the values of P_k defined by the mean flow profile. However, because of the existence of flow perturbations, the transit time effect will be divided among all the instantaneous velocities occurring round the mean $\bar{v}_k$ in proportion to their occurrence frequency, i.e., $p_k(v)$. This division of the transit time effect between the velocity distribution is expressed by a convolution of the functions $p_k(v)$ and $N(0, \sigma_k)$ for each mean velocity $\bar{v}_k$.

By transforming the velocity axis into the frequency one according to the Doppler formula, we obtain a complete approximation of the spectrum as

$$S_s(\omega) = \sum_{k=1}^{L} \left[P_k N(\omega_k, \sigma_k) * p_k(\omega) \right]. \tag{36}$$

Equation (36) is the final form of our model of the power spectrum of the Doppler signal.

5. Mean value and the standard deviation of frequency in the power spectrum

From the final form of the spectrum approximation, we can calculate its mean value and the standard deviation, in order to investigate the relationships between these quantities and the flow parameters.

We obtain, as the mean frequency in the spectrum,

$$\overline{\omega}_s = \frac{\int\limits_{-\infty}^{+\infty} \omega S_s(\omega)\, d\omega}{\int\limits_{-\infty}^{+\infty} S_s(\omega)\, d\omega} = \frac{\sum\limits_{k=1}^{L} P_k \omega_k}{\sum\limits_{k=1}^{L} P_k}. \tag{37}$$

In view of the direct relationship between ω_k and v_k, the mean frequency in the spectrum corresponds to the mean bulk velocity weighted in the sample volume. The weights P_k are defined by the power distribution in the sample volume and its position with respect to the flow profile. We can note that the mean frequency does not depend on the transit time effect or the possible perturbations. This results from our assumptions as to the effects mentioned above. In practice, some nonsymmetricities can certainly occur, as a result of the out-of-parrallel character of the velocity vectors with respect to the vessel axis and the nonsymmetricity of the transit effect $B_k(\omega)$, described by equation (26).

It is much more interesting to consider the result of the calculations of the standard deviation of the power spectrum. By calculating the variance of the spectrum $S_s(\omega)$, we obtain

$$\sigma_s^2 = \frac{\sum\limits_{k=1}^{L} P_k \omega_k^2}{\sum\limits_{k=1}^{L} P_k} - \overline{\omega}_s^2 + \frac{\sum\limits_{k=1}^{L} P_k \sigma_k^2}{\sum\limits_{k=1}^{L} P_k} + \frac{\sum\limits_{k=1}^{L} P_k \sigma_{pk}^2}{\sum\limits_{k=1}^{L} P_k}, \tag{38}$$

where σ_{pk}^2 is the variance of the distribution $p_k(\omega)$.

The expression describing the variance σ_S^2 of our approximation of the spectrum contains three distinguishable components. The first is the effect of the mean velocity gradient. We denote it as

$$\sigma_G^2 = \frac{\sum\limits_{k=1}^{L} P_k \omega_k^2}{\sum\limits_{k=1}^{L} P_k} - \overline{\omega}_s^2. \tag{39}$$

The variance σ_G^2 defines the spectrum width when the effect of the transit time and the flow perturbation are negligible. Another one, denoted by σ_T^2, is related

to the effect of the finite time of the particle passage through the sample volume:

$$\sigma_T^2 = \frac{\sum_{k=1}^{L} P_k \sigma_k^2}{\sum_{k=1}^{L} P_k}. \tag{40}$$

A third component in turn is related to the flow perturbations:

$$\sigma_Z^2 = \frac{\sum_{k=1}^{L} P_k \sigma_{pk}^2}{\sum_{k=1}^{L} P_k}. \tag{41}$$

Both σ_T^2 and σ_Z^2 are certain mean values of the influence of the effects of the transit time and flow perturbations, related to the power distribution in the sample volume and its position with respect to the mean profile of flow through the values of P_k.

By using the new notation, we can write the total variance of the spectrum as

$$\sigma_S^2 = \sigma_G^2 + \sigma_T^2 + \sigma_Z^2. \tag{42}$$

The numerical model presented here permits the calculation of the shape and parameters of the power spectrum and the separation of the contributions from the different factors to the spectrum, and, by it, also, an accurate measurement of the flow parameters, namely σ_{pk}^2. For we can, by identifying σ_S^2 through measurements, calculate the values of σ_G^2 and σ_T^2, and then calculate the value of σ_Z^2. When we assume that σ_{pk} is constant throughout the sample volume, σ_{pk} is equal to σ_Z.

6. Experimental studies on the model of the power spectrum of the Doppler signal

By using the numerical synthesis of the power spectrum of the Doppler signal given above, we calculated the spectra of a signal for laminar flows. The results obtained were compared with the measured results. Thus, we verified the calculations of the effect of the velocity gradient in the sample volume and the effect of the transit time on the shape and parameters of the spectrum.

Looking at the results we can say that the elaborated description of the Doppler signal corresponds well to reality. We observed, however, a certain difference between the mean frequencies of the measured and calculated spectra, which is absent from Figs. 3 and 4, for it was compensated for in the course of matching the peaks of respective curves. The existence of this difference can be explained by an inacuracy of the model and also by the differences

between the real and calculated positions of the sample volume, or by slow changes in the output of the pump in the course of recording signals. These differences were compensated for numerically by a change in the value of the maximum velocity used as the calculation parameter. We should point out that these differences were always smaller than 2.5% of the maximum velocity; thus, quite low.

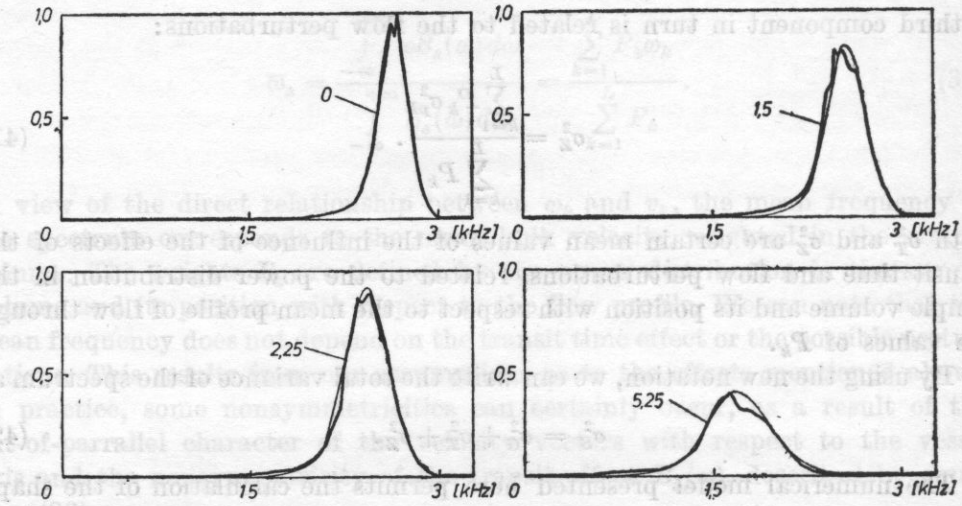

Fig. 3. The measured and calculated power spectra of the Doppler signal for flow with the Reynolds number $Re = 1450$. Thick line — measurements, thin line — calculations

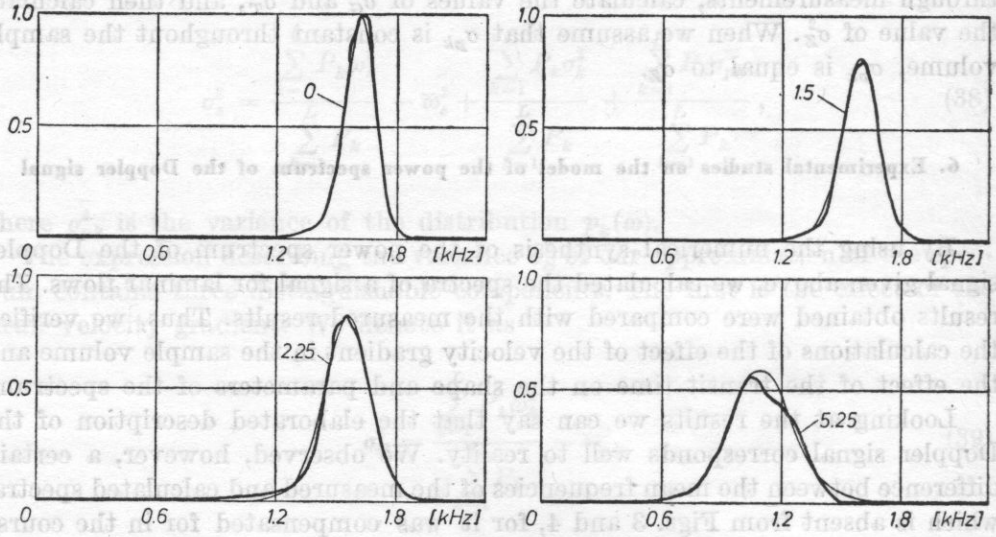

Fig. 4. The measured and calculated power spectra of the signal for flow with the Reynolds number $Re = 700$. Thick line — measurements, thin line —calculations

The parameters of the spectra shown in Figs. 3 and 4 are given in Table 1. It contains the mean values and the standard deviations of the measured spectra f_m and σ_m and the calculated ones, f_s and σ_s, and also the values of the relative errors between these quantities.

Table 1

Re	Sample volume position	f_m [Hz]	f_s [Hz]	[%]	σ_m [Hz]	σ_s [Hz]	[%]
1450	0	2619.30	2623.29	0.20	119.34	118.70	0.50
	1.5	2542.61	2536.71	0.17	159.89	148.98	6.82
	2.25	2543.70	2428.20	0.14	179.58	176.59	1.56
	5.25	1656.30	1666.80	0.63	231.64	232.55	0.39
700	0	1677.40	1616.50	0.17	77.01	173.31	4.80
	1.5	1610.20	1608.30	0.14	94.41	94.44	0.30
	2.25	1571.50	1571.40	0.01	114.28	113.53	0.66
	5.25	1091.90	1092.97	0.10	146.41	152.49	4.15

The differences between the parameters of the measurement curves and the results of a numerical synthesis of the spectrum, contained in Table 1, are random in nature. They suggest, however, the necessity for a more precise implementation of measurements. In the present case, the pipe wall caused a deformation in the sample volume with respect to the assumed symmetry. This explains perhaps the irregular shape of the spectra for the position "5.25" of the sample volume.

The experimental studies on the correctness of the model, though still distinctly incomplete, confirmed the usefulness of the approximation of the finite transite time effect. These studies confirm that the present model traces well the relative changes in the contribution in the spectrum width of the mean velocity gradient and the effect of the transit time.

7. Turbulence index

The achieved relationships between the parameters of the spectrum and the flow, (37) and (38), indicate that the initially discussed perturbation index, defined by the parameters of the spectrum, can significantly deviate from values characterizing the velocity distribution.

We now present the results of the application of the classical perturbation index and those obtained when using the corrected turbulence index in the case of the application of these indices for turbulent flow with a Reynolds number of 5000. As was mentioned above, equation (42) can serve in determining the effect of the flow parameters on the power spectrum. By transforming this

equation slightly, we obtain

$$\sigma_Z^2 = \sigma_S^2 - \sigma_T^2 - \sigma_G^2. \tag{43}$$

If we assume that the presented results of the verification of the model prove its correctness, the value of the calculated variance σ_S^2 is equal to the variance σ_m^2 which was measured. The sum of the variance σ_T^2 and σ_G^2 is the variance of the power spectrum for laminar flow with the same profile as the mean one of the perturbed flow under study. The value of this sum, denoted by σ_{SL}^2, can be calculated by means of our model. Thus, we obtain the following expression of the averaged flow perturbations, determined from formula (41),

$$\sigma_Z = \sqrt{\sigma_m^2 - \sigma_{SL}^2} \tag{44}$$

In other words, the expansion of the spectrum, caused by flow perturbations, equals a square root from the difference between the measured and calculated spectrum variances for the mean profile of perturbed flow.

Table 2 shows the values of the perturbation index, defined classically as σ_m/f_m, the index calculated from numerical results of σ_s/f_s and the values of the corrected perturbation index σ_Z/f_m.

Table 2

Re	Sample volume position	σ_m/f_m [%]	σ_{SL}/f_{SL} [%]	σ_Z/f_m [%]	$\frac{\sigma_Z}{f_m}\frac{\Delta\sigma_Z}{\sigma_Z}$ [%]
1450	0	4.56	4.52	0.47	±4.34
	1.5	6.29	5.87	2.28	±1.50
	2.25	7.38	7.27	1.30	±1.26
	5.25	13.99	13.95	1.24	±15.88
700	0	4.76	4.52	1.46	±1.42
	1.5	5.86	5.87	0.15	±23.61
	2.25	7.22	7.27	0.83	±6.26
	5.25	13.47	13.95	3.90	±4.99
5000	0	12.06	2.66	11.76	±0.59

It follows from the data given in Table 2 that for laminar flows under study, the values of the corrected perturbation index are, however, different from zero. It means a lack of correctness in evaluating the flow perturbations by means of this method. By analyzing the effect of error on the evaluation of perturbations, we can explain these inaccuracies.

From equation (44), we can determine the effect of the error involved in the calculations of the spectrum variance, on the effect of the error characteristic of the calculated flow perturbations:

$$\frac{\Delta\sigma_Z}{\sigma_Z} = \frac{1}{1-\sigma_m^2/\sigma_{SL}^2}\frac{\Delta\sigma_{SL}}{\sigma_{SL}}, \tag{45}$$

where $\Delta\sigma_Z/\sigma_Z$ is the relative error in evaluating the value of perturbations; $\Delta\sigma_{SL}/\sigma_{SL}$ is the relative calculation error.

Fig. 5 represents two curves illustrating this dependence on two different values of the ratio σ_m/σ_{SL}. For $\sigma_{SL} \ll \sigma_m$, the effect of the velocity gradient and the transit time effect on the spectrum variance is small compared with

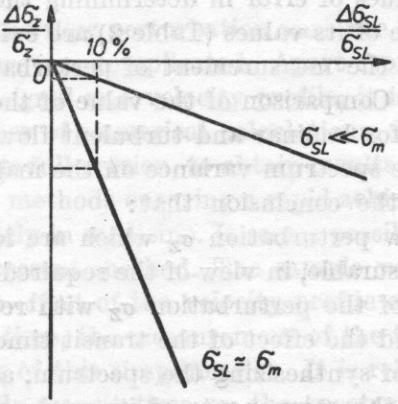

Fig. 5. The relative error of the calculation of the flow perturbation variance $\Delta\sigma_Z/\sigma_Z$ as a function of the relative error of numerical calculations $\Delta\sigma_{SL}/\sigma_{SL}$

the effect of perturbations. In this case, the calculation inaccuracy is hardly significant for the exactness of the perturbation determination. Unfortunately, in the opposite case, if perturbations are small compared with the other effects expanding the spectrum, $\sigma_m \simeq \sigma_{SL}$. Then, even small error in the calculation σ_{SL} causes error of as much as dozens of % in estimating the perturbation degree. In this case, the achieved magnitude of the corrected perturbation index can involve such significant error that it cannot be interpreted as a result of real flow perturbations.

On the basis of the relative differences between the values of σ_m and σ_S, in Table 1, we are justified in stating that the accuracy of the calculations of $\Delta\sigma_{SL}/\sigma_{SL}$ is better than 10%. With this assumption, error in estimating the magnitude of the corrected perturbation index was calculated from formula (44). The absolute value of this error was set in the last column of Table 2.

8. Discussion and conclusions

The conclusions from the application of the corrected perturbation index for the flows under study are as follows:

1. In keeping with the predictions from Section 3, the effect of the mean velocity gradient and that of the transit time on the spectrum is similar to the

effect of perturbations. Thus, the perturbation index is not unambiguously related to the flow perturbations. Its values obtained for the position "5.25" of the sample volume and laminar flow are greater than those for turbulent flow.

2. The corrected perturbation index determines much better the real perturbations in flow. However, it is much more complicated to calculate its value, requiring knowledge of the flow parameter, which the mean profile is.

3. The enormous values of error in determining the corrected perturbation index, obtained for some of its values (Table 2) are evidence of the low sensitivity of the method for the measurement of perturbations through spectrum variance measurements. Comparison of the value of the corrected perturbation index and its accuracy for laminar and turbulent flows, and also the analysis of the dependence of the spectrum variance on the magnitude of perturbations (formula (45)) lead to the conclusion that:

— values of the flow perturbation σ_Z which are low with respect to σ_{SL}, are particularly not measurable, in view of the required measurement accuracy;

— for large values of the perturbation σ_Z with respect to σ_{SL}, the effect of the mean gradient and the effect of the transit time are actually negligible.

The numerical way of synthesizing the spectrum, as presented here, makes it possible to calculate the components of its variance, corresponding to the contributions from the mean velocity gradient and the transit time effect. This permits the calculation of the mean variance of perturbations in the sample volume, from relation (42). It is also the basis for the evaluation and interpretation of the results of perturbation measurements, and also of the optimization of the parameters of equipment, depending on the measured flow parameters.

However, relation (38) is concerned with the variance of full spectrum distributions. In practice, we are forced, as a result of the occurrence of equipment noise, to fix the lower level to which the measured results are considered significant. This can introduce inaccurracies in using this relation, since, usually, the sum of the variances of cut-off distributions is different from the variance of the cut-off resultant distribution.

In the extreme cases, the present model reduces, for the laminar flow, to the forms described in the literature:

— when the transit time effect is negligible, the spectrum obtained from calculations corresponds to the velocity distribution in the sample volume [15];

— when the mean velocity gradient in the sample volume is negligible, the spectrum has the shape of a Gaussian function with its width proportional to the velocity. It corresponds to the results achived by GABRINI [6].

For perturbed flow, when the mean velocity gradient and the transit time effect are negligible, the shape of the spectrum corresponds to the occurrence frequency of the instantaneous velocity averaged over the sample volume. We can calculate the mean perturbation variance from in vivo measurements. The necessary data include:

a. the mean flow profile, which can be determined e.g. by a multi-gate pulsed flowmeter;

b. the position of the sample volume, which can be determined e.g. by selecting for the multi-gate analysis a signal from one gate of the profile-measuring equipment;

c. the shape of the sample volume which we can determine irrespective of the flow under study.

The calculations of the flow perturbation variance, as presented in the previous sections, are, however, complicated. Apart from measurements of the power spectrum of the signal and velocity profile, it is necessary each time to carry out a large number of numerical calculations. This prevents the use of the present method, in its full version, to obtain results in real time. It is a serious difficulty, since only methods ensuring a rapid achievement of results can be expected to be used widely in medicine. It seems possible, in turn, to use a simplified version of the present method. The sample volume applied should be so small as to make the effect of the velocity profile on the spectrum variance negligible. At the same time, the measurement of the flow profile would ensure control of permissibility of this simplification. It is relatively easy to calculate the effect of the particle transit time on the spectrum variance in this case. By identifying this effect and detracting it from the spectrum, we obtain quite an accurate value of the mean variance of the flow perturbations.

Acknowledgement. The author wishes to thank Prof. L. FILIPCZYŃSKI for discussion and a number of valuable remarks in the course of preparing this paper.

References

[1] B. A. J. ANGELSEN, *A theoretical study of scattering of ultrasound from blood*, IEEE Trans. Biom. Enging., **27**, 2 (1980).

[2] W. R. BRODY, I. D. MEINDL, *Theoretical analysis of the C. W. Doppler ultrasonic flowmeter*, IEEE Trans. Biom. Enging., **21**, 3, 183–192 (1974).

[3] L. FILIPCZYŃSKI, R. HERCZYŃSKI, A. NOWICKI, T. POWAŁOWSKI, *Blood flows — hemodynamics and ultrasonic Doppler measurement methods* (in Polish), PWN, 1980.

[4] L. FILIPCZYŃSKI, *Detectability of gas bubbles in blood by the ultrasonic method* (in Polish), Archiwum Akustyki, **18**, 1, 11–30 (1983).

[5] F. K. FORSTER, *The applications and limitations of Doppler spectral broadening measurements for the detection of cardiovascular disorders*, Ultrasound in Med. Biol., D. White, R. Brown (eds.), Plenum Press, **3B**, 1223–1226 (1977).

[6] J. L. GABRINI, F. K. FORSTER, J. E. JORGENSEN, *Measurement of fluid turbulence based on pulsed ultrasound techniques*, Part 1 and Part 2, J. Fluid Mech., **118**, 445–470, 471–505 (1982).

[7] J. E. JORGENSEN, D. N. CAMPAU, D. W. BAKER, *Physical characteristics and mathematical modelling of pulsed ultrasonic flowmeter*, Med. Biol. Enging., **12**, 4, 404–420 (1973).

[8] J. P. MOUTET, *Etudes des modifications de l'ecculment induites par une stenose arterielle, these de doctorat,* es — sciences naturelles, Paris, 1981.

[9] V. L. NEWHOUSE, P. J. BENDICK, L. W. VARNER, *Analysis of transit time effects on Doppler flow measurement, IEEE,* Trans. Biom. Enging., **23**, 5 (1976).

[10] A. NOWICKI, *Ultrasonic Doppler pulsed method and equipment for blood flow measurements in the circulation system* (in Polish), D. Sc. Thesis, IPPT PAN, Warsaw, 1975.

[11] A. V. OPPENHEIM, R. W. SCHAFER, *Digital signal processing,* Prentice Hall, Inc., Englewood Cliffs, New Jersey, 1975.

[12] A. PAPOULIS, *Probability, random variables and stochastic processes* (in Polish), WNT, Warsaw, 1972.

[13] P. PERRONNEAU, M. PIECHOCKI, J. P. MOUTET, *Contribution des conditions de mesure et des caracteristiques de l'ecoulement sanguin a la genese des spectres Doppler,* Colloque sur les Ultrasons et l'acoustique phisique, Paris, November 1982.

[14] M. PIECHOCKI, *Ultrasonic Doppler methods of measurements of perturbed blood flows* (in Polish), D.Sc. Thesis, IPPT PAN, 1983.

[15] T. POWAŁOWSKI, *Mesaurement of fluid flow by the ultrasonic Doppler C.W. method* (in Polish), D. Sc. Thesis, IPPT PAN, Warsaw, 1976.

[16] K. K. SHUNG, R. A. SINGLEMANN, J. M. REID, *Scattering of ultrasound by blood,* IEEE, Trans. Biomed. Enging., **23**, 6, 460–467 (1976).

[17] E. TULISZKA, *Fluid mechanics* (in Polish), PWN, Warsaw, 1980.

[18] J. WESŁOWSKI, *Experimental and clinical studies on the usefulnees of ultrasound in vascular surgery* (in Polish), Ass. Prof. Thesis, Reports IPPT PAN, Warsaw, 1982.

ARCHIVES OF ACOUSTICS
10, 3, 303–314(1985)

NON-INVASIVE ULTRASONIC METHOD FOR THE BLOOD FLOW AND PRESSURE MEASUREMENTS TO EVALUATE THE HEMODYNAMIC PROPERTIES OF THE CEREBRO-VASCULAR SYSTEM

TADEUSZ POWAŁOWSKI, BOGUMIŁ PEŃSKO

Institute of Fundamental Technological Research, Polish Academy of Sciences
(00–049 Warsaw, ul. Świętokrzyska 21)

This paper presents a method for using ultrasonic measurements of the blood velocity and the motion of the walls of the blood vessel in simultaneous, noninvasive determination of the blood pressure and blood flow rate. The measurements were carried out in carotid arteries in people aged 25 to 40. On the basis of the results obtained, the vessel impedance was determined by the method of discrete Fourier transform. Analysis of the distribution of the impedance modulus and phase permitted the calculation of the parameters of the substitute cerebro-vascular model, such as resistance, inertia and compliance. By applying the model assumed the authors performed a computer simulation of the blood flow in the common carotid artery on the basis of the pressure determined from the movements of the walls of the artery under study. The results obtained coincide with the flows measured by the Doppler method in healthy persons.

1. Introduction

The description of the properties of man's vascular system requires the knowledge of a number of hemodynamic quantities, such as blood flow, blood pressure, vascular resistance, elasticity of blood vessel walls, capacity and resistance of the vascular bed. In 1959 McDonald and Taylor [13] suggested that the determination of the input vessel impedance might be the simplest way of describing these properties. The investigations carried out in a large number of laboratories in the world ever since in order to determine the impedance have confirmed this suggestion [1, 3, 12, 14, 22].

The input impedance of the vascular system is defined as the ratio between the blood pressure inside the vessel and the flow rate of blood flowing through this vessel, measured at the same time and over the same vessel cross — sec-

tion. When assuming the vascular system investigated as linear, the impedance Z can be determined by the Fourier transform of the time dependent pressure P and the blood flow Q, according to the formula

$$Z(2\pi nf) = P(2\pi nf)/Q(2\pi nf), \tag{1}$$

where $n = 0, 1, 2, \ldots$ and f is the frequency of the heart.

In the literature, the vessel impedance is most frequently represented in the form of modulus and phase as functions of frequency. Mutual relationships are sought among the modulus and phase distributions and the properties of the vascular system. In addition, the vessel impedance can contain information about the reflection sites of the waves of the pressure and flow at the branching points of blood vessels or their narrowings or blockages, which can be of significant values in diagnosing the patency of blood vessel in regions inaccessible to the currently used measurement methods.

The determination of the vessel impedance requires the simultaneous measurement of the instantaneous values of the blood flow and pressure. It is possible to carry out noninvasive measurements of the blood velocity in vessels by using ultrasonic Doppler methods [4, 7]. However, the pressure measurement offers considerable problems. It requires the introduction of a pressure transducer into the vessel studied. This restricts greatly the experimental possibilities, limiting practically the investigations to animals and very large vessels, for the introduction of the pressure transducer into the vessel perturbs the blood velocity measured simultaneously.

It would be possible to achieve a further extension of studies on the vessel impedance by finding noninvasive methods proposed by the authors, consisting in the determination of the blood pressure from the measurement of the displacement of the blood vessel walls [15]. At the Ultrasonic Department, Institute of Fundamental Technological Research, Polish Academy of Sciences in Warsaw an ultrasonic device was constructed for the simultaneous measurement of the blood vessel wall movement and the velocity of blood flowing through these vessels. This device was applied in measurements in man's carotid arteries. A computer, connected on line to the measurement device, calculates the blood pressure and blood flow rate, and the vessel impedance.

2. Relationship between the blood pressure and the displacement of the vessel wall

The magnitude of changes in the diameter of the blood vessel as a function of blood pressure depends on the mechanical properties of the vessel, its shape and size, and on the position of the vessel with respect to the heart. The determination of the functional relationship between the pressure and the wall displacement requires the assumption of some, of necessity, simplified mechanical model of the blood vessel. Most frequently, large vessels are regarded as

axially symetric cylinders with thin walls built of a homogeneous, elastic and incompressible material exhibiting transverse isotropy. Such cylinders are subjected to loads which also show axial symmetry, and the only effect of this loading is a change in the radial component of strain. Investigations carried out in a large number of centres on the properties of blood vessel have confirmed the justifiability of using the above simplifications [1, 2, 6, 16].

The direct application of the onedimensional Hooke law in the direction of the vessel radius leads to the simplest relationship between changes in the radius and changes in the pressure

$$\Delta P = E_P \frac{\Delta R}{R_0}, \tag{2}$$

where ΔP is the pressure difference causing a change in the vessel radius R_0 by a value ΔR, E_p is the elastic modulus "corresponding" to Young's modulus.

It follows from formula (2) that the dependence of E_p on the pressure or radius signifies a deviation from the Hooke law, i.e. elastic nonlinearity. E_p has repeatedly been observed to vary [8, 17]. There have been attempts to "improve" the modulus E_p by taking into account finite wall thickness, introducing the Poisson's ratio etc. [1, 2, 8].

With time variable dynamic loads, vessel walls can show viscoelastic properties. For sinusoidal load changes, the complex elastic modulus E^* can be introduced in the form

$$E^* = E_{\text{dyn}} + j\eta\omega, \tag{3}$$

where E_{dyn} is a dynamic elastic modulus and η is the coefficient of viscosity. Investigations carried out by a large number of authors have shown that the phase lag between the pressure and the radius change does not exceed 10° and that the inequality $\eta\omega \leqslant 0.1\ E_{\text{dyn}}$ is valid [8, 17]. This permits the viscoelastic effect to be neglected in the simplified model.

A successive approximation of the wall reaction to the internal pressure is the assumption that the pressure change is in the direct proportion to the relative change in the vessel volume [18]

$$\Delta P = K \frac{\Delta V}{V}, \tag{4}$$

where V is the volume of a vessel section and K is the elastic modulus. When the vessel cross-section is circular, then formula (4) becomes

$$P - P_0 = K \frac{R^2 - R_0^2}{R_0^2}, \tag{5}$$

where R_0 is the vessel radius at the pressure P_0 and R is the vessel radius at the pressure P.

In addition to the attempts to describe the relationship between the vessel radius and the pressure, mentioned above, in the literature [19, 21] there has also been the suggestion that this relationship is described by an exponential function.

In view of the large variety of descriptions of the relationship between the pressure and the vessel radius, the authors undertook an attempt to carry out their own evaluation of this function. On the basis of mathematical analysis introduced by GREEN [10] for an elastic system with axial symmetry subjected to large-amplitude strains and of SIMON's experimental results [19], the following dependence was assumed:

$$P(R) = P_0 \exp(\gamma R^2). \tag{6}$$

The parameters P_0 and γ can be determined by substituting in formula (6) the values of P and R in systole (P_s, R_s) and in diastole (P_d, R_d). Relationship (6) becomes then

$$P(R) = P_d \exp\left[\left(\frac{R^2 - R_d^2}{R_s^2 - R_d^2}\right) \ln \frac{P_s}{P_d}\right]. \tag{7}$$

Fig. 1 shows the function $P(R)$ calculated from the above relationship. For comparison, experimental data given by SIMON for canine abdominal aorta and the results of numerical calculations carried out on the basis of dependencies presented by GREEN are also given. In the calculations, the values $R_d = 4.4$ mm, $P_d = 46$ mmHg, $R_s = 5.2$ mm and $P_s = 199$ mmHg were assumed. It can be seen that the exponential function (formula (7)) approximates very well the experimental results and those of the numerical calculations.

It should be emphasized that in the case of small ratios $\Delta P/\Delta R$ all the relationships between the pressure and the vessel radius, mentioned above, give results close to each other. However, in view of the limited reaction of the vessel walls to large pressures, the authors assumed the exponential function as the more probable physiological dependence compared with a linear or quadratic function.

3. Measurement equipment

An ultrasonic device containing a bi-directional C.W. Doppler flowmeter and an echo system was constructed for the simultaneous measurement of the blood velocity and the instaneous diameter of the blood vessel. The parameters of the device were selected from the point of view of applications in measurements in carotid arteries. The ultrasonic probes, connected with the flowmeter and the pulse system, were focussed in tissue at depth between 1 and 3 cm. In the measurement of the blood velocity, the frequency of the transmitted ultra-

sonic wave is 4.5 MHz, while the frequency used in the measurement of the diameter of the vessel is 6.75 MHz. The resolution of the pulse system in tissue is 0.5 mm and permits the measurement of the internal diameter of the carotid artery. The measurement device contains a digital unit for tracing and measuring the motion of the blood vessel walls [9]. The accuracy of mapping the vessel wall displacements is 0.03 mm.

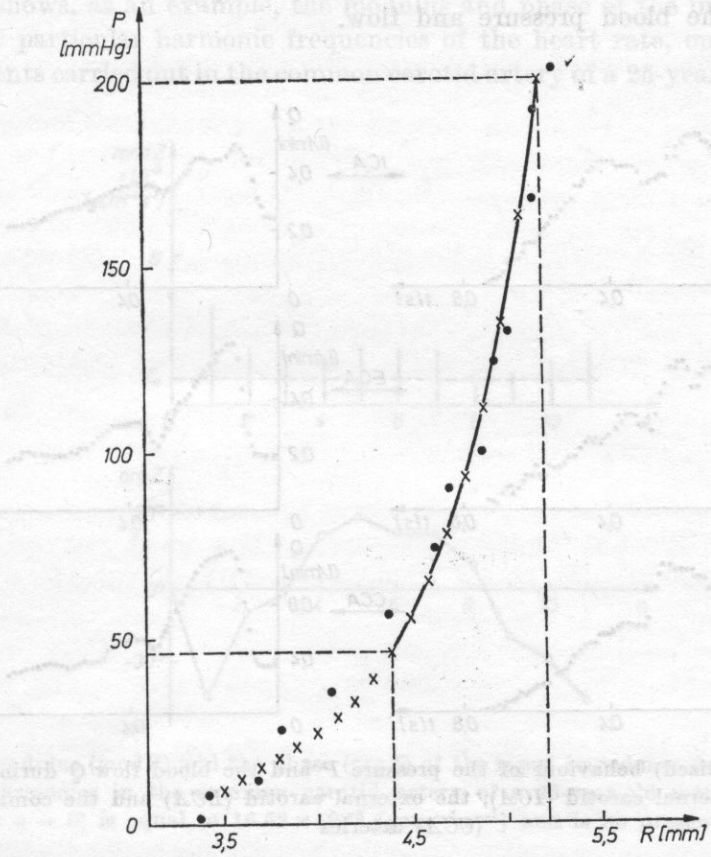

Fig. 1 The blood pressure versus the vessel radius (•) experimental points, according to SIMON, for canine abdominal aorta, (×) the results of numerical calculations, solid line — dependence from formula (6)

The device is equipped on line with a computer (MERA 60 — a Polish equivalent of PDP—11), which on the basis of the measured blood velocity, vessel diameter and the displacements of its wall, calculates the blood flow rate and the accompanying changes in the blood pressure. Each time the calculated results were averaged from three cycles of the heart rate.

The pressure (formula (7)), determined from displacements of the vessel walls, in the carotid arteries was calibrated in absolute values by the systole

pressure P_s and the diastole one P_d measured in the brachial artery. The quantities P_s and P_d were measured with a cuff in a lying patient, at the height of the carotid artery.

Fig. 2 shows, as an example, the blood pressure and flow determined by the authors using the device described in the internal (*ICA*), external (*ECA*) and common (*CCA*) carotid arteries of a 40-year-old man. It is possible to see a difference between the external and internal carotid arteries in the form of changes in the blood pressure and flow.

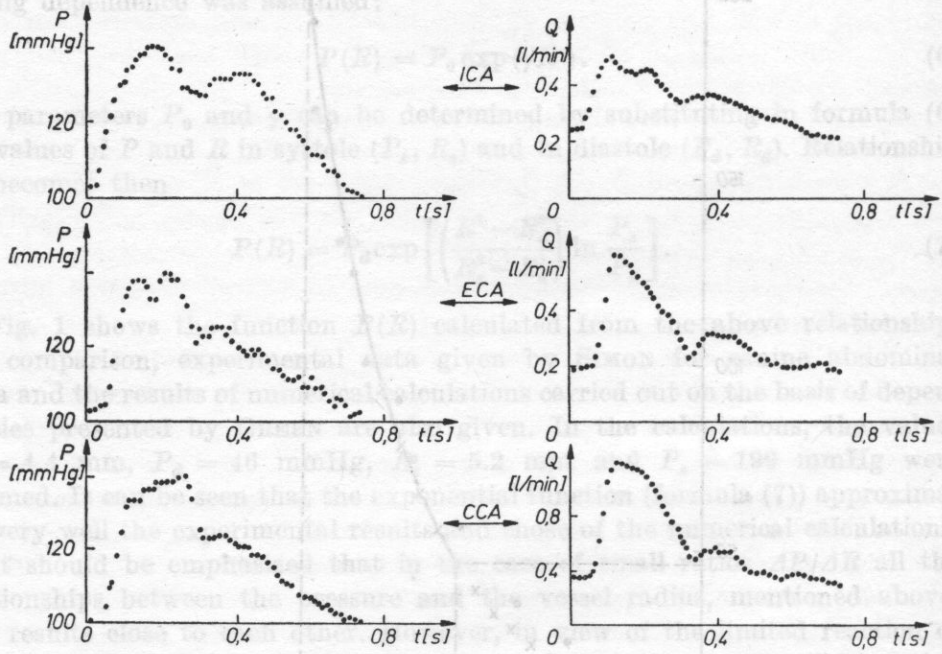

Fig. 2. (Quantitized) behaviour of the pressure P and the blood flow Q during a cardiac cycle in the internal carotid (*ICA*), the external carotid (*ECA*) and the common carotid (*CCA*) arteries

4. Impedance and the equivalent model of the vessel system

The simultaneous measurement of the blood pressure and blood flow in the same cross-section of the vessell permits the determination of the vessel impedance, which is a functional relationship between these quantities (see formula (1)). By using the equipment constructed, the authors carried out measurements of the vessel impedance in the common carotid artery in 10 men aged between 25 and 40 years. In all the cases the investigations were carried out at 2–3 cm before the bifurcation.

The modulus and phase of the vessel impedance were determined by the fast Fourier transform (*FFT*) from the time functions of the blood pressure and flow. For each heart cycle, 64 discrete values of the pressure and flow were used in the calculations. The impedance was determined independently of three successive cardiac cycles, and subsequently the average value was calculated from the results obtained.

Fig. 3 shows, as an example, the modulus and phase of the impedance calculated for particular harmonic frequencies of the heart rate, on the basis of measurements carried out in the common carotid artery of a 25-year-old man. In

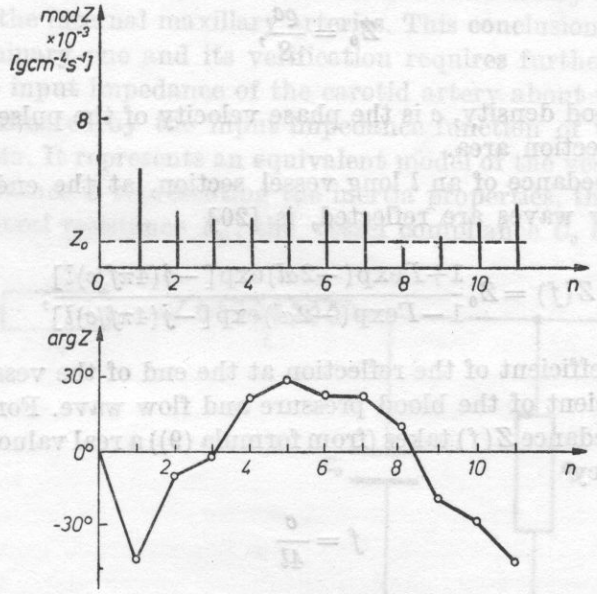

Fig. 3 The modulus (mod Z) and the phase (arg Z) of the input impedance determined for n successive harmonics in the common carotid artery of a 25-year-old man. DC value of mod Z (for $n = 0$) is equal to 16.52×10^{-3} [gcm^{-4} s^{-1}] and is no presented in figure

the interpretation of impedance, 12 first harmonics were considered. The other harmonic frequencies were eliminated, for their values are quotients of components with very small amplitudes, whose share in the spectrum of the signal of the blood pressure and flow velocity is negligibly small.

In all the 10 men examined, it was observed that the modulus of the vessel impedance has two characteristic minima, accompanied by a zero value of the phase. The first minimum occurs between the 3th and 4th harmonics, the other between the 7th and 10th harmonics, depending on the patient. From the viewpoint of the authors, the first minimum is related to the compliance, inertia and resistance of carotid arteries and brain vessels. The negative phase of the impedance for harmonics below a minimum is related to the compliance pro-

perties. The positive phase values for harmonics above the minimum corresponds to the inertance properties.

The other impedance minimum is probably the effect of the reflection of the pressure and velocity wave propagating along the carotid arteries. By analysing the phenomenon of the reflection, the authors assumed, just as McDONALD [14] did, a simplified model of the vessel system in the form of vessel sections with constant hemodynamic properties. By analogy, these sections can be regarded as sections of a transmission line with the characteristic impedance Z_0. For large blood vessels and higher harmonics, this impedance has a real character and is [18].

$$Z_0 = \frac{\varrho c}{S}, \tag{8}$$

where ϱ is the blood density, c is the phase velocity of the pulse wave and S is the vessel cross-section area.

The input impedance of an l long vessel section, at the end of which the pressure and flow waves are reflected, is [20]

$$Z(f) = Z_0 \frac{1+\Gamma \exp(-2\alpha l)\exp[-j(4\pi f/c)l]}{1-\Gamma \exp(-2\alpha l)\exp[-j(4\pi f/c)l]}, \tag{9}$$

where Γ is the coefficient of the reflection at the end of the vessel and α is the attenuation coeficient of the blood pressure and flow wave. For real values of Z_0 and Γ, the impedance $Z(f)$ takes (from formula (9)) a real value for a harmonic with the frequency

$$f = \frac{c}{4l} \tag{10}$$

corresponding to 1/4 of the wavelength of the pulse wave in the vessel. In addition, it reaches a minimum value, less than the characteristic impedance, when the reflection cofficient Γ has a positive value.

The above conclusions confirm the author's earlier suggestion that the second minimum of the input impedance for the common carotid artery can be caused by reflection of the pulse wave. Fig. 3 shows that the impedance at the second minimum has a real character (with zero phase) and is lower than the characteristic impedance Z_0 calculated from relationship (8).

In determinig the hypothetic site of reflection the authors assumed that the impedance measured in the common carotid artery before the bifurcation depends on the input impedances of the external and internal carotid arteries. It signifies that the observed minimum of the input impedance of the common carotid artery can be a result of reflection in the external or internal artery. Assuming approximately that the phase velocity c is independent of the frequency, the authors estimated the distance l between the measurement point

and the reflection point from dependence (10). The velocity c in this depedence was determined from measurements, on the basis of the formula [18]:

$$c^2 \simeq \frac{1}{\varrho} \frac{P_s - P_d}{S_s - S_d} S_d, \tag{11}$$

where P_s and P_d are systole and diastole pressures and S_s and S_d are the vessel cross-section areas for the two pressures. The distance between the reflection point and the measurement point estimated in this way varied between 15 and 18 cm, depending on the person examined. It suggests that the second minimum of the impedance measured in the common carotid artery can be related to reflection from the bifurcation of the external carotid artery into the superficial temporal and the internal maxillary arteries. This conclusion should be regarded as a preliminary one and its verification requires further studies. The behaviour of the input impedance of the carotid artery about the first minimum can be approximated by the input impedance function of the elastic system shown in Fig. 4a. It represents an equivalent model of the vessel system and includes the inertance L representing the inertia properties, the vessel resistance R_0, the peripheral resistance R_p, the vessel compliance C_0 and the peripheral

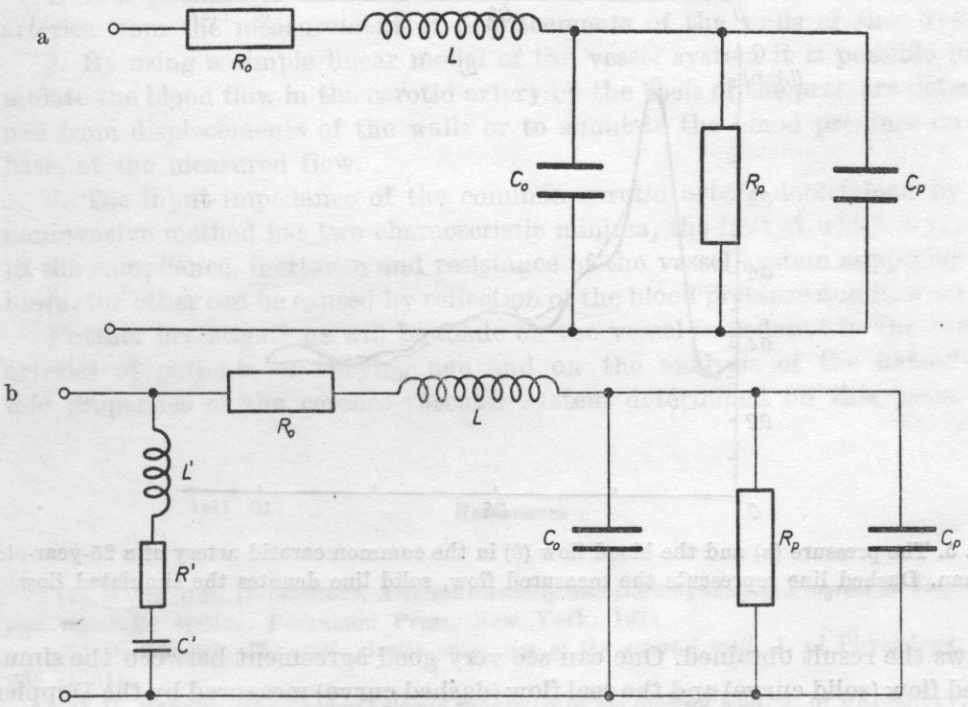

Fig. 4a. The electric equivalent model of the vessel system

Fig. 4b. The electric equivalent model of the vessel system simulating two minima of the vessel impedance

compliance C_p. This model is a slight modification of the vessel model proposed by BROEMSER and RANKE [5, 11], which is used by a large number of authors to interpret the impedance measured in the aorta [12, 22].

By applying the model shown in Fig. 4*a*, a computer simulation of the blood flow rate in the common carotid artery was carried out on the basis of the pressure determined from displacements of the walls of this artery. Fig. 5

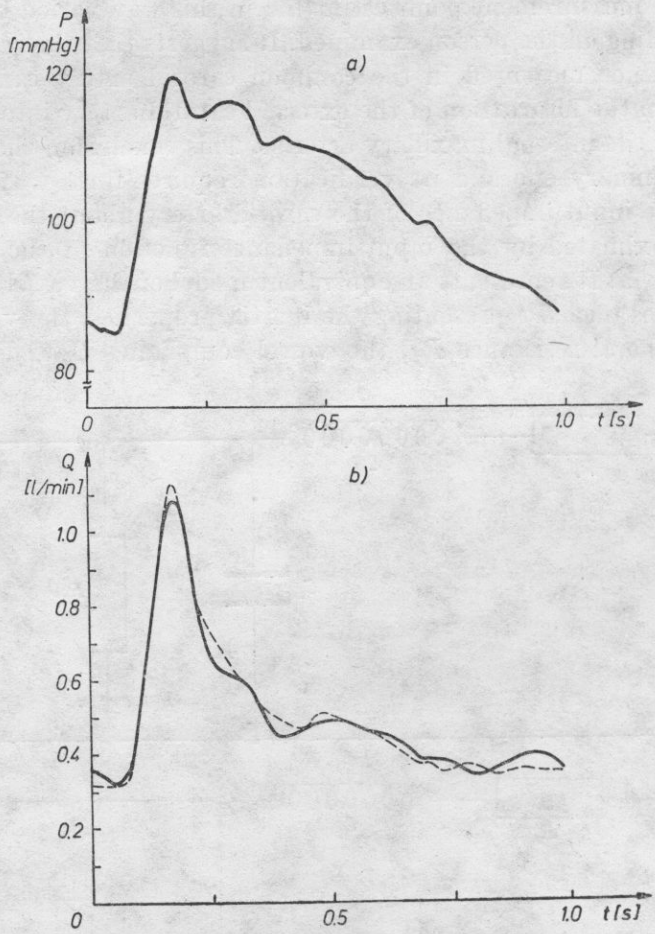

Fig. 5. The pressure (*a*) and the blood flow (*b*) in the common carotid artery of a 25-year-old man. Dashed line represents the measured flow, solid line denotes the simulated flow

shows the result obtained. One can see very good agreement between the simulated flow (solid curve) and the real flow (dashed curve) measured by the Doppler method. The calculated results were essentially uneffected by neglecting the second minimum of impedance in the modelling (for the model assumed describes only the first minimum). It can be explained by the fact that those har-

monics for which the impedance takes the second minimum contribute little energy to the blood pressure and flow spectrum.

The second impedance minimum can be simulated by including a series resonance circuit L', R', C' (Fig. 4*b*) in the equivalent system. The impedance of such a system describes much better the real impedance. However, this model requires further studies and is only an example of a possible successive step towards modelling a vessel system.

The presented example of modelling the blood flow in the common carotid artery was obtained from a 25-year-old man. The parameters of the equivalent system, calculated from the vessel impedance determined for this patient (see Fig. 3), were $R_0 = 2480$ gcm^{-4}s^{-1}, $R_p = 14040$ gcm^{-4}s^{-1}, $L = 56$ gcm^{-4}, $C_p + C_0 = 3.3 \times 10^{-5}$ g^{-1}cm^{4}s^2.

5. Conclusions

The investigation results presented in this paper permit the following conclusions to be drawn.

1. It is possible to determine changes in the blood pressure inside carotid arteries from the measurement of displacements of the walls of thse vessels.

2. By using a simple linear model of the vessel system it is possible to simulate the blood flow in the carotid artery on the basis of the pressure determined from displacements of the walls or to simulate the blood pressure on the basis of the measured flow.

3. The input impedance of the common carotid artery determined by the noninvasive method has two characteristic minima, the first of which is related to the compliance, inertance and resistance of the vessel system supplying the brain, the other can be caused by reflection of the blood pressure and flow waves.

Further investigations will be made on the vessel impedance in the carotid arteries of patients of varying age and on the analysis of the hemodynamic properties of the cerebro-vascular system determined on this basis.

References

[1] D. Bergel, D. Schultz, *Arterial elasticity and fluid dynamics, Progress in biophysics and molecular biology*, Pergamon Press, New York, 1971.

[2] D. Bergel, *The static elastic properties of the arterial wall*, J. of Physiology, **156**, 458 (1961).

[3] D. Bergel, *The dynamic elastic properties of the arterial wall*, J. of Physiology, **156**, 458 (1961).

[4] K. Borodziński, L. Filipczyński, A. Nowicki, T. Powałowski, *Quantitative transcutaneous wave Doppler methods*, Ultrasound in Medicine and Biology, **2**, 189–193 (1976).

[5] P. H. BROEMSER, O. F. RANKE, *Über die Messung des Schlagvolumens des Herzens auf unblutigem Wege*, Z. Biol., **90**, 467–507 (1930).

[6] T. CAREW, R. VAISHNAV, D. PATEL, *Compressibility of the arterial wall*, Circ. Res., **23**, 61 (1968).

[7] L. FILIPCZYŃSKI, R. HERCZYŃSKI, A. NOWICKI, T. POWAŁOWSKI, *Blood flow – hemodynamics and ultrasonic Doppler measurement methods*, PWN, 1980.

[8] B. GOW, M. TAYLOR, *Measurement of viscoelastic properties of arteries in living dog*, Circ. Res., **23**, 1, 111 (1968).

[9] D. H. GROVES, T. POWAŁOWSKI, D. N. WHITE, *A digital technique for tracking moving interfaces*, Ultrasound in Medicine and Biology, **8**, 2, 185–190 (1982).

[10] A. GREEN, J. ADKINS, *Large elastic deformation*, Clarendon Press, Oxford, 1970.

[11] T. KENNER, *Models of arterial system. The arterial system, dynamics, control theory and regulation*, 80–87, Springer Verlag, 1978.

[12] S. LAXMINARAYAN, P. SIPKENA, N. WOESTERHOF, *Characterization of the arterial system in the time domain*, IEEE Trans. on Biomedical Eng., **BME—25**, 2, 177–184 (1978).

[13] D. A. MCDONALD, M. G. TAYLOR, *The hydrodynamics of the arterial circulation*, Progress in biophysics and biophysical chemistry, **9**, 105 (1959).

[14] D. A. MCDONALD, *Blood flow in arteries*, E. Arnold, London, 1960.

[15] T. POWAŁOWSKI, B. PEŃSKO, Z. TRAWIŃSKI, L. FILIPCZYŃSKI, *An ultrasonic trascutaneous method of simultaneous evaluation of blood pressure, flow rate and pulse wave velocity in the carotid artery*, Abstracts of Satellite Symposium of the XIIIth World Congress of Neurology, Aachen, 1985, M–68.

[16] D. PATEL, D. FRY, *The elastic symmetry of arterial segments in dogs*, Circ. Res., 24 (1969).

[17] D. PATEL, F. FREITAS, J. GREENFIELD, D. FRY, *Relationship of radius to pressure along the aorta in living dogs*, J. of Applied Physiology, **18**, 6, 111 (1963).

[18] T. J. PEDLEY, *The fluid mechanics of large blood vessels*, Cambridge University Press, 1980.

[19] B. SIMON, A. KOBAYASHI, D. STRANDNESS, C. WIEDERHIELM, *Large deformation analysis of the arterial cross section*, J. of Basic Eng., **93***D*, 2 (1971).

[20] J. L. STEWART, *Circuit analysis of transmission lines*, John Wiley, New York, 1958.

[21] T. TANAKA, Y. FUNG, *Elastic and inelastic properties of the canine aorta and their variation along the aortic tree*, J. of Biomech., **7**, 4, 357 (1974).

[22] N. WESTERHOF, G. ELZINGA, G. C. VAN DEN BOS, *Influence of central and peripheral changes on the hydraulic input impedance of the systemic arterial tree*, Medical and Biol. Eng., 710–721 (1973).